A stochastic model of root gravitropism

Robert Frederick Thomas

Department of Biological Sciences

University of Leeds

A thesis submitted for the degree of

Doctor of Philosophy

30th September 2017

Acknowledgements

This thesis could not have been completed without the support of my fantastic friends and collegues. Firstly I would like the thanks my supervisors Stefan Kepinski and Netta Cohen, you have both been great and I feel lucky to have worked with you.

I would also like to thank Suruchi, Ryan, and Marta along with all the Kepinski lab members for helping someone new to Biology figure out how everything works, and for making it fun while I do. Special thanks go to Katie for measuring a seemlingley endless number of roots without which I would have had nothing to model.

I would like thank Chris Wolverton for our talks about ROTATO, it's been good to get the input of someone who has done this before.

To Pete and Joe, you've both been great housemates. I would like to thank you for not getting too annoyed when I've spent too much time working and not enough looking after the house, and for always being up for a beer when needed. Thanks must also go to my climbing partners, Sandy, Charlotte, and all the others. Without people to climb with I think I would have gone a bit mad.

Lastly I would like to thank my family. Chris and Linda, thank you for your support throughout this project. It's been good to known you'll be there if I've ever needed it.

There are many more people who have made my time on this project thoughourly enjoyable. It has at times been frustrating when nothing has worked for a week, but even then I don't think there's anything else I would rather have been doing.

Abstract

Gravitropism is a vital process determining plant architecture. As plant architecture is key to resource aquisition a better understanding of gravitropic behaviour may have a great impact on our future food security. Recent models of gravitropism have focussed on understanding specific mechanisms involved in gravitopic response. However our understanding of gravitropism at the behavioural level remains limited, with little known about the factors that determine a response and the timescales involved. We show that gravitropic behaviour is best treated as an angle dependent stochastic system exhibiting fast angle detection and relatively slow response with limited to no hysteresis. A minimal stochastic model of root gravitropism is presented which provides a description of gravitropic behaviour at the population level as well making informative predictions about the behaviour of the mechanisms involved. The root is treated as having a probability of making a discrete bend in a given time that is directly proportional to the current angle. The angle dependent probability combined with the size of a bend determines the expected response, while the bend size determines the variation in response. The time step of a bend limits the timescale of the response to a few minutes. The need to analyse the noisy response of roots to gravity has necessitated the development of equipment to precisely control the angle of a root tip over long time periods, as well as automated data analysis tools capable of handling large datasets.

Contents

List of Figures

Chapter 1

Introduction

1.1 The role of tropisms in plant growth

Like all organisms, plants require a variety of resources to survive and reproduce. Being sessile, plants must be capable of maximising the amount of resources captured from their surroundings. A plant's shape, or architecture, is an important aspect of resource optimisation, with different architectures maximising the capture of different resources available for uptake. For example topsoil tends to contain a greater concentration of nutrients but is often drier than than deeper soil layers (Lynch, 1995). It has been shown that in beans, a shallow and highly branched root system allows for more effective nutrient uptake (Lynch and van Beem, 1993) than a deeper root system. Conversely, it has long been known that in desert plants a deep root system with near vertical roots allows plants to better survive dry conditions (Cannon, 1911). Shoot architecture is equally important for maximising the utilisation of the light available. For example the tropical tree *Terminalia catappa* has been shown to display branching angles optimum for light capture in its environment (Honda and Fisher, 1978).

Plant architecture is not fixed; many plants are able to actively adapt to the conditions they find themselves in. This has been demonstrated in the bean *Phaseolus vulgaris* which under different conditions will adapt its root architec-

ture to maximise the overall uptake of water or nutrients (Ho et al., 2004), with more vertical roots being produced in nutrient rich or water poor conditions. In herbaceous plants particularly, changes in shape can occur over short timescales due to directed growth in response to stimuli. By actively directing growth in response to stimuli the plant is able to move and adapt to rapidly changing conditions despite its sessile nature. These processes known as tropisms have been studied since Darwin wrote "The power of movement in plants" (Darwin and Darwin, 1880) in 1880.

Tropic responses can be triggered by a range of stimuli. Gravitropism is a response towards or away from the direction of gravity, allowing roots to bend downwards or shoots upwards. Phototropism causes shoots or roots to bend towards or away from light. Thigmotropism is a response to touch, and hydrotropism a response to water content (Esmon et al., 2005). In many cases multiple stimuli will be present and driving conflicting responses, in this situation the plant must be able to integrate multiple conflicting responses and maintain a coherent response to complex stimuli. Such ability in an organism lacking a centralised controller such as the nervous system seen in animals is impressive. The following sections outline some of the processes involved in generating an active and coherent growth response with an emphasis on gravitropic mechanisms and behaviour in *Arabidopsis thaliana* .

1.2 Growth control in herbaceous plant roots

1.2.1 Bending as a growth response

Organs capable of tropic response have well defined structures that must be maintained while directional growth is achieved. Because of this it not simply sufficient to grow when a stimulus is present, instead growth must be coordinated across the organ in order to produce a bend towards or away from the stimulus.

In Arabidopsis, post-embryonic root growth is governed by the longitudinal elon-

gation of epidermal cells. When a stimulus is present, cell expansion becomes asymmetrical across the root differentiation zone, causing the root to bend. A simple explanation for this can be obtained from the geometry of a bend over a small distance. Assuming the bend over a small distance (say one cell-length) is constant, we can describe the mid-line of the root with width w as an arc on a circle. Since root growth is mainly longitudinal, the width of the root can be considered constant. If we look at the two sides, the inner side I and outer side O, their edges will be arcs along circles with radius r and r + w, respectively. (see figure 1.1 for an illustration). This is described by Equation 1.1, where θ is the angle of the arc describing both sides in radians. If we rearrange Equation 1.1 we find that $\theta = \frac{O-I}{w}$. Therfore in an ideal root (or shoot) with constant width we would expect a bend proportional to the difference in length between the opposite sides. It is worth noting that the direction of the observed bend is towards the shorter side of the organ.

In order for tropic growth to be achieved it is sufficient for an organ to produce asymmetrical growth rates such that the side of the organ in the direction of the intended bend is elongating slower than the opposite side. This could be achieved by increasing growth rates on the outside of the intended bend, decreasing growth rates on the inside, or through some combination of the two.

A similar analysis, along with measurements confirming the consistency of bending can be found in Perbal *et al.* (Perbal et al., 2002).

$$\theta = \frac{I}{r} = \frac{O}{r+w} \tag{1.1}$$

1.2.2 Auxin concentration determines growth rate

Cellular elongation is limited by the stiffness of the cell wall. The elongation itself is driven by the turgor pressure of the cell (Cleland, 1987), when the turgor pressure exceeds the yield stress threshold of the cell wall, the cell will expand, with the growth rate given by equation 1.2 where P is the turgor pressure, Y is
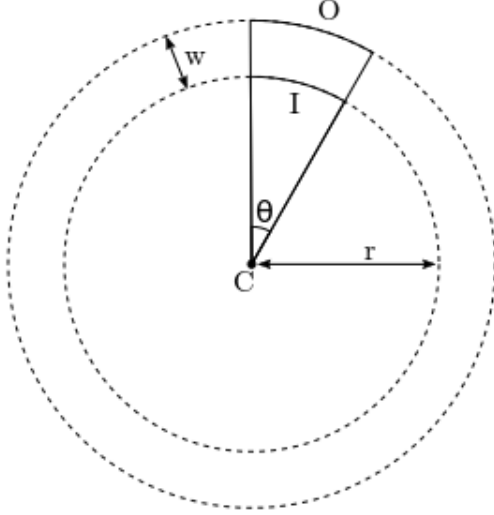
Figure 1.1: Assuming uniform curvature over small distances the inner and outer sides of the root can be treated as arcs along circles with radius r and $r + w$. The angle of the segment is given by θ.

the yield stress, m is an extensibility coefficient, and V is the volume of the cell. Unidirectional, longitudinal growth occurs because the structure of the cell wall, with bands of cellulose which ring the cell, strongly resists elongation along the radial axis of the cell (Schopfer, 2006). To produce differential growth either the turgor pressure or the cell wall yield stress must be varied.

$$\frac{\delta V}{\delta t} = m \cdot (P - Y) \tag{1.2}$$

The hormone Auxin (indole-3-acetic acid) is a key growth regulator that has been widely accepted as the most significant player in tropic growth. Auxin is capable of regulating cellular elongation rates by changing the stiffness of the cell wall (Nakahori et al., 1991). A recent detailed review of the biophysical basis of cell wall extensibility is given by Crosgrove in (Cosgrove, 2015). As the turgor pressure forces the cell to elongate it behaves viscoelastically (Cosgrove, 1993), with the weakening of the cell wall being accompanied by the deposition of new wall material making the process irreversible (Schopfer, 2006). In the root, in-

creased auxin content inhibits cell elongation, whereas in the shoot it promotes elongation (Fendrych et al., 2016). Although there is limited data available on the precise relationship between auxin concentration and elongation rates in the *Avena* coleoptile it appears to be sigmoidal, with initial increases in auxin concentration promoting elongation which quickly plateaus as the concentration is increased further (Cleland, 1972). However this relationship is known not to hold in the Arabidopsis root where increasing auxin levels cause a decrease in the elongation rate (Fendrych et al., 2016; Swarup et al., 2005). It is plausible however that a similar sigmoidal function may be displayed in the Arabidopsis root, where at low values the turgor pressure is insufficient to overcome the yield stress of the walls, and at high concentrations the elongation rate is limited by other processes (such as the speed of wall deposition).

The mechanism by which auxin inhibits cellular elongation in the root is still up for debate. In the shoot the acid growth theory is used to explain the mechanism behind auxin induced cellular elongation. The acid growth theory claims that auxin triggers the activation of proton pumps on the cell membrane, leading to acidification of the apoplast. The reduction in pH in the apoplast then activates cell wall loosening enzymes, such as expansins, allowing the cell to elongate (Hager, 2003). Recent studies have shown that in the root increases in auxin concentration can lead to alkalinisation of the apoplast, and that this in turn inhibits cellular elongation (Barbez et al., 2017), suggesting the acid growth theory may apply to roots as well as shoots.

The expansins are a super-family of cell wall loosening enzymes thought to play a role in determining cellular expansion during gravitropic response (Cosgrove, 1997; Sampedro and Cosgrove, 2005; Zhang and Hasenstein, 2000). The structure of the cell wall largely consists of rigid load-bearing cellulose microfibrils bound together by hemicelluloses and pectins (Cosgrove, 2005), with elongation occurring due to slippage between cellulose microfibrils (Cosgrove, 2000). Expansins facilitate the movement of the cellulose microfibrils by disrupting the binding between the microfibrils and the supporting pectins and hemicelluloses (Cosgrove, 2000), this allows the cellulose microfibrils to move apart in response to the turgor pressure within the cell.
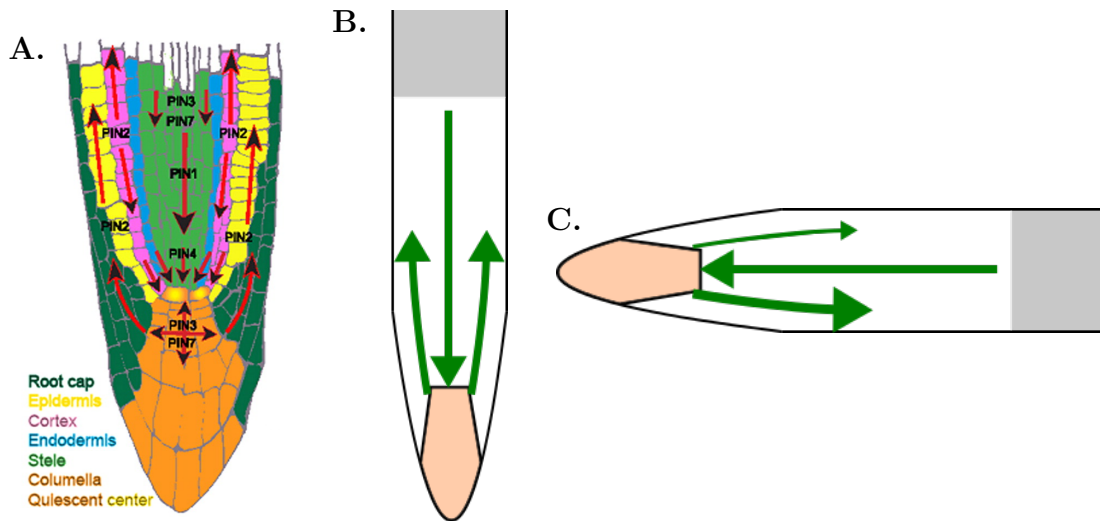
Figure 1.2: **A.** The location of PIN expression and auxin flow in the root tip, image adapted from (Feraru and Friml, 2008). **B.** The auxin transport pattern in an Arabidopsis root. Auxin is moved down the vasculature towards the tip. The columella (shaded beige) redistributes the auxin laterally through the lateral root cap and back up and away from the tip into the epidermis. The auxin dependent regulation of cell elongation occurs behind the tip in the elongation zone (shaded grey). **C.** During graviresponse auxin is preferentially distributed to the lower side.

1.2.3 Auxin distribution drives behaviour

The Cholodny Went model of tropic behaviour, proposed in the 1920's (Cholodny, 1927; Went, 1927), states that tropic growth is driven by the distribution of the plant growth regulator auxin. In both the Arabidopsis root and shoot the flow of auxin follows a distinctive pattern. In the root the flow of auxin forms an inverted fountain with auxin flowing down the vasculature in the centre of the root to the root tip, more specifically the stem cell niche and columella cells of the root cap. From here the auxin is moved laterally and back up the root to the epidermis via the lateral root cap, where it flows up and away from the tip (see Fig. 1.2). Elongation then occurs further back from the root tip in a region known as the elongation zone. In the Arabidopsis root increased auxin concentration leads to decreased elongation.

Auxin is synthesised primarily in young leaves and the root tip (Ljung et al., 2005), although all cells have the capability to produce auxin. After synthesis auxin is transported through the plant in two ways. Long distance transport of auxin takes place in the vascular system and allows relatively rapid movement of auxin. Short distance polar auxin transport relies instead on the chemical properties of auxin and on the activity of efflux carriers (such as the PINs) and influx carriers (such as AUX1) (Marchant et al., 1999), the locations of which determine the flow of auxin though the organ (Benková et al., 2003; Grieneisen et al., 2007; Robert and Friml, 2009). Inside the cell auxin is deprotonated, the pH gradient between the cell and the surrounding cytoplasm then prevents it from diffusing across the plasma membrane. AUX1 is an auxin efflux protein in the AUX/LAX family required for polar auxin transport. Loss-of-function AUX1 mutants show a reduction in auxin transport rates which causes a loss of gravitropic ability in the roots (Marchant et al., 1999).

Where the AUX/LAX family consists of auxin efflux proteins, the PIN family consists of auxin influx proteins. In Arabidopsis eight members of the PIN family have been identified (Vieten et al., 2007), of which PINS 1,2,3,4, and 7 have been shown to be expressed in the root tip (Petrášek and Friml, 2009) (Fig. 1.2), loss of function in *pin2* produces an agravitropic phenotype while *pin3pin4pin7* mutants show decreased gravitropic ability as an auxin gradient cannot be maintained in the elongation zone.

As these PIN proteins are required for auxin transport out of the cell, the location of the PINs within the cells of the root cap determines the direction of auxin flow out of the tip. While the mechanisms determining PIN polarity in the columella are not know, in other tissues cellular distribution is controlled by the antagonistic action of the phosphatase PP2A and the protein kinase PID (Fozard et al., 2012; Michniewicz et al., 2007) with phosphorylated PINs localising on the upper face of cells, and loss of PID function causing dephosphorylated PINs to relocalise to the lower face of cells (Kleine-Vehn et al., 2009; Sukumar et al., 2009). Fozard *et al.* produced a model of PIN phosphorylation and localisation which shows that unique stable equilibrium levels of phosphorylated PINs exist given different levels of PID and PP2A (Fozard et al., 2012). This would support the idea that

reliable gravitropic growth could be produced by a variation in levels of PID or PP2A in the columella controlling the flow of auxin out of the root tip by varying the amount of PINs localised at the upper and lower faces of the cells in the columella.

In the Arabidopsis root, gravitational stimulation causes an increase in auxin output on the lower side of the columella which then leads to an auxin gradient further back in the elongation zone. The increase in auxin on the lower side of the elongation zone causes it to grow more slowly than the upper side leading to a downwards bend in the root.

Auxin response can be either transcriptional or non-transcriptional. While very little is known of the latter there are two families of transcription regulators that have been demonstrated, AUXIN/INDOLE-3-ACETIC ACID co-repressor proteins (Aux/IAA) and AUXIN RESPONSE FACTORS (ARFs). ARFs can be divided into two broad classes, those that activate and those that repress transcription. Dimerisation occurs between activating ARFs and AUX/IAA co-repressors which results in transcriptional repression at the targeted locus. Auxin acts to promote gene expression by promoting the ubiquitinisation and subsequent degradation of AUX/IAAs thus relieving the repression (Tiwari et al., 2001).

The auxin dependent degradation of Aux/IAA proteins has been used as the basis for an auxin biosensor. By binding a portion of the Aux/IAA complex that is responsible for auxin-induced instability to a yellow fluorescent protein (YFP) one can create create an inverse marker for auxin concentration. R2D2 is a ratiometric auxin marker consisting of DII-VENUS, a degron from domain 2 of Aux/IAA IAA28 fused to GPF, and nuclear localised red fluorescent protein (RFP). Auxin causes the degradation of DII-VENUS, this acts as an inverse reporter where the presence of auxin reduces the YFP fluorescence (Liao et al., 2015). As the RFP is stable it is able to act as a control allowing more accurate auxin measurements than DII-VENUS alone.

By using DII-VENUS alone it is possible to get a good approximation of auxin distribution within the root and other tissues. Although DII-VENUS levels are not directly proportional to auxin levels, a system of ODE's (ordinary differential

equations) has been produced which is able to map the levels of DII-VENUS to auxin (Band et al., 2012).

Analysis of auxin distribution using DII-VENUS has shown an auxin gradient across the lateral axis of gravistimulated roots as expected, however the results suggest that the distribution of auxin at different angles does not change smoothly as previously thought. Instead of a smoothly changing auxin gradient, the magnitude of which depends upon the angle of orientation, a tipping point was observed. When rotated by 90° there was a large change in auxin distribution within the first few minutes of reorientation. Interestingly the auxin gradient was lost around the mid point of gravitropic bending (at an orientation of approximately 48°) after which it was hypothesised that continuing bending is due to downstream products of auxin which persist after the auxin asymmetry has dissipated (Band et al., 2012). It is suggested that statocytes act as a tilt switch outputting a binary auxin signal with an auxin gradient being formed if and only if the statocyte is reorientated above a threshold angle. In this case bending to the vertical could be the result of deceleration over time after the root tip has moved below the threshold angle. Given this it is not clear how gravitropic growth could occur after reorientation to an angle of below the 48° threshold value. Additionally if an organ is held at different orientations the rate of gravitropic growth should form a step function, or sigmoid. While there is not a large amount of fixed orientation data available the results of Mullen *et al.* (Mullen et al., 2000) do not seem to show the rates of reorientation predicted by the tipping point model, instead showing a smooth increase in bend-rate as the angle increases.

A model of PIN positions within cells in the arabidopsis root has shown that the distribution of PIN's in the columella is able to produce a lateral auxin gradient across the root (Grieneisen et al., 2007), as would be required by the Cholodny Went hypothesis. However this model is based on simplified cellular geometries, models including more complex cellular geometries highlight the necessity of efflux proteins such as AUX1 in generating realistic auxin distributions (Band et al., 2014). This builds upon previous work which models the relationship between auxin concentration and D2-Venus, making it possible to determine the concentration of auxin across the root during graviresponse (Band et al., 2012)

Statocytes and statoliths

The most widely accepted explanation of how gravity sensing cells detect the direction of gravity is the starch-statolith theory (Sack, 1991, 1997), originally proposed by the German botanist Fritz Noll in 1897. Most plants have specialised gravity sensing cells known as statocytes which contain dense specialised amyloplasts called statoliths. This is supported by the fact that removal of the statocytes in the Arabidopsis root tip by laser ablation has been shown to reduce gravitropic response (Blancaflor and Masson, 2003). The statoliths consist of one or more starch granules contained within a membrane. Being denser than the surrounding medium the statoliths are able to sediment at the bottom of the statocyst, this sedimentation is thought to be involved in the detection of gravity. It is not known how the placement of statoliths affects the auxin signal outputted by the cell (Morita and Tasaka, 2004) but it seems likely that the signal depends upon the number of statoliths in contact with the membrane. Recent work suggests that statoliths act as angle sensors rather than force sensors (Chauvet et al., 2016) though whether it is the absolute number which is detected or the force of statoliths pressing on the membrane is still an important question. It is also possible that the there are in fact 2 mechanisms involved in signal production: the presence of statoliths on the side wall of the cell, may determine magnitude of response, and their presence (or absence) on the top or bottom face of the cell may determine direction.

The starch-statolith theory is well supported by several pieces of evidence. For example Arabidopsis mutants which lack the ability to produce starch are less sensitive to gravity than those able to produce starch normally (Kiss et al., 1989), while retaining the ability to respond to other stimuli (Kiss et al., 1996). Others have shown that in *Salix viminalis* root bending only occurs after statoliths have developed (Fjell, 1985), and that in decapitated *Zea mays* roots gravitropism is only shown in roots which have developed statoliths which are capable of sedimentation (Hillman and Wilkins, 1982). However some gravitropic response does still occur in starch-less Arabidopsis mutants, which is consistent with the idea that while starch-statoliths are involved in sensing the direction of gravity, starch-less

statoliths may still be able to sediment on the bottom of the cell (Sack, 1991).

Statolith movement

There have been some attempts to model the movement of statoliths within the cell. For example Audus *et al.* (Audus, 1964) made a physical model of a cell containing polythene "statoliths". They found a good fit between the number of statoliths on the long edge of the model cell and reported magnitude of gravitropic responses at different orientations. To simulate this Audus used a perspex box of of a similar shape to a central columella cell containing between 30 and 36 polythene statolith models, which was then filled with paraffin. The box was then rotated and the number of statoliths in contact with the long wall of the box counted. They found that the log of the number of contacts between statoliths and the cell wall was a close match to the reported gravitropic responses in previous literature. This suggests a relationship between the strength of gravitropic output and the number of statoliths touching the lower side of the cell, but the relationship is unlikely to be linear. Before Audus it had been suggested that statoliths did not normally sink directly to the lowest point in the cell, rather that they have a tendency to clump together and move along the cell wall, and there is evidence that statolith movement is affected by interactions with the cell's cytoskeleton which would not have an equivalent in Audus's model (Palmieri and Kiss, 2005).

There are a number of factors which may alter the behaviour of statoliths within the cell. The movement and position of statoliths will depend on both the statoliths interactions with other parts of the cell, and with each other. It has been shown that the movement of statoliths in cells does not depend entirely on the effects of gravity, but that statoliths movements are actively affected by vacuoles within the cell and the cell's cytoskeleton(Moulia and Fournier, 2009; Palmieri and Kiss, 2005).

In Arabidopsis, statoliths show saltatory movement (consisting of short abrupt jumps), which ceases when the cytoskeleton is disrupted using latrunculin B (Palmieri

and Kiss, 2005; Saito et al., 2005) which implies that the statoliths are being actively propelled around the cell. It is also possible that saltatory movements are due to statoliths becoming ensnared by the cytoskeleton and releasing stored potential energy as they escape. Disruption of the cytoskeleton also reduces statolith movement in general, though it is not known whether this is due to the same mechanism. It has also been found that treatment of *Arabidopsis* hypocotyls with latrunculin B causes increased gravitropic curvature (Palmieri and Kiss, 2005). It has been suggested that the increase in curvature is due to increased contact time between statoliths and vacuoles in the cell which may be necessary for signal transduction (Saito et al., 2005). The idea that statolith-vacuole interactions are involved in gravitropism is supported by the finding that mutations causing abnormal vacuole formation inhibit gravitropic response (Morita et al., 2002).

1.3   Root behaviour

1.3.1   Gravitropic behaviour and the Sine Law

In his 1882 work "Uber orthotrope und plagiotrope Pflanzenteile" (Sachs, 1882), Julius von Sachs hypothesised that the gravitropic response of a root or shoot should be determined by the component of gravity at a right angle to the long axis of the organ. This idea, also known as the Sine Law for gravitropism, predicts that when an organ is displaced the magnitude of response is proportional to the sine of the angle of rotation (Dumais, 2013) and has since become a commonly used model of gravitropism.

The Sine Law was formally described as "the intensity of the gravitropic change in tip angle for a given stimulation time t_s and a given gravity g is proportional to the sine of the stimulation angle of the plant relative to the direction of the gravitational field vector" (Moulia and Fournier, 2009).

As the response is determined by the component of gravity acting across the organ, the rotation is measured from the vertical, so an organ displaced hori-

zontally would show the greatest response. When discussing the Sine Law, the response of an organ is defined by the rate of gravitropic curvature, or the rate at which the angle of the displaced organ returns to its initial angle. This leads to equation (1.3), where θ is the orientation of the organ relative to gravity, and t is time. c represents a rate coefficient subject to the following constraints: in positively gravitropic organs (those that bend downwards) $c < 0$, while in negatively gravitropic organs (which bend upwards) $c > 0$.

$$\frac{\delta \theta}{\delta t} = c \sin \theta \tag{1.3}$$

The Sine Law describes the relationship between a given a stimulation angle and response. As an organ responds to a given rotation this in turn changes the angle. In order to measure only the initial rotation, and so a known stimulus, the Sine Law was proposed for cases where the stimulation time equals the reaction time of the organ (the time at which the organ starts to reorientate) (Moulia and Fournier, 2009). When longer stimulation is applied the response does not always fit a straight Sine Law, with some evidence that for many plants the maximum gravitropic response occurs when the plant is reorientated by approximately 120° (Audus, 1964; Larsen, 1969), not 90° as would be predicted. Empirical modifications to the Sine Law have been described which attempt to capture the behaviour at angles above 90°. Some examples of these modified Sine Laws include the addition of offsets in the detected angle as shown in Eq. 1.4 (Mullen et al., 2000), and the introduction of cosine terms such as in Eq. 1.5 (Metzner, 1929) and Eq. 1.6 (Larsen, 1969). In these instances k, k_1, and k_2, represent various tuning parameters which can be adjusted to fit the observed response.

$$\frac{\delta \theta}{\delta t} = c \sin (\theta + k_1) + k_2 \tag{1.4}$$

$$\frac{\delta \theta}{\delta t} = c \sin \theta (1 - k \cos \theta) \tag{1.5}$$

$$\frac{\delta\theta}{\delta t} = \frac{c\sin\theta}{\sqrt{k^2 + 2k\cos\theta + 1}} \tag{1.6}$$

Due to the continuous change in angle over time, it is difficult to determine whether a change in response is due to the change in angle or the time since reorientation. However by using the ROTATO system (a feedback system able to constrain root tip angles for long time periods) it has been shown that the response does not appear to be time-dependent, and that an organ actively maintained at an angle away from its normal growth angle will continue to respond consistently to its displacement long after it would otherwise have stopped bending (Mullen et al., 2000). Mullen *et al.* fit the observed response to the modified Sine Law given in Eq. 1.4, where $y \propto \sin(\theta - 14.7)$, this gives a maximum response of approximately 105°, which lies between that predicted by the Sine Law and that observed by others (Audus, 1964; Larsen, 1969). It should be noted however that this modification to the Sine Law is purely empirical and, while it is able to fit the data, it departs from the fundamental assumption of the model, that response is proportional to gravity acting across the organ.

As the Sine Law only describes tip angle when applied to the root, it does not predict the final shape of the plant. Indeed in the case of soft roots being driven by growth occurring behind the tip the mechanics are complicated and there is no guarantee that the path of the root will follow that of the tip. However the Sine Law would suggest that a root whose tip has been displaced and maintained at a nearly vertical angle would form a gentle curve, compared to one which has the tip maintained at a near horizontal angle which would be tightly curved.

It is worth noting that while the Sine Law is intuitive, a simple model of the movement of sedimentary particles in a box would not obviously give a Sine Law. If the number of statoliths is large, and they are able to move around the cell freely in response to gravity, the statoliths can be modelled as a liquid collecting at bottom of the cell. Assuming the cell is rectangular, the number of statoliths in contact with the lower edge of the cell approximates to equation (1.10). Where V is equal to the volume of statoliths, θ is the orientation of the cell, and θ_{max} is the angle at which the entire cell face is in contact with statoliths.
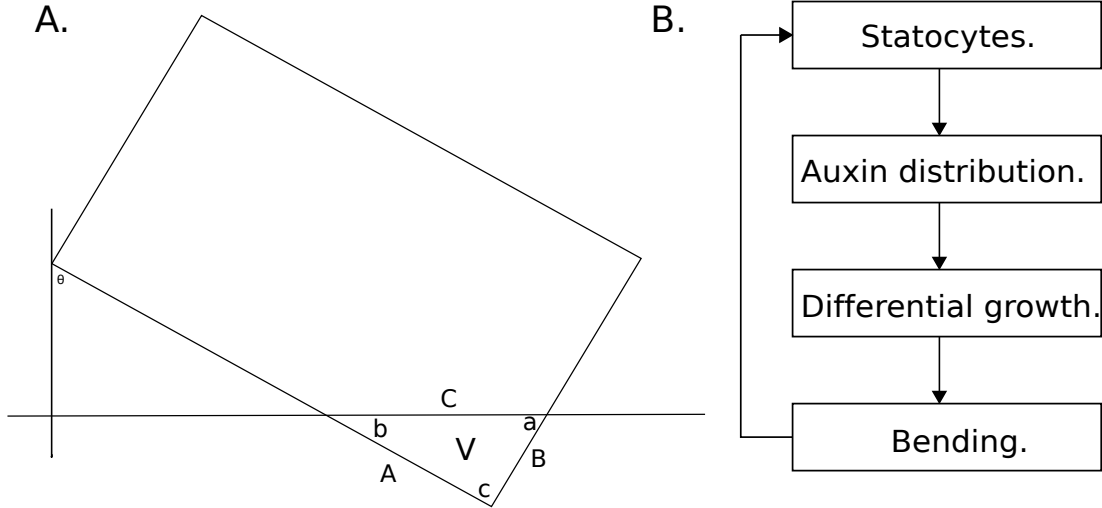
Figure 1.3: A. Position of liquid model statolith in a rotated cell. B. The feedback loop between gravity detection in statocytes and response to gravity.

Given a cell rotated from the vertical by an angle θ and a volume of statoliths V, the statoliths form a right-triangle as shown in Figure (1.3). The volume V is given by equation (1.7). Given that we are assuming a rectangular cell, and the statoliths form a right-triangle, we know $a = \theta$, and so can multiply equation (1.7) by $\tan\theta$ (1.8). This gives A^2 in terms of V and θ as shown in equation (1.9). Taking the square root of equation (1.9) gives the length of the covered side A, and dividing by the length of the cell wall gives the predicted fractional activation, A_frac of the gravitropic response in equation(1.10).

$$2V = AB, \tag{1.7}$$

$$\tan\theta = \frac{A}{B} \tag{1.8}$$

$$A^2 = 2V\tan\theta \tag{1.9}$$

$$A_{frac} = \frac{\sqrt{2V \tan \theta}}{\sqrt{2V \tan \theta_{max}}} \qquad (1.10)$$

While the Sine Law is a commonly used model of gravitropic behaviour it is not a complete description of behaviour. For example Bastien *el al* (Bastien et al., 2013) suggest that the Sine Law alone cannot explain gravitropic behaviour in shoots, and that some proprioceptive component is necessary to achieve a stable orientation. Due to the shape of shoots a curvature near the base of a shoot will affect the orientation of the shoot further away from the base. Unlike in roots, gravitropic growth in shoots occurs along the length of the organ. The Sine Law would predict that the stem of a rotated plant would repeatedly overshoot the vertical as the base would still be responding to a change in the direction of gravity as the tip was approaching vertical. The minimal model to account for this requires a balance between gravitropic curvature and basipetal straightening. A large number of plant shapes seen among different plants can be modelled by using a *bending number, B* which represents the ratio of these two responses. Unlike the Sine Law alone the addition of a proprioceptive term allows the equilibrium shape of the organ to be defined, providing at least one tropism is distributed and external forces are negligible.

Despite these questions the Sine Law remains a commonly used model in many situations (Galland, 2002).

1.3.2 Gravitropic set-point angle and the anti-gravitropic offset

In many plants the primary shoot and root will grow vertically upwards and downwards respectively, however many plant organs are maintained at a non-vertical angle (Roychoudhry and Kepinski, 2015). While it has been suggested that non-vertical growth is due to a lack of gravitropic ability it has now been shown that non-vertical orientation is actively maintained and that this is not simply due to a weak gravitropic response, as when reorientated both shoots and roots are able to

bend either upwards or downwards to return to their previous orientation (Digby and Firn, 1995; Mullen and Hangarter, 2003; Roychoudhry et al., 2013). It is important to note that in different species not all plant organs are gravitropic. Organs can be gravitropic only at specific stages of development (Sievers and Volkmann, 1977), and some organs do not display gravitropic behaviour at any point. Organs can also be orientated relative to gravity due to being attached to a gravitropic organ, but not be gravitropic themselves (Blancaflor and Masson, 2003).

Some early studies of gravitropism considered horizontal growth to be distinct from vertical growth, with horizontally growing organs being referred to as plagiotropic or diageotropic. However as a single organ can vary in angle throughout its lifetime, and in response to a number of factors, it has been concluded that these behaviours are the result of variation along a continuum of gravitropic response (Digby and Firn, 1995). The angle at which an organ is maintained was defined as the gravitropic set-point angle (or GSA), and is the point at which there is no gravitropic curvature. The GSA of an organ is given as an angle between 0° and 180°, with 0° being vertically downwards and 180° being vertically upwards (see Figure 1.4). As gravity sensing in the root is confined to the root tip the angle maintained is the tip angle (Figure 1.4, in shoots where gravity sensing and response occurs along the length of the organ the angle must be measured along the organ. The existence of a GSA was proposed by Digby and Firn who observed that the *Tradescantia fluminensis* shoot, over the course of its development, will maintain a range of angles between almost vertically upwards to almost vertically downwards; as shown in Figure 1.5. The power of this observation is in its descriptive value, the orientation of any organ can be described by its GSA allowing models to be produced which can describe a range of organ shapes using a single system of gravitropic growth.

Non-vertical GSA, such as is seen in lateral roots and shoots, can be explained by a gravitropic and an anti-gravitropic response (or offset) which act in opposing directions, these responses are balanced in a stable equilibrium when the organ is at its GSA. This anti-gravitropic force has been observed by subjecting Arabidopsis to clinorotation. In the absence of a constant gravitropic response the

A.

B.
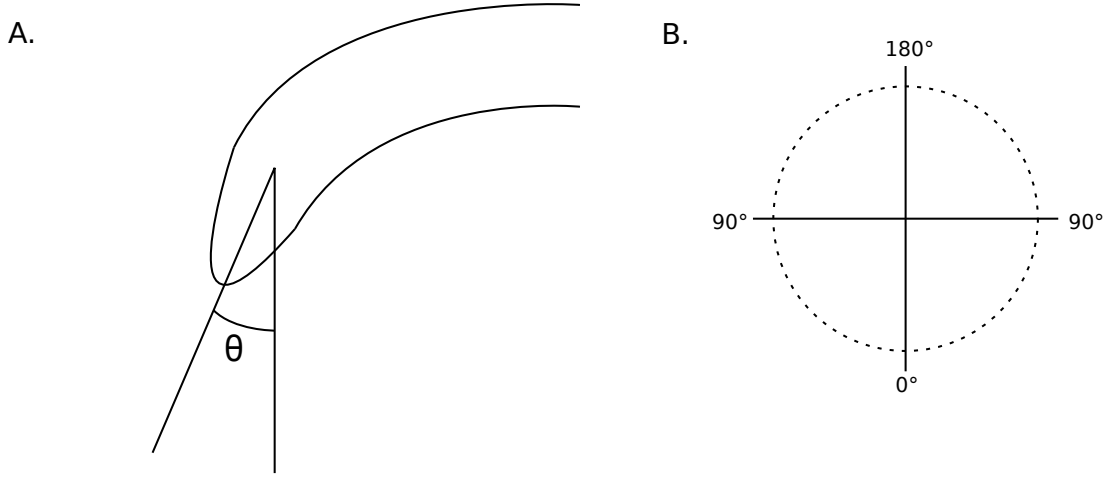
Figure 1.4: A. A reorientated root in the process of a gravitropic response, the effective angle of the root is given by θ. B. GSA is measured as 0° being vertically downwards, and 180° being vertically upwards.

lateral branches will bend back upon themselves, as the anti-gravitropic offset is no longer being balanced by a gravitropic response (Roychoudhry et al., 2013). The same effect is also seen in roots suggesting a common mechanism is shared by both roots and shoots.

A constant (or slow to react) anti-gravitropic offset combined with a gravitropic response which varies depending on orientation may be able to explain how an organ can be maintained at a non vertical angle, and also allows for similar behaviour observed in primary and lateral organs when reorientated. This would lead to a modified Sine Law for non-vertical GSA's shown in Eq.1.11, with an offset O. A vertically orientated primary root or shoot can be treated as a special case of an organ where the anti-gravitropic offset is equal to 0.

$$\frac{\delta\theta}{\delta t} = c\,\sin(\theta) + O \tag{1.11}$$
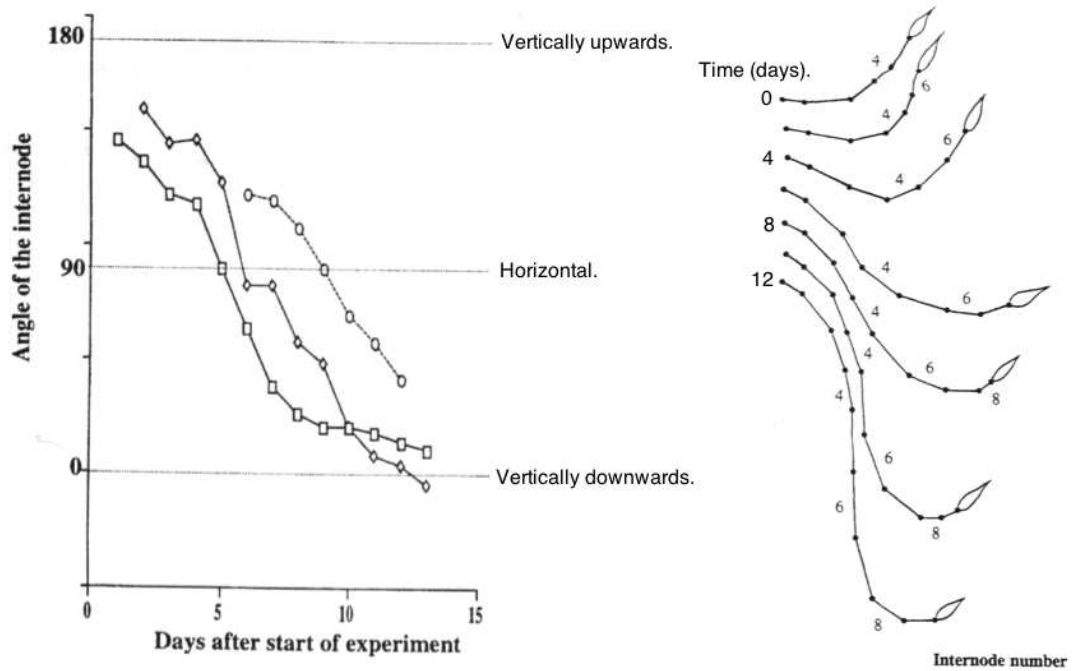
Figure 1.5: The GSA of *Tradescantia fluminensis* shoots at different stages of development. A shoot is shown at different times over 12 days, and points along the shoot are tracked. Points are numbered sequentially starting from the base, and new points are added as the shoot grows. The GSA of these points is shown over time, with □, ◇, and ◯ representing points 4, 6 and 8, respectively. This shows a smooth change in GSA over the time period measured. Figure adapted from Digby and Firn, 1995 (Digby and Firn, 1995).

1.3.3 Non-gravitropic behaviour

When at GSA, roots display a range of non-tropic behaviour. Most notable at the large scale are waving and skewing. When grown on a two dimensional surface Arabidopsis roots grow in a distinct sinusoidal pattern (Figure 1.6). The reasons for this are not fully understood but a number of processes are thought to be involved including circumnutation and gravitropism (Simmons et al., 1995). The role of gravity in root waving is still unclear however as plants grown in microgravity can display stronger waving phenotypes than under 1G (Paul et al., 2012; Roux, 2012). It is clear that root-gel interactions are important for skewing to occur. In a three dimensional environment Arabidopsis roots will grow in a corkscrew pattern, but when confined to a 2D surface, such as on agar plates, this corkscrew becomes flattened forming the waving pattern in Fig. 1.6. As the root digs further into the gel on one half of the corkscrew it is unable to move as freely across the surface. This produces a bias in the back and forth motion of the root tip which manifests as a skew in the direction of growth, as shown in Fig. 1.6. Physical interactions with the surrounding environment play an important role in the final shape of the root, as impedance of the root tip can cause buckling as it is forced into the growth media which has the effect of accentuating existing curvature (Thompson and Holbrook, 2004). This is supported by the observation that on inclined plates root skew is increased as the gravitropic response digs the root tip further into the media.

While not directly relevant to the work in this thesis, it is important to remember that these processes are continuing through the course of any gravitropic response. Unlike behaviours such as phototropism we cannot remove this background response of the plant (as much as we would like to), nor it's mechanical interactions with the environment. As such any behaviour observed under gravistimulation will be a combination of gravitropic and other behaviours.
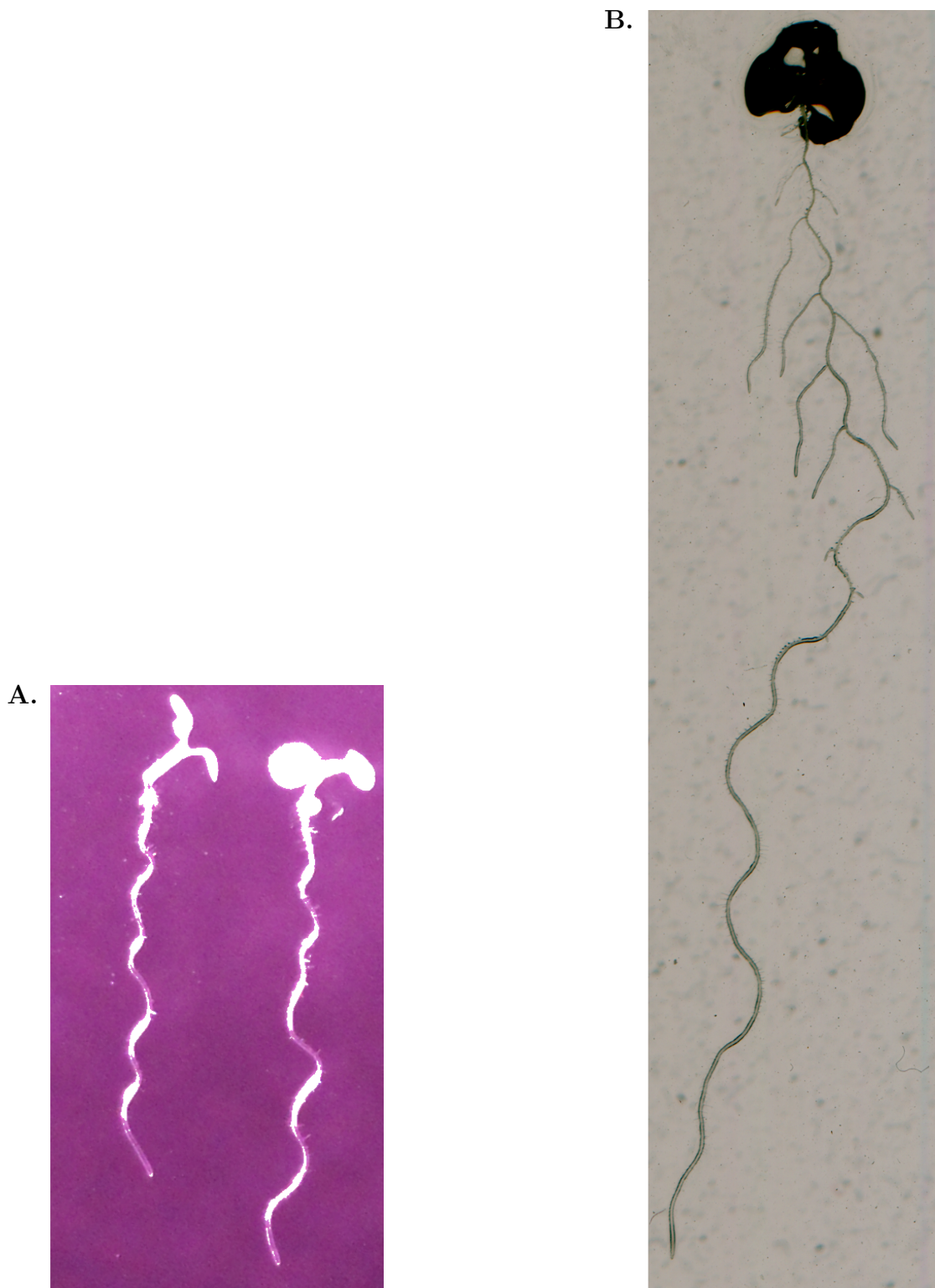
Figure 1.6: **A.** 5 day old Arabidopsis seedlings at GSA (imaged under near infrared light). Note the sinusoidal waving of the roots, neither root tip it as the GSA. **B.** An older root displays skewing behaviour caused by root-gel interactions.

1.4 Context and project aims

To date recent models of root gravitropism have tended to focus largely on individual mechanisms involved in the gravitropic response, such as the role of influx/efflux proteins in determining the flow of auxin across the root (Band et al., 2014). While bottom-up models of gravitropism have had considerable success describing physiological features of a gravitropically stimulated root, they have not yet been able to predict the response at a behavioural level. At the behavioural level gravitropic behaviour is still largely described by the Sine Law and it's variants (see section 1.3.1). However while the Sine Law performs well at low angles modifications are needed in order to accurately describe high angle responses (where the root is above the horizontal). These models can produce reasonable descriptions of gravitropic behaviour but they lack explanatory power, as does the unmodified Sine Law. Alternative models such as the tipping point model described previously (section 1.2.3) are unable to explain behaviour at low angles. Many behavioural questions remain unanswered by current models such as the time-scales of the response, the presence or lack of hysteresis (the effect of a roots history on its future behaviour) at the behavioural level, and the precise nature of the angle-dependent response.

In this project we aimed to create a behavioural model of gravitropic response that can accurately describe gravitropic behaviour over a wide range of angles, from vertically downwards to above the horizontal, as well as to determine what factors determine this behaviour and under what conditions it occurs. Additionally we aim to provide a link between behaviour and the mechanisms involved in a response allowing us to limit the range of possible mechanisms.

Chapter 2

Materials and Methods

2.0.1 Seed sterilisation

Arabidopsis seeds were sterilised using chlorine gas. Open 1.5 ml Eppendorf tubes containing the seeds were left in a bath of chlorine gas for 3 hours, the seeds were then allowed to ventilate for 1 hour. Chlorine gas was produced by mixing 3 ml of hydrochloric acid and 100 ml of bleach containing sodium hypochlorate.

2.0.2 Plant growth media

Arabidopsis plants were grown on sterile Arabidopsis salts (ATS) growth media, the composition of which is given in Table 2.1.

2.0.3 Kinetics experiments and analysis

Arabidopsis seeds were vernalised at $5°C$ in the dark for 2 days, Plants were grown on ATS for 5 days in controlled conditions at $20°C$ with a light/dark cycle of 16 hours light and 8 hours dark.

In order to remove phototropism as a confounding effect on response, all plants

Ingredient	Concentration
KNO_3	5 mM
KPO_4	2.5 mM
$MgSO_4$	2 mM
$Ca(NO_3)_2$	2 mM
$Fe - EDTA$	50 μM
H_2BO_3	70 nM
$MnCl_2$	14 mM
$CuSO_4$	0.5 mM
$ZnSO_4$	1 mM
Na_2MoO_4	0.02 mM
$NaCl$	10 mM
$CaCl$	0.01 mM
Sucrose	1%
Plant agar	0.8%

Table 2.1: ATS constituents.

were imaged under near infra-red light (840 mn wavelength). All plants were given a 1 hour acclimatisation period under NIR lighting before reorientation. Plates were then manually reoriented so that the root tips were at the desired angle and images were taken by a modified Canon camera with the IR filter removed. Imaging was performed at 1 minute intervals for at least 6 hours. Manual measurement of the root-tip angle was done on images at 10 minute intervals using ImageJ Schneider et al. (2012).

For kinetics experiments plants were grown in either 92 mm x 16 mm round petri dishes, or 120 mm x 17 mm square dishes. Plants were placed roughly 5 mm-10 mm apart resulting in around 20-30 plants per plate.

We exclusively used the Col-0 ecotype, with seeds obtained from Katelyn Sageman-Furnas.

2.0.4 ROTATO experiments

In order to be consistent with the kinetics experiments all seeds were seeds were vernalised at $5°C$ in the dark for 2 days, Plants were grown on ATS for 5 days

in controlled conditions at $20°C$ with a light/dark cycle of 16 hours light and 8 hours dark. Imaging was done under near infra-red light (840 mn wavelength) using a dinolite microscope with plants imaged every minute (see chapter 3 for details).

On ROTATO smaller 60 mm plates were used to reduce the weight on the stage. A single plant was used per plate as it is not possible to constrain multiple plants simultaneously.

We exclusively used the Col-0 ecotype, with seeds obtained from Katelyn Sageman-Furnas.

Chapter 3

Development of a ROTATO system

3.1 Introduction

When modelling any system it is important to properly understand which factors determine the response of the system, under what conditions a given response occurs, and over what timescales. In the case of root gravitropism there are a number of factors which may affect the behaviour of the root. Perhaps the most obvious of these is the root-tip angle. Sine-law dictates that response is proportional to $\sin\theta$ based on the idea that the response depends only upon the magnitude of the gravitational force acting across the organ at the time of response. However this is not the only possible mechanism which may produce similar behaviour. It seems likely that at small enough time scales the necessity of transmitting a signal from the columella to the elongation zone will add a temporal component to the response. Over short times one may expect the root's recent history to be the determining factor of response due to the delay between angle detection, signal transmission, and response. The ROTATO system uses a feedback mechanism to maintain root tip angles over long time periods, while this has previously been used to show that gravitropic responses can be consistently

maintained(Mullen et al., 2000), this has only been tested over a limited range of angles and timescales. Even within the limits imposed by Sine Law there are time-dependent mechanisms which could produce such behaviour. Consider the case of a pendulum where the instantaneous force acting on the bob produces a sinusoidal velocity over time. It is conceivable that a similar mechanism could produce time-dependent Sine Law like behaviour given an initial reorientation.

Traditional reorientation experiments where a root is given some initial stimulus and allowed to respond struggle to separate the effects of changing angle and time since reorientation, given only an initial reorientation it is also impossible to fully control the angular history of a root throughout an experiment. In essence it is hard to distinguish between differences in response over time and difference due to the change in angle throughout the course of the reorientation.

The ROTATO system is based on the design used in Mullen *et al.*, where a single plant is placed on a computer controlled rotating stage. A plant is placed so that the root tip is at the centre of rotation of the stage with a camera positioned to observe the tip (see Fig 3.1). Using computer vision software the tip angle is measured periodically (normally once per minute) and the stage is rotated to bring the tip to the desired angle. The measured angle of the root tip and the rotation of the stage are logged allowing the response to the measured over the experiment. The system was developed in order to allow increased control over root-tip angle over time by constant measurement and adjustment of the tip angle (Mullen et al., 2000). In theory this allows for the angle to be fully controlled over long time periods while the response is measured simultaneously. This high level of control over root-tip angle allows the contributions of angle and time to be determined independently by, for example, constraining a root at a given angle and observing the rate of response while the angle remains unchanged.

While the system is designed primarily to constrain roots the adjustment step can be individually controlled allowing either high resolution traditional reorientation experiments, or periods of constrained and free response.

As we were unable to replicate previously published results, nor were our results consistent with those presented elsewhere in this document, we did not continue
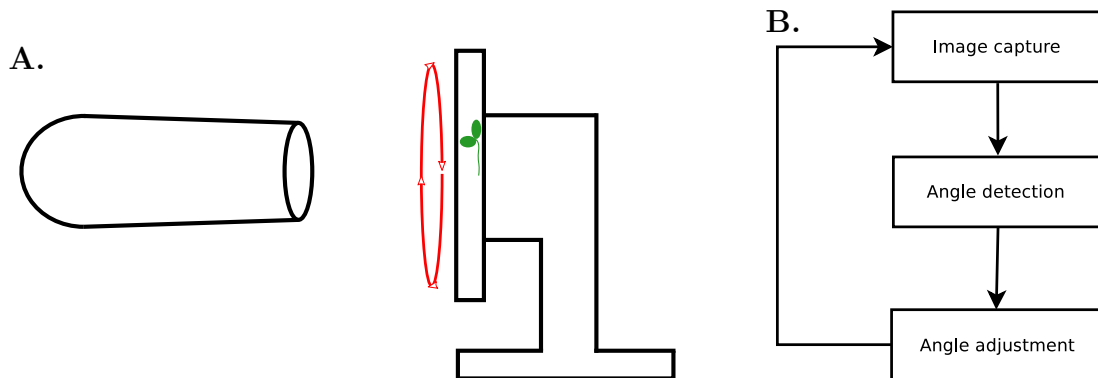
Figure 3.1: **A.** A simple schematic of the ROTATO system. A plant is placed on a rotating stage with a camera positioned to image the root tip. **B.** The ROTATO feedback loop. The root is imaged and the tip-angle is detected, the plant is then rotated to maintain the desired tip-angle.

working with the ROTATO system after the initial testing and experimentation was complete. However as this is likely due to limitations of the hardware used it is our hope that the system design may prove useful to others attempting to create a similar system.

3.2 Hardware

3.2.1 Camera

When choosing a camera for the ROTATO system there are a number of considerations. It is important to have a sufficient resolution and field of view (FOV) to accurately measure the root-tip angle while ensuring that the tip does not move out of the FOV during the course of the experiment. While the tip is initially placed at the centre of rotation for the plate, ensuring there is no translation as the stage is rotated, the placement is by necessity inexact. Under the sort of magnifications necessary to accurately determine the tip angle, even small deviations from the centre of rotation can lead to large movements of the tip in the image. Compounding this is the growth of the root. Even an initially perfectly

centred root-tip will move away from the centre as it grows, and once off the centre of rotation can quickly move out of the field of view. The lighting conditions to image under are also important considerations. As the ROTATO system is designed to measure purely gravitropic response it is important to minimise the effects of other behaviours, including phototropism. Visible light cameras are easier to obtain, with a wide variety of readily available lighting set-ups, however any visible light in the system may induce a phototropic response in the root.

If we assume the computer vision is perfect we will be able to draw a straight line from the end of the root to the back of the columella. Assuming this line joins two pixels in the image we can calculate the angular resolution from the length of the line. Given a tip at pixel position $(0, 0)$ the second point must exist on the circle with radius L pixels around the point $(0, 0)$. If we can resolve to 1 pixels length along this circle then given that in radians the length of an arc is given by $s = r \cdot \theta$; the minimum resolvable angle is equal to $\frac{1}{L}$. Converting into degrees gives us Equation 3.1, values for a reasonable range of columella lengths are given in table 3.1. While this calculation does not take into account discretisation of length along different directions (a move along the diagonal of a pixelated circle will give a different resolution to a change along the flat) or the effects of techniques designed to overcome the pixelisation of the image, this does give us an indication of the scale required for accurate measurements. To be accurate to within $1°$ we will need a resolution sufficient to give a columella length of at least 60 pixels, without taking into account inaccuracy due to the computer vision. This must be done while also maintaining sufficient FOV to ensure the root does not leave the visible area of the plate over the course of an experiment.

$$\theta_{resolution} \approx \frac{1}{L} \cdot \frac{360}{2 \cdot \pi} = \frac{180}{\pi \cdot L} \tag{3.1}$$

When choosing conditions to image under there is a trade-off between the clarity of image and the phototropic response induced in the root by the lighting. The original ROTATO system used a back-lighting system where the plant is placed between a light source and the camera. The advantage of this method are a high

L (pixels)	Resolution (°)
10	5.73
20	2.86
30	1.91
40	1.43
50	1.15
60	0.95
70	0.82
80	0.72
90	0.64
100	0.57
110	0.52
120	0.48
130	0.44
140	0.41

Table 3.1: Approximate limits of angular resolution given length of columella in pixels.

contrast between the root and the image background. As the light is directional but perpendicular to the plane of gravitropic response there should not be any direct interference between phototropic and gravitropic response, additionally any phototropic response will be perpendicular to the imaging plane and so should not produce a change in measured angle from the point of view of the camera. An alternative to back lighting is front lighting. Like back lighting the direction of illumination is perpendicular to the plane of response. Unlike back lighting, front lighting places the illuminates the sample from the direction of the camera. The advantage of this is that the physical set-up takes up significantly less spaces and it is easier to produce an even illumination without specialist equipment. This comes at the cost of some image contrast. However both the above methods assume a separation between gravitropic and phototropic responses which may not be valid. As both phototropism and gravitropism work to produce an auxin gradient across the affected tissue (Pandey and Chaudhary, 2016) it is unlikely that the two responses can be treated independently even when working across different axis.

One solution to this is to image under infra-red light which has been shown not

to induce a phototropic response (Iino and Carr, 1981). This does present some practical problems as infra-red cameras of the type needed for the ROTATO system are expensive, as are lighting systems. While it appears that infra-red light does not produce phototropic responses there is some evidence to suggest that in Oats IR lighting can effect growth angles (Johnson et al., 1996), so even here care should be taken to minimise exposure.

We have used a Dino Lite AM7013M-FIT for the following reasons. The camera has high enough resolution to allow accurate angle detection and while maintaining sufficient field of view to maintain tracking for decent lengths of time. The camera works in the near infra-red range (940 nm wavelength) allowing imaging in similar conditions to our reorientation experiments and minimising the effects of phototropism. In order to minimise the potential for phototropic effects even from infra-red lighting, front lighting is used which does not require as high an illumination as back lighting. Using lower levels of illumination also allows for better control over temperature and makes the system more compact and easier to use. While there are technically superior cameras in terms of resolution, focal distance, or magnification, the Dino Lite is a good compromise between between technical specifications and affordability. It is also compact enough to be easy to use in a small environment and the technical limits are offset by the fact that only a single root can be maintained on a plate at a time limiting the needed resolution and FOV.

3.2.2 Stage

The ROTATO system needs to be able to accurately rotate the sample by a given amount over a potentially unlimited number of rotations. We used a Agilis AG-PR100 rotation stage from the Newport Corporation which is capable of adjustments as small as 0.001° with no maximum rotation amount.

A diagram of the physical system is shown in Fig. 3.2
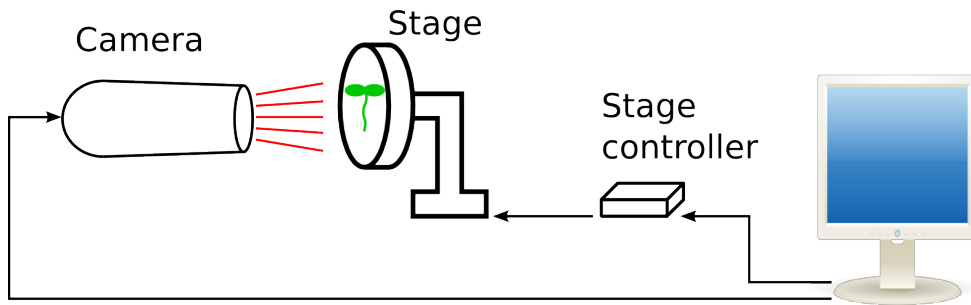
Figure 3.2: The ROTATO hardware consists of an infra-red camera and a rotation stage controlled by a computer, the rotation stage is connected via an intermediate controller.

3.3 Software

3.3.1 System design

The core of the ROTATO system is the measure-adjust cycle. Conceptually there are 3 main components to the software. First is the hardware control which provides an interface for the physical control of the equipment, and provides feedback on actions carried out. It also provides simple image acquisition controls allowing different cameras to be used if necessary. Second is the image analysis software. This is the most complex part of the software, and provides an easy interface for the extraction of root features from raw images. This part of the software consists of an analyser object which is capable of operating fully independently of the rest of the ROTATO system (see Chapter 5). Lastly is the control system. This runs a ROTATO experiment, it provides an interface allowing experimental parameters to be set, manages data acquisition, analysis, and storage, and maintains the central control loop. The design of the central control system interacts minimally with the hardware and the image analysis system, and exclusively through the public methods provided by those components. This should allow alternative hardware or image analysis methods to be simply swapped in if desired.

The ROTATO software is designed to be easy to set up and run. The system is controlled by a "MATATOobject" class (see section 3.3.2). The class controls all the stages of an experiment, including managing and storing the data collected.

To use the software first ensure the sample is correctly mounted to the stage and the camera is in focus, with a clear view of the root tip. Once the physical set-up is complete a "MATATOobject" class must be instantiated, then call the "setup" method which allows the user to enter the experimental conditions. Lastly the "stepMATATO" method must be called within a loop. To allow for parallelisation waiting is not performed in step so a delay should be included in the loop. An example script is given in appendix A, and an outline of the experimental process is given in Figure 3.3.

The software is written exclusively in MATLAB due to its ease of use, large library of inbuilt functions, good hardware interface support, and cross platform support. An early prototype was written using Python and OpenCV but this was not continued due to the time needed to recreate features already available in MATLAB. For an example script running a ROTATO system see appendix A.

3.3.2 Control system

The control system consists of a single "MATATOobject" class (MATATO being shorthand for MATLAB ROTATO). The details of the "MATATOobject" will not be covered in full here but an outline of the object is as follows. The object itself has two methods which are necessary to run a ROTATO experiment and are defined below. The first of these is the constructor. The constructor takes experimental parameters (outlined below), a camera type, and a connection object. As the Agilis stage controller takes a serial connection it is necessary to create a single connection which can be shared between instances rather than creating a separate connection for each instance. The second method is the "stepMATATO" method which completes a single step of the measure-adjust cycle and returns the time taken by the step. As pausing in MATLAB completely blocks execution it is not possible to include the wait in the step and maintain the option for concurrent experiments. Instead timing must be performed outside the MATATO object.

1. **MATATOobject = constructor(jitter, constrain, lateral, camType, stageID[optional], camID[optional], connection[optional]):** "jitter" and "constrain" are boolean experimental type parameters. Jitter causes the root to be periodically moved around a central point. Typically this is done by +1,-1 degrees at each step. This can be used to test whether the act of moving a root causes a difference in behaviour. If the constrain flag is on the root will be constrained at the initial angle specified during set-up, otherwise the root will be allowed to respond without interference. CamType is a string containing one of various different camera and lighting types used during testing. It determines which of a number of preset image
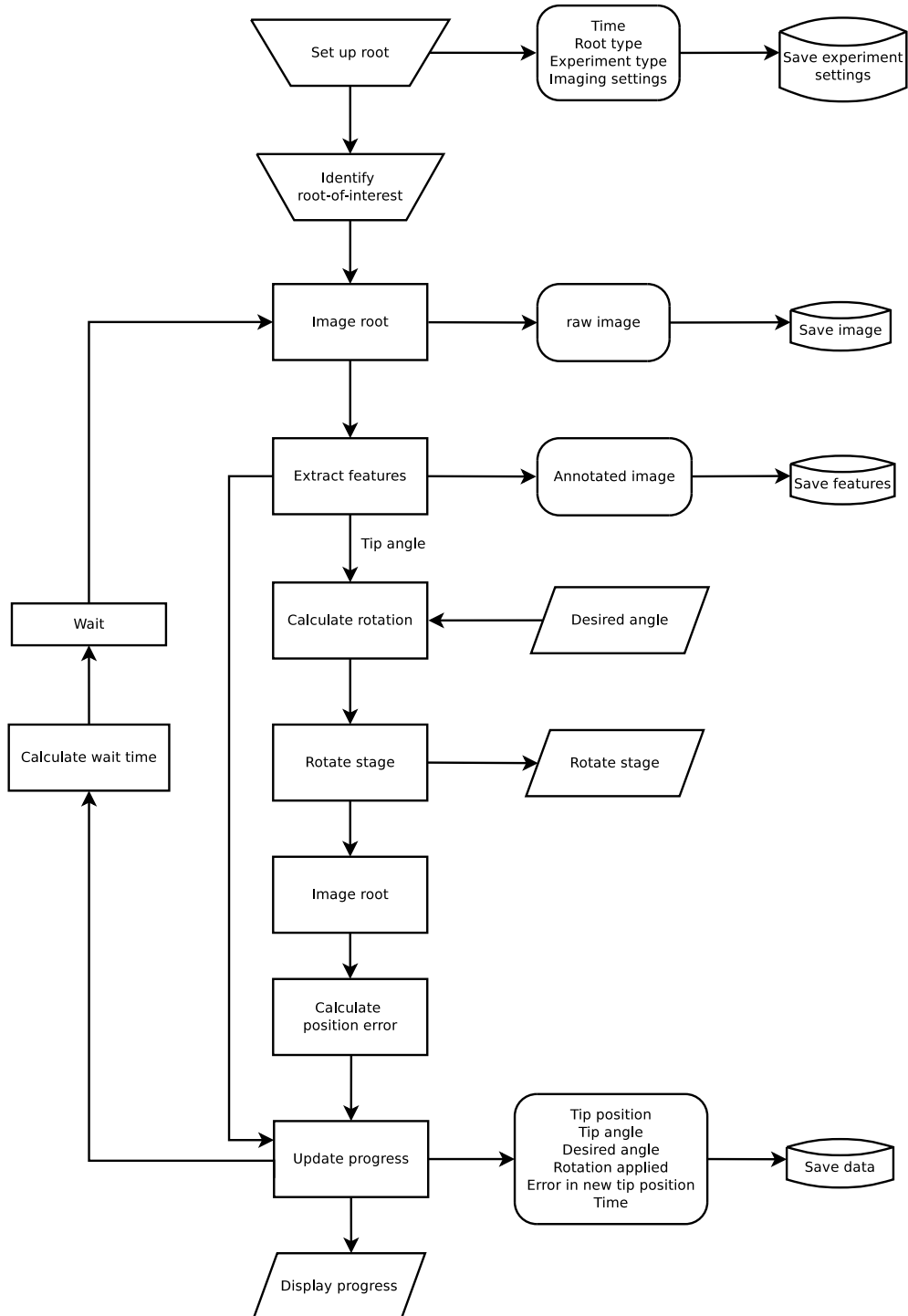
Figure 3.3: An overview of the ROTATO software. The central loop performs the analyse-adjust cycle while raw and processed data is saved to disk. Experimental conditions and settings can be changed in the initial set-up stage. Progress is displayed during the experiment to allow manual adjustments to image conditions and error correction.

analysis parameters will be used. Both "stageID" and "camID" are the ID's of the camera and stage to be used if more than one of each is detected. Connection is an optional argument containing a serial port connection. This connection will be used to interact with the stage.

2. **timeTaken = stepMATATO()**: This performs a single step of the measure-adjust cycle and updates the internal state of the MATATOobject instance. It also saves the updated state and the raw images to disk. The return value "timeTaken" is the time taken by the step (in seconds).

The "MATATOobject" provides a "setup" method which prompts the user for experimental conditions and allows the user to perform initial quality tests before the experiment commences. When run the "setup" method will take the user through the following steps:

1. A live video of the camera feed is displayed. This gives the user a chance to ensure that the root of interest is squarely in the field of view, in focus, and that the lighting conditions are good.

2. When prompted by the user a snapshot is taken and an annotated image is taken. This displays the boundary, centre-line, and tip position of the root as determined by the analysis software (see Fig. 3.16 for an example image). The tip angle is displayed for verification. If this does not appear correct the user can adjust the camera and restart the process.

3. If the analysis appears correct the user will be prompted to enter any notes on the experiment. This could include anything unusual or noteworthy that may not be stored in the standard condition fields.

4. The user is next prompted for an angle to constrain at. The root is then rotated to the given angle, based off the initial angle detected in step 2. If the constrain flag has been previously set to 1 the root will be constrained at this angle, otherwise it will be allowed to reorient freely.

5. A second snapshot is taken and the angle detected is provided. This gives the user a final chance to check that the set-up is correct and the stage is

correctly calibrated. This also gives the user an indication of the drift in tip position caused by imperfectly centred tip position. Folders are created to store the images and the user is prompted to start. If the user accepts the prompt the set-up is complete.

A measure-adjust step is at the heart of the ROTATO system. The "step-MATATO" method is designed to encapsulate the entire measurement, analysis, adjust, process in one package. At each step the method saves both the raw image data and an annotated copy of the data for easy visualisation, allowing manual verification or reanalysis at a later time. The internal state of the MATATOobject is updated with the analysed data and a visualisation of the experiments progress is provided. A "stepMATATO" call has the following stages:

1. A snapshot of the root is taken.

2. The raw image is saved to disk.

3. The image is analysed and key features are identified. This includes the tip angle and position, as well as an annotated image identifying the roots outline, midline, and tip position.

4. The annotated image is saved to disk.

5. The necessary rotation is calculated. Maximum and minimum bounds are set for the rotation, both to reduce unnecessary adjustments due to noise and to prevent erroneous readings from incorrect analysis.

6. The stage is rotated, and the actual rotation as returned by the stage is stored.

7. The root is imaged a second time with the root at the new position.

8. The image is analysed and the error between the new angle and the expected angle is recorded.

9. The object is updated with the data for this step.

10. An updated summary of the experiments progress is displayed.

11. The time since the step began is recorded and returned. The step ends.

3.3.3 Computer vision

The image analysis software is designed to extract and analyse root features from individual images of an Arabidopsis root. While designed for the ROTATO system the analysis software is flexible enough to cope with other imaging set-ups providing the image quality is good and the area surrounding the samples is clear of obstructions.

Challenges

Extracting features accurately and robustly is vital for the ROTATO system. Key to this is good image quality with a clearly defined root and a consistent background. While care has been taken to ensure good image quality there are still a number of challenges to accurate feature detection. In a clear image, as shown in Figure 3.6, the root is sharply contrasting with an either constant or nearly constant background. There are no other objects in the image, and the root has a strong water meniscus all the way to the tip giving it a well defined outline and a consistent shape. This is not the case in all instances, Figure 3.4 shows an example of a low contrast root which is most likely lacking a water meniscus. Other problems can be caused by foreign objects or features in the image, this includes imperfections in the agar surface (bubbles, indentations, etc), dirt or grit on the plates lid, or marks on the backing material that forms the background of the image. If such features occur in the image the software must be able to distinguish them from the desired root. In some cases such as small specular features this is easily possible, in other cases such as with impressions in the agar this is very difficult to achieve simply be looking at the properties of the feature. Figure 3.5 shows an example of an indentation left in the gel by the root. In this case the root was poorly aligned with the centre of the plate and was re-centred, leaving an impression of the same size and shape as itself.
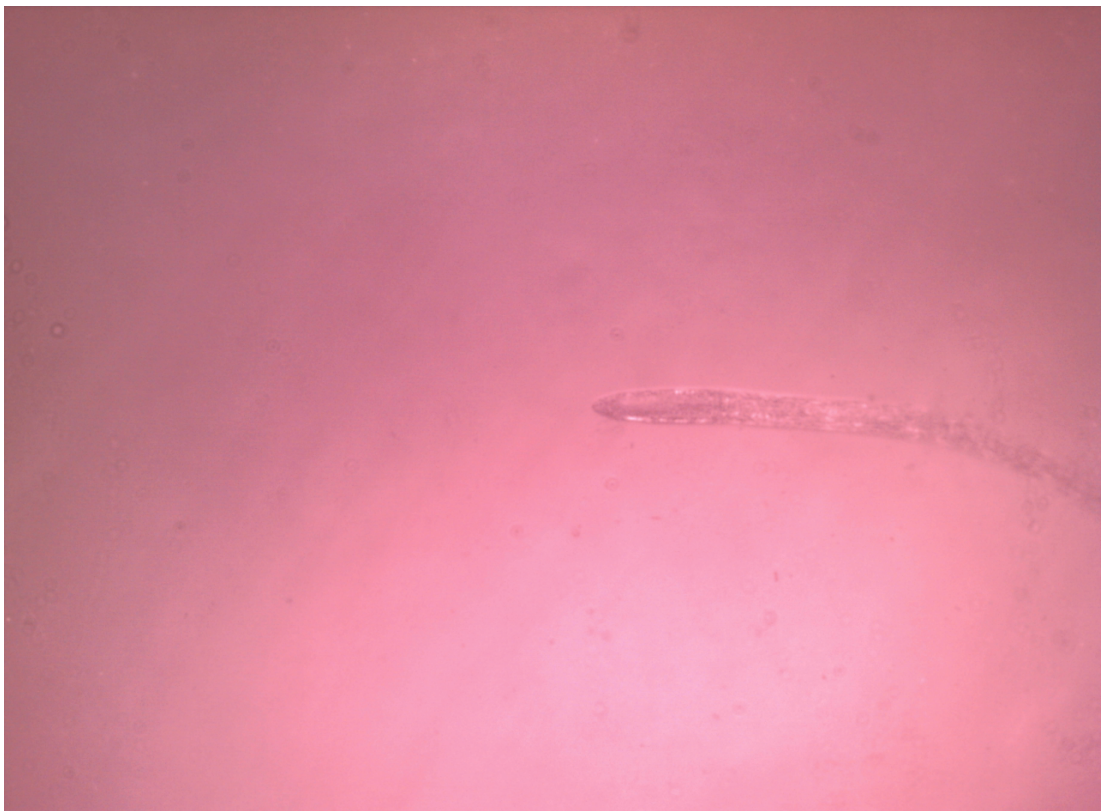
Figure 3.4: An example of a low contrast root lacking a water meniscus. It is possible the root has grown into the agar.

Figure 3.5: An example of a foreign feature in the image. In this case the root was poorly aligned with the centre of the plate and was re-centred, leaving an impression of the same size and shape as itself. Features such as this are very difficult to separate from actual roots based on properties such as size, shape, or colour.

Figure 3.6: An example ROTATO image with a dark root on light background. Under these lighting conditions the root is transparent with only the edge clearly defined. Specular reflection makes the edges inconsistent.

The analysis pipeline

Figure 3.6 shows an example root image. The following section will go through the analysis process step-by-step until the initial feature detection stage is complete.

Traditionally many image processing operations assume a light object on a dark background, examples of this include many morphological operations such as dilation and erosion, as well as common thresholding methods. Under our lighting conditions we have a dark root on a light background, the first step of the processing is to complement the image. This results in the image seen in Figure 3.7.

The next stage of the pipeline is to convert the image to greyscale. The images are natively stored in RGB, the obvious greyscaling methods are to either take a

Figure 3.7: A reversed image with a light root on a dark background. Many of the features of the raw image are still present, such as transparency and inconsistent colouration.

Figure 3.8: The complemented image transformed to greyscale by taking the green channel.

single channel or average across the channels. In general the green channel was clearer than either the red or blue channels, with a reasonable amount of contrast around the root and a consistent background (see Figure 3.8). Taking the mean pixel intensity across channels gave reasonable results but not as good as the green channel alone. The result of greyscaling in our example image is shown in Figure 3.8.

While taking the green channel produces a relatively uniform background, there is still a noticeable change in intensity where the lighting is centred, whereas ideally we want a distinct root on a uniform background. We equalise the background by taking the difference between each pixel intensity and the mean intensity of its surrounding area. This keeps "small" features such as the root while removing gradual gradients such as that produced by an uneven background, conceptually

this is similar to a high pass filter. A clear example of this can be seen by comparing Figure 3.8 from before the filtering with Figure 3.9 showing the same image after filtering (and scaled for legibility). Notice how the dark patch in the centre of the image has been removed but the root remains clear. This background subtraction step also has the convenient effect of setting the background intensity to approximately 0, note that due to the image subtraction our image intensities are now in range the -255 to 255. Averaging is done by performing convolution with a uniform circular kernel, while the size of the kernel can be set in the software a default value of 71 pixels is used (approximately one root width of a typical primary root).

As we are looking for a light root on a dark background, and we have effectively set the background colour to 0, we can then discard any negative intensities (by setting them to 0), this gives us the image shown in Figure 3.10. The process so far has taken a 3 channel image with an unknown and uneven background and unknown root colour and produced a single channel image with a background value of around 0 and a lighter root.

At this point we are able to threshold the root and produce a good estimation of the roots outline. While there are standard techniques to pick a threshold such as Otsu's method (Otsu, 1979), under the known conditions of the ROTATO system a manually set threshold was more consistent than calculating a different threshold for each image. After thresholding we typically get a root outline as shown in Figure 3.11.

Morphological closing is used to fill in the root outline. As we know the approximate width of the root this can be done reliably and without significant artefacts being produced near the tip. As shown in Figure 3.12 (and Figure 3.16) good filling and root tip identification can be achieved by closing. There is a tendency to fill in areas between root hairs which would make this method unsuitable for applications needing accurate identification of the roots midline past the differentiation zone, however that is not required by the ROTATO system.

A second opening process with a small kernel is applied to the image to remove the root hairs (Figure 3.13). Failure to remove hairs can lead to problems in the

Figure 3.9: The intensity of the greyscaled image relative to the local area. A local averaging filter is applied to the image and the difference between the original and the local average is taken. This example uses a circular mean filter with a radius of 71 pixels (the default value used for the experiments performed in section 3.5), approximately equal to 1 root-width. As the intensities are typically low the image was been scaled for visibility.
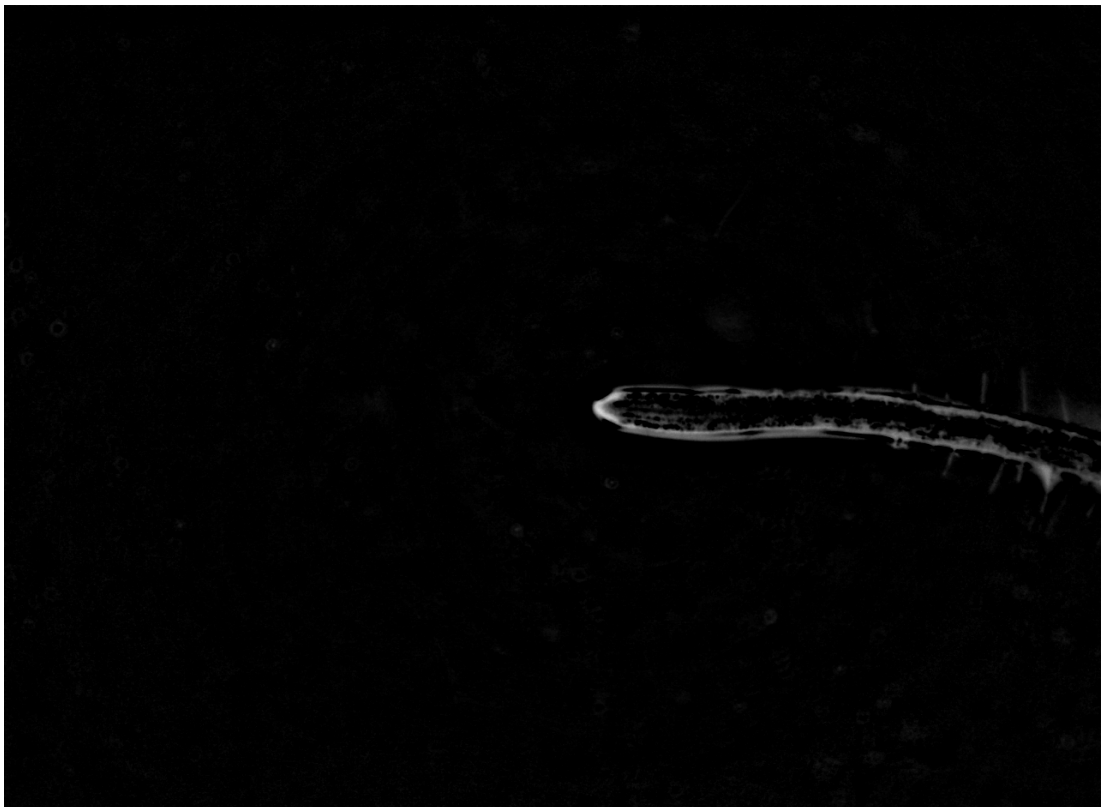
Figure 3.10: The positive values of the relative intensity values from Figure 3.9. Obtained using the transform $pixel_{(i,j)} = max(0, pixel_{(i,j)})$. As the intensities are typically low the image was been scaled for visibility.

Figure 3.11: A threshold applied to the filtered image shown in Figure 3.10. The roots edge has been extracted but the transparent centre has not.

Figure 3.12: Morphological closing applied to the root outline. The outline has been filled at the expense of accuracy in the differentiation zone. Some hairs are present and the area between hairs has been incorrectly identified as belonging to the root.
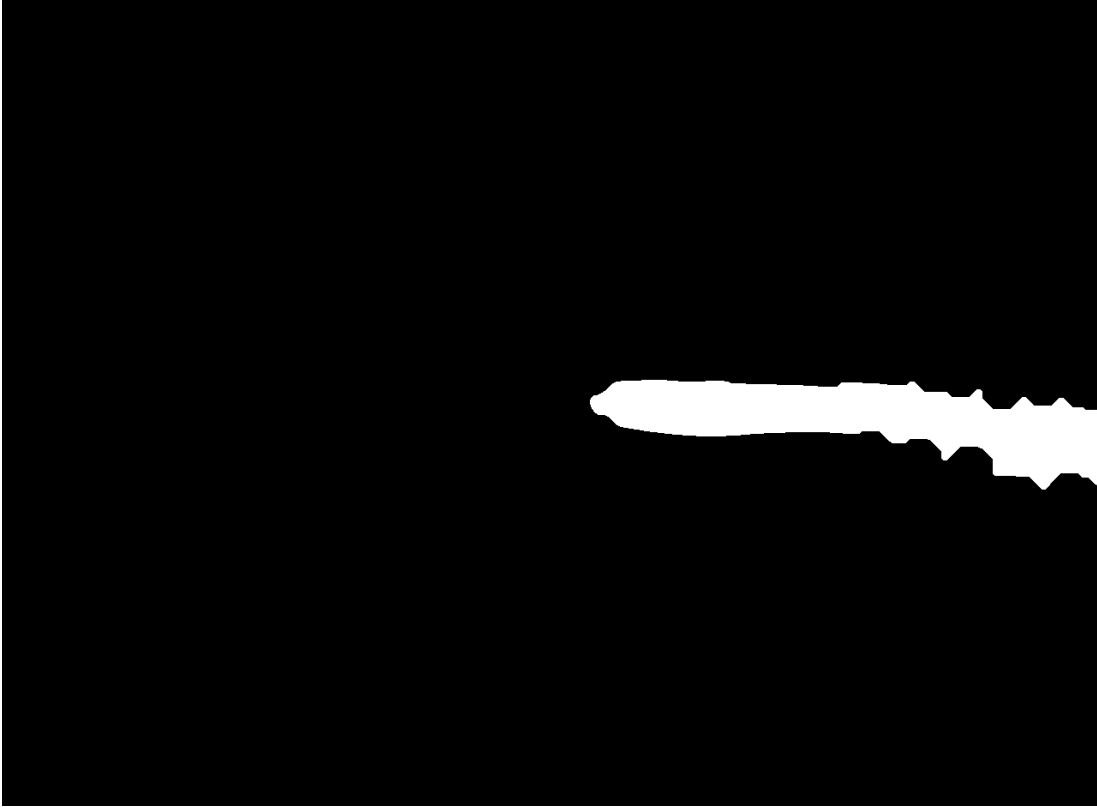
Figure 3.13: Morphological opening gets rid of the hairs, but does not affect the root tip.

next stage where the skeleton is obtained.

The root midline is identified my finding the morphological skeleton of the root. A skeletonisation method used was taken from Lam et al (Lam et al., 1992) as implemented in MATLAB's "bwmorph(thin)" function. This was found to produce better results than the default MATLAB "skel" skeletonisation method. In some instances however the skeletonisation can produce "forked" results, with a split midline, as can be seen in Figure3.14. In this case we cannot tell which branch of the split is correct (or indeed if either is correct). Similarly small spurs can be erroneously identified as tips. In order to deal with these issues small spurs are removed from the skeleton. This is done in a way that does not effect components of midline of a size greater than a given threshold. Figure 3.14 shows a split skeleton section after spur removal. The final midline is shown in Fig. 3.15

A.

B.
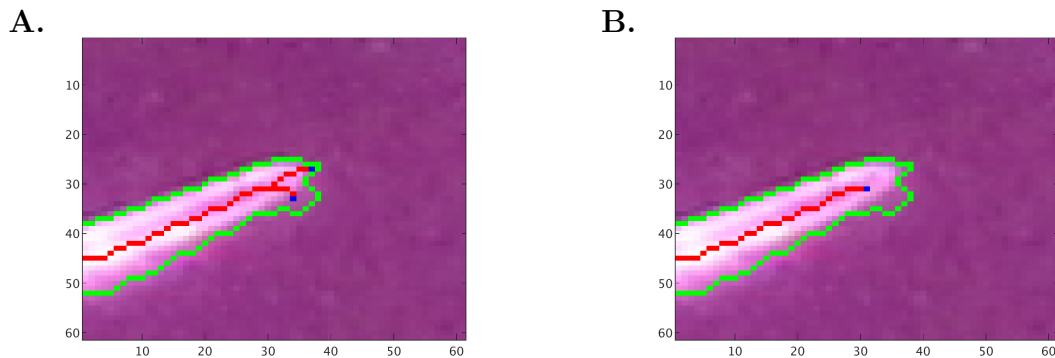
Figure 3.14: **A.** Poor segmentation has caused a "split end" (shown in red) making the tip position and angle hard to determine. Two potential tip positions are shown in blue, and the segmentation is outlined in green. **B.** By removing small spurs we can obtain a more accurate and consistent measurement of tip position and angle. This is the same segmentation as in Figure 3.14 after spur removal. There is now only a single candidate tip position.

Figure 3.16 shows the final result of the analysis pipeline. The estimated outline of the root is shown in green, with the midline in red. In general the root outline is accurate, in this case with 2 notable exceptions. First the specular reflection off the root tip has produces 2 indentations in the extracted outline. This is not a common problem, being specific to the particular lighting in the example image, however problems of this sort do have the potential to produce inaccurate angle measurements. This specific example gives an angle of 96.6° compared to 94.7° given by manual measurement, an error of 1.9°. In general problems caused by lighting are transient as the movement of the stage is sufficient to change the angle of illumination, while this does mean that they can occur unexpectedly during an experiment it also means that, to a degree, this sort of problem is self-correcting. The second notable problem with the outline detection is around the root hairs. Detection of hairs during the initial steps leads to overestimation of the boundary of the root. While this can be mitigated to a degree by removing the hair itself (the opening step of the pipeline), and at the skeletonisation stage removing spurs from the midline, it is difficult to remove entirely. However as the distance between the tip and the beginning of hair growth is much larger than the length of the tip the inaccuracies in segmentation do not affect the measured

50
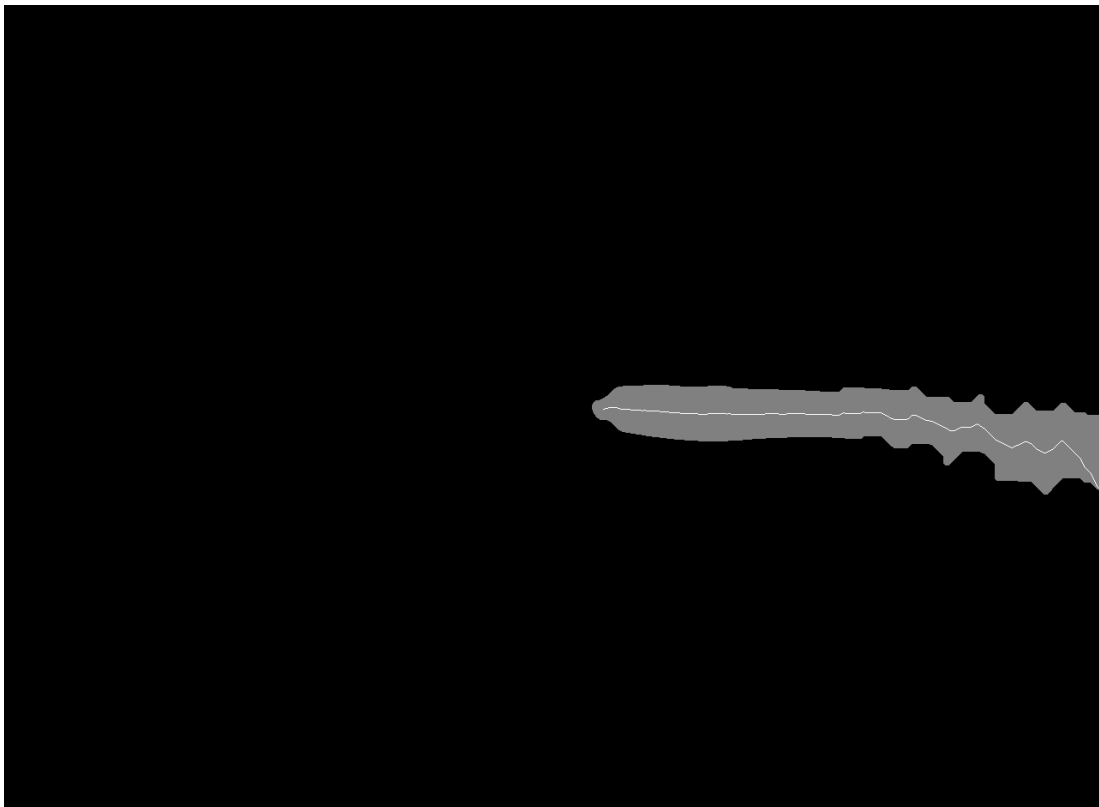
Figure 3.15: Skeletonisation is used to find the midline of the root. Small spurs are removed leaving only the central line. The skeleton extends to approximately $\frac{1}{2}$ root-widths from the tip.

Figure 3.16: An annotated root image. The green border gives the roots outline, while the red line shows the roots midline. The background image has been converted to greyscale for clarity.

tip angle. There is the potential for spurs in the midline caused by root hairs to be erroneously identified as the root tip but this is mitigated by the spur removal process. For a more in-depth analysis of the vision systems accuracy see section 3.5.

While it would be considerably more efficient to run the above processing pipeline only on a region of interest the movement of the root tip during the adjustment step precludes this. While the root tip is aligned to the centre of the stage during the initial setup, the growth of the root moves it away from the centre point as the experiment progresses. This introduces lateral movement when the plant is rotated that can be large relative to the scale of the image, because of this we do not know the position of the root tip at the start of each analysis step.

nn	AA	xx

Table 3.2: The Agilis motor command format. "nn" is the axis of the stage, "AA" is a 2 character command, "xx" is an optional parameter depending on command type. (Corporation, 2012)

3.3.4   Stage control

The stage control software consists of a single stage class, which provides a simple interface between the stage and the control software. The details of the hardware interface are abstracted away allowing physical stages to be swapped with minimal changes. Two versions of the stage controller have been developed, an initial version working with a simple stepper motor stage used for prototyping, and a final version that uses the Agilis stage. Both provide the same interface to the ROTATO system, but as the stepper motor code was only used for prototyping it will not be covered in detail.

The Agilis motors themselves connect to a control box which connects to a computer via serial connection. Each stage is identified by a port and channel which are determined by which physical socket the stage is connected to. Communication is done by sending newline terminated commands in ASCII, with the form shown in table 3.2(Corporation, 2012). The motor control code wraps around the serial commands and provides a number of methods with the same general structure. With a few exceptions the command methods have the following structure:

1. Move to the correct channel

2. Construct a string to send to the device

3. Write the string to the serial port

4. Wait for a reply

5. Return the reply

All the commands available to the Agilis stage have been implemented but not all are necessary for the ROTATO system, for details on the full list of com-

mands available see the Agilis user manual (Corporation, 2012). As many of the commands available to the Agilis motor, are specific to the motor a higher level set of commands is used by the ROTATO software. By far the most commonly used command is the "stepByAngle" function which converts an angle given in degrees, into a number of steps, which is then sent to the stage. Positive values cause a rotation in one direction while negative values cause a rotation in the other direction, which direction is which depends on the physical layout of the stage and can be changed in software. As channel and axis information is contained within the object this then provides a hardware independent way of interfacing with the stage.

As the Agilis stage works in terms of steps, with a step-size not being well defined, calibrating the stage is very important. The Agilis version of the motor control code also includes a calibration method with the following steps:

1. The Stage is manually set to 0° using the markings on the outside of the stage.

2. The controller will attempt to turn the stage clockwise by 90°.

3. The actual rotation as given by the markings on the stage is entered, and the clockwise step-size is calculated.

4. The controller then attempts to turn the stage counter-clockwise back to the original position at 0°.

5. The actual angle of the stage relative to 0 is entered and the counter-clockwise step-size is calculated.

3.4 Evaluation

3.4.1 Stage accuracy

Ensuring the accuracy of the stages rotation is vitally important for gathering reliable data. While an error in rotation is unlikely to seriously compromise the root tip angle, if the rotation done is consistently different to that recorded the bend-rate will not be correctly measured. Initial accuracy tests were performed in much the same way as the stage calibration. The angle of the stage as given by the reference mark on the front is recorded, the stage is told to rotate by a set amount, and the angle after rotation is recorded. As it is important to determine not just relative error but absolute error this has been performed with both 30° and 90° turns. As can be seen on Fig. 3.17 the accuracy of the stage is good for 30° turns, however for large single reorientations drift does occur.

However, single large rotations are not representative of the behaviour when the system is in use. Given a measurement frequency of 1 minute, and assuming a fast bending root we would typically not expect rotations of more than around $1° - 2°$ at any one time. In practise the maximum rotation allowed when the system is in operation is $\pm 2°$ in order to protect against erroneous measurements. Given the precision of manual measurements we cannot determine the accuracy of the stage over a single rotation on this scale. However, given a cumulative error in rotation it is possible to determine any bias in rotation over a long series of movements. In order to test the stage accuracy in representative conditions the stage is set to perform a random walk of 500 rotations of $\pm 2°$, equivalent to almost 1.5 times the maximum number of rotations performed in a typical 6 hour experiment. Under these conditions considerable errors accumulated leaving the final rotation out by around 25 degrees (Fig. 3.17). As the error is highly consistent is is likely that this is the result of a miscalibration rather than a problem with the hardware itself. Unfortunately we were not able to consistently achieve a more accurate calibration than presented here. In order to test the drift on a repeatable set of movements a patterned walk was used. This consists of 100 alternating pairs of $(+1°, -1°)$, and $(-1°, +1°)$ rotations, with each pair returning the stage to it's
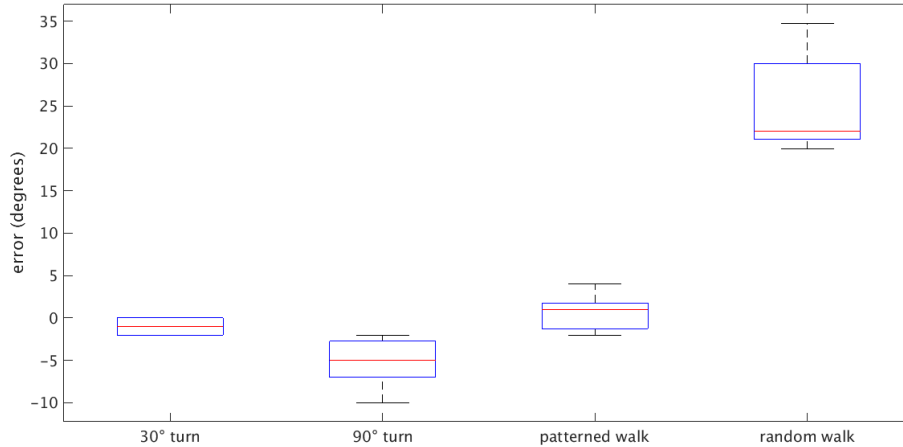
Figure 3.17: The error in the rotation of the motorised stage. Turns consist of a single turn of the specified size. The patterned walk consisted of 100 pairs of alternating $+1°,-1°$ turns. The random walk consisted of 500 random turns of between $-2°$ and $+2°$, giving an average magnitude of $1°$. Drift occurs after a large number of turns, as shown in the random walk trial. Given the consistency of the error it is likely this is due to the limits of the calibration method. N = 5

initial position. After 100 sets of rotations no appreciable error was seen. One would naively expect the error to be proportional to the number of steps taken but this does not appear to be the case, the reason for this is unclear.

3.4.2 Computer vision accuracy

Correct identification and measurement of the root is key to the accurate control of root tip angle. Given small errors in mechanical adjustment, as seen in section 3.4.1 the accuracy at which the root is maintained at the desired angle is approximately equal to the accuracy at which the angle is measured. In order to quantify the accuracy of the vision system roots were placed in the ROTATO system and time-lapse images were taken by the camera used for the ROTATO. These images can then be both hand measured and passed into the ROTATO vision system and the results compared. As can be seen in Figure 3.19 the system performs well. In two out of the three cases the system performed well with the

measured values equally distributed above and below the manual measurements and a mean error of less than 1° (Figure 3.19, table 3.3). The third root is more interesting, where the computer vision consistently overestimated the angle by up to 15°. The cause of this is a bubble forming at the edge of the root approximately 4 hours into the bend (see Figs. 3.18 and 3.20). As problems such as this are difficult to foresee or to compensate for, but easy to spot visually, in instances such as this data was discarded if appropriate.

When comparing manual and automated measurements which typically differ by less than 2° (table 3.3) it is often not possible to determine which measurement is "correct". As the resolution of the angle detection by the Arabidopsis root tip is unlikely to be capable of distinguishing such small differences, at this scale the difference between manual and automated results is not a useful form of analysis. However in order to minimise disturbance to the root and erroneous adjustments to the noise in the angle detection is is useful to determine the degree of noise present in the detection. This has been done by approximating the true root path using a smoothing spline and calculating the residuals from this. Using this method for all the roots tested we consistently see an average image by image error of approximately 1°, with 95% of measurements falling within $\approx 2°$ of the true value as given by the fitted spline (see Figure 3.21).

Given the average error on a successful experiment is of the order of 1° we should be able maintain root tip angles to within a few degrees of the desired angle. The vision system has shown itself to be highly consistent with a noise level of approximately 1°, and 95% of measurements have less than 2° of noise. Given this we can largely eliminate noise in response by setting the minimum adjustment size to 2°, the point at which we can be 95% confident that a reading represents a real change in root tip angle.

As can be seen in figures 3.19 and 3.20, it can on occasion be difficult to accurately segment the root. In this instance a bubble forming near the root tip has been identified as part of the root, but other features such as impressions in the gel, or roots burrowing into the gel can present similar problems (figures 3.4 3.5). While it is often possible to identify cases such as these before an experiment begins, in

	Mean error	Std error	Mean noise	Std noise
root 1	0.8482	4.089	-2.961e-17	0.8736
root 2	5.999	4.131	1.974e-16	1.143
root 3	0.608	3.938	8.142e-17	0.9679
all roots	2.485	4.753	8.306e-17	1

Table 3.3: Distribution of error from the manual and noise in the detection, as shown in Figs. 3.19 and 3.21. Errors are calculated from the difference between matching manual and automated measurements, noise is calculated from the residuals of a smoothing spline applied to the automated results. Due to the use of a smoothing spline we would expect the mean noise to equal 0.

some cases problems only before apparent during the experiment. In instances where the computer vision is unable to correctly identify the root tip it is best to discard such experiments. In properly monitored experiments this is uncommon, occurring in less than 10% of experiments, although it is necessary to ensure the root does not move out of the field of view.

3.5 Results

3.5.1 Experimental methods

When running constrained ROTATO experiments, a 5 day old seedling was initially placed in the ROTATO equipment to acclimatise for 1 hour before reorientation. After acclimatisation the plant was reoriented such that the root tip was at the desired angle, the angle was then adjusted by a maximum of ± 2 degrees at 1 minute intervals to maintain the tip angle. This was continued for up to six hours, or until the system failed (typically due to root growth moving the root tip out of the field of view of the camera). Roots were imaged in dark conditions, under NIR light with a wavelength of 940 nm. Root tip angle, desired angle, adjustment made, time of measurement, and tip position were measured each time an adjustment was made. For the full experimental details see section 2. For a full table of experimental settings see appendix B
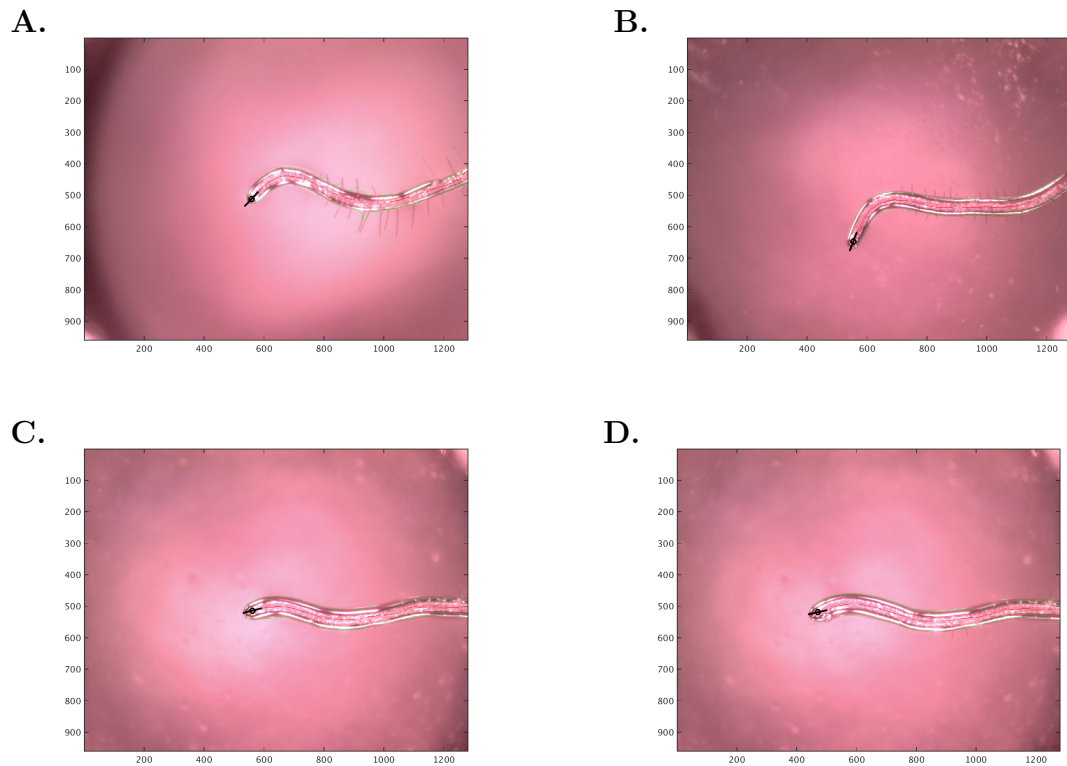
Figure 3.18: **A.** Example segmentation and angle visualisation of a root tip. The tip position and angle is overlaid in black. **B.** Example segmentation and angle visualisation of a root tip. The tip position and angle is overlaid in black. **C.** Example segmentation and angle visualisation of a root tip. The tip position and angle is overlaid in black. **D.** An example of a poorly analysed root tip angle. What appears to be a bubble in the agar is affecting the segmentation and pulling the centre line off centre.
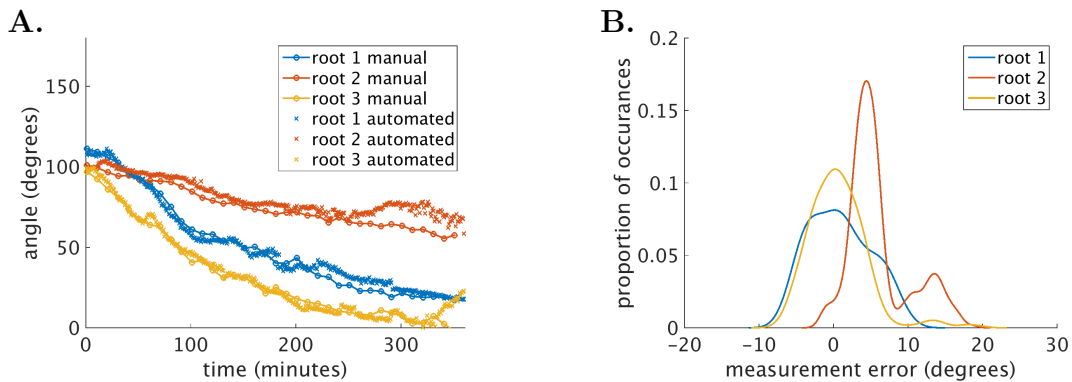
Figure 3.19: **A.** Example traces for reorientated roots, manual measurements are taken every 10 minutes automated measurements every minute. The traces shown here correspond to the images given in Figs. 3.18 **B.** Estimated error distribution for the root traces given in **A.** The overall mean error is $2.5° \pm 4.75°$, distributions were calculated using a kernel-smoothing estimator with a Gaussian kernel.

3.5.2   Experimental results

In order to compare bend rates over a range of angles, constraint (where the root tip is held at a constant angle) experiments were performed at 0°, 20°, 30°, 60°, and 90°. As expected we found continuous bending at all angles throughout the duration of the experiments, as shown in Figure 3.22. Beyond this the data is highly variable. In order to determine the average bend rate we perform a least-squares fit for linear fit through the cumulative bend over time, constrained to pass through $(0, 0)$. The gradient of this line is then gives us the mean bend rate of the data. This model was chosen at it represents the expected behaviour if the response is fully angle-dependent with no change in behaviour over time.

Bend rates have been calculated from the mean response of the populations constrained at the angles given above. Unlike previous work (Mullen et al., 2000) we do not see a clear trend of increasing bend rates at higher angles (Figure 3.22. Although we do see a strong correlation between angle and bend rate ($c \approx 0.88$), we see significantly faster bending at both 30° and 60° than would be predicted by the Sine Law or a simple linear model. The fact that we see the greatest bend rates at 60° is cause for concern. Previous constraint work has found a maxi-
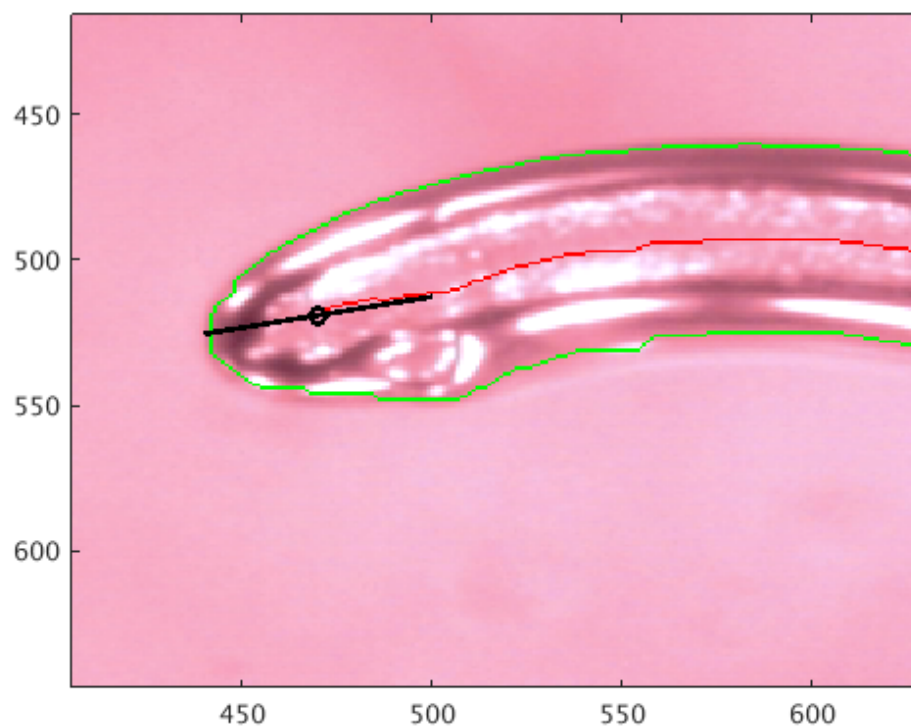
Figure 3.20: A bubble has been erroneously identified as part of the root throwing off the tip angle. The tip angle is given as 77.9° compared to 61° when measured manually, an error of over 16°. The black circle marks the detected tip position while the line shows the angle.

A.

B.
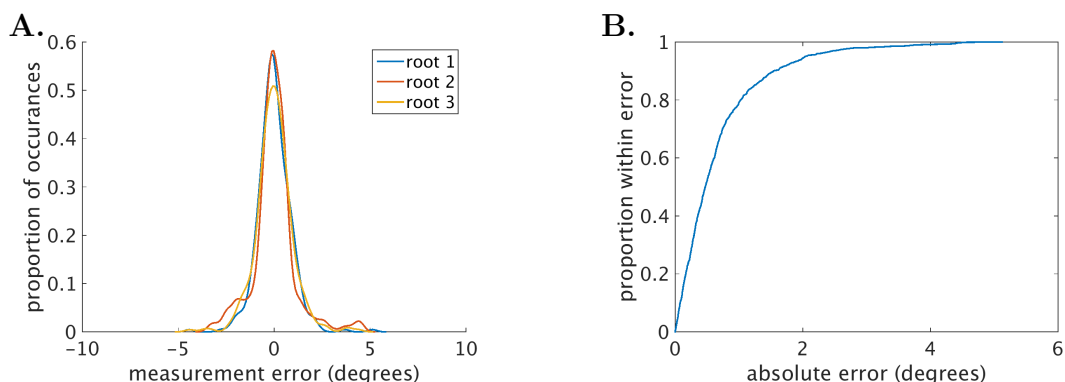
Figure 3.21: **A.** The residuals given when comparing the measured angles to a smoothed path. This demonstrates the distribution of the noise around the "true" root tip angle as measured by the system. The distributions were calculated using a kernel-smoothing estimator with a Gaussian kernel. **B.** The cumulative error distribution of the residuals when comparing the measured angles to a smoothed path for all 3 roots. 50% of measurements are within $\approx 0.5°$ of the smooth path and 95% are within $\approx 2°$.

mum bending angle of around 105°, while in reorientation kinetics experiments the maximum response is reported to be in the 120° to 130° range.

As we are fitting to the mean of each population's cumulative bend over time we are not easily able to determine the range of bend rates observed within a population. This could be done by fitting to individual roots within each population and determining the spread from the individual bend-rates, however when looking at individuals it is apparent that at the individual level bending is not constant. Figure 3.22 shows 3 example traces from 90° constraint experiments. Of these three only a single root (root 2) displays a constant rate of bending of a long period of time, from around 90 minutes into the experiment until the root is lost after 5 and a half hours. Given this inconsistency we cannot meaningfully describe individual by simply taking the mean bend rate, although this is appropriate at the population level.
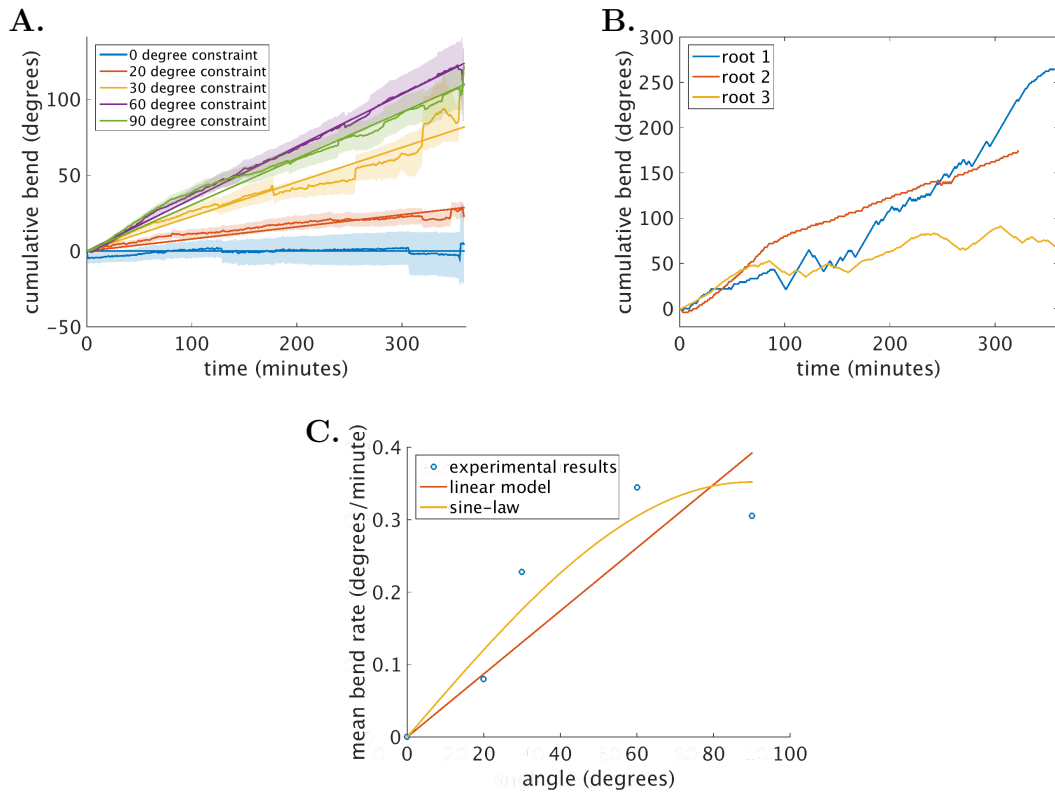
Figure 3.22: **A.** Cumulative bending over time for 0°, 20°, 30°, 60°, and 90° constrained roots ($N \geq 11$). Large changes in angle are due to roots getting lost and being removed from the dataset. **B.** Example traces for 3 individual roots constrained at 90° for 6 hours. Only one of three shown displays a consistent rate of bending. **C.** Mean bend rate for 0°, 20°, 30°, 60°, and 90° constrained roots. While there is a strong correlation $c \approx 0.88$ between angle and bend-rate the results we see the maximum response at 60° which is not consistent with the free response data presented in chapter 4. ($N \geq 11$)

3.6 Discussion

A working ROTATO system has great potential usefulness due to the ability to control gravitropic stimulation over long periods of time. Previous ROTATO systems have demonstrated persistent gravitropic responses for long time periods, following a modified Sine Law. While we were able to observe persistent responses at the population level, individual results were highly variable. Additionally we could not confirm any angle-dependent model of gravitropic response beyond the fact that higher angles tend to produce a greater response. Surprisingly we saw the greatest response at 60° which does not agree with previous measurements which place the maximum response at 105° in constraint experiments and around 130° in free response. Due to the disagreement between these results and previous studies, as well as the reorientation kinetics discussed elsewhere in this document, it is likely that the system was failing to either maintain the desired angles, or that other sources of error were present in the experiments we could not account for. Although it should be mentioned that in general the bend rates are comparable with bend rates of up to $0.35°/minute$ compared to approximately $0.5°/minute$ in free response over the same range of angles.

There are 3 principal possibilities which could account for the inconsistency between the results observed on ROTATO and in reorientation experiments. Firstly there may have been a failure in controlled conditions. While every effort was made to ensure consistent growth and experimental conditions it is possible that this was not sufficient. Failure in conditions is most likely during the course of a ROTATO experiment, as while the system was placed in a controlled temperature environment we were not able to account for any heating of the sample due to waste heat from the ROTATO equipment or absorption of the IR light used for imaging. The second possibility is a failure to accurately identify the root tip angle. If the vision system incorrectly measured the root tip angle for a prolonged period of time it is possible that the root was actually being maintained at a different angle to that reported. This seems unlikely however for a number of reasons. Firstly the root is checked periodically during the course of each experiment specifically in order to ensure good tracking and to adjust the

camera if necessary. In cases where a root was not able to be tracked accurately the experiment was discarded. Secondly the ROTATO system produces annotated images for every measurement taken allowing for manual verification for the tip measurement. Thirdly it is unlikely that difficulties tracking the root tip angle would occur for long periods of time. While it is not uncommon for single frames to report inaccurate results, in order for the results observed inaccurate readings would need to be taken consistently and that if highly likely to have been observed. The third possibility is perhaps the most likely, which is that the amount bent does not match that recorded. The mechanical stage used does not include a feedback system to measure the actual angle rotated. While under test conditions the stage shows good accuracy under realistic rotations and conditions, it is possible that this is not always the case. Poor accuracy in the stage would manifest as the root being correctly maintained at the desired angle (within some limits imposed by the accuracy of the stage and the angle detection), but inaccurate bend rates would be recorded. A related problem is mechanical slippage either of the stage or of the plant itself. Again this would appear as correctly maintained roots however the recorded bend rate would be incorrect.

Improvements to the system could certainly be made. The addition of back lighting could significantly improve the initial stage of root segmentation, allowing for more accurate and reliable angle detection. This is likely to improve the throughput of the system as with the current system experiments are manually monitored and discarded should the angle detection fail. As the ROTATO is only able to process a single root at a time, and experiments can be long, loss of the root tip can significantly impact the number of successful experiments. The use of a rotation stage capable of verifying its position would rule out the most likely source of error in the current system. This would reduce the reliance on the initial stage calibration and provide confirmation that the reported reorientation is correct. While confirmation of correctness is in theory possible based on the angle detection alone (by comparing the angle after reorientation with that expected), the error in detection is of the same order of magnitude as the desired adjustments. In this case we cannot detect small errors in reorientation as stage inaccuracy is likely to be smaller than the error in angle detection.

While the ROTATO system has limitations it may still be useful for maintaining a constant angle for a long period of time. Even assuming we are not able to accurately report the bend rate of a root within the system we are still able to maintain root tip angles over long periods of time, and to verify the correctness of this maintenance. Indeed the software developed here has now been ported to the original ROTATO hardware as presented in Mullen *et al.* where it is performing well.

Chapter 4

Gravitropic response is noisy and angle-dependent.

4.1   Introduction

The most widely used behavioural model of gravitropic response is the Sine Law
(see section 1.3.1). Although the Sine Law has been validated experimentally,
it is not without its flaws. The mechanistic basis for the Sine Law is that the
response is proportional to the force of gravity acting across the organ, this is
a reasonable assumption if the gravity sensing mechanism in the root-tip acts a
force sensor. The magnitude of the perceived deviation from the vertical could
then easily be proportional to the force acting across the organ, which could easily
lead to a Sine Law like response. However there is recent evidence that the root
tip acts not as a force sensor, but as an angle sensor. In this case the theoretical
case for a Sine Law becomes significantly less clear. This is compounded by the
large body of evidence suggesting that the angle of maximum response lies in the
region of 120°-140° (Audus, 1964; Galland, 2002; Larsen, 1969). This suggests
that, in essence, gravitropic response is not linked directly to the force across the
root, which is further supported by the fact that in shoots, gravitropic response is
constant over a range of effective gravities (Chauvet et al., 2016); the presence of

a non-horizontal angle of maximum response also detracts from Sine Laws power as a descriptive model. Taken together one could argue that Sine Law as a model has been shown to lack a theoretical basis as well as having limited powers of prediction.

As discussed in section 1.3.1, the role of time-dependence in gravitropic response has not been thoroughly investigated. A tipping point mechanism has been proposed in which the statocytes act as a binary tilt switch (Band et al., 2012). In this model an auxin asymmetry of constant magnitude is present above 48° from vertical, with no auxin asymmetry present below this angle. Presumably then any difference in response would not be due to the magnitude of the response to the current gravitational stimulus, but due to other effects such as time since reorientation. Certainly for a reoriented root to achieve vertical growth in a system which maintains no response below approximately 48° requires at least some level of hysteresis. An exclusively time-dependent response is problematic for non-zero GSA maintenance over long time periods, while it is not impossible to imagine a time varying process where the gravitropic and anti-gravitropic responses remain balanced; such a system would be hard pressed to display to robustness seen by lateral roots.

The purpose of this chapter is twofold. Firstly it is to determine the magnitude of any time-dependent effects, or hysteresis, on gravitropic response. Second is to determine more generally the accuracy and limits of Sine Law as a model, and evaluate alternative relationships between root-tip angle and gravitropic response. To do this a large (N = 368) set of Arabidopsis reorientation kinetics from a range of initial reorientations has been collected and analysed to determine the extent of time and angle dependent effects.

4.2 Results

4.2.1 Definitions

To avoid confusion following terminology and definitions will be used:

- **Angle**. Angle refers to the orientation of the root-tip (specifically the columella) with respect to gravity. Angle is defined as the difference in angle between a root-tip and the gravity vector, this is measured in degrees with an angle of $0°$ representing a root pointing vertically downwards, and an angle of $180°$ representing a root pointing vertically upwards. Angle is represented by the character θ.

- **Bend rate**. Bend rate is the rate of change of angle with respect to time. This is a vector quantity with positive values representing upwards bending and negative values representing downwards bending. The unit is $\frac{degrees}{minute}$ and it is written as $\frac{\delta\theta}{\delta t}$.

- **Proportional bend rate**. Proportional bend rate is the proportion of the root-tip angle bent per minute. Conceptually this is similar to the "decay rate" found in many physical and chemical processes. The unit is $minutes^{-1}$, and it is represented by the character λ.

- **Curvature**. Curvature is the change in angle with respect to length. This is a vector quantity with positive values representing upwards bending in the tip-wards direction and negative values representing downwards bending in the tip-wards direction. The unit of curvature is $\frac{degrees}{cm}$ and it is written as $\frac{\delta\theta}{\delta l}$.

A large set of 368 Arabidopsis reorientation kinetics were measured. Plants were imaged under infra-red light at 1 minute intervals with manual measurements taken at 10 minute intervals for 6 hours (see section 2). Experimental work and measurements were performed jointly with Katelyn Sageman-Furnas (Sageman-Furnas, 2016). In order to ensure that a wide range of angle/time points were covered, initial reorientations were done at $30°$, $60°$, $90°$, $120°$, and $150°$. The

Reorientation angle	Initial N	N after re-binning
30	47	52
60	61	81
90	91	87
120	84	71
150	87	65
170	0	14

Table 4.1: N values of the reorientation kinetics data-set before and after re-binning.

number of roots at each reorientation angle can be seen in table 4.1 and Figure 4.1. As shown in Figure 4.1 these is significant overlap between the initial angles of roots with different initial reorientations. The pre-reorientation angles follow a widely dispersed distribution with approximately 50% of roots more than $10°$ from 0, and 20% more than $20°$ from 0 (see Fig. 4.2). With the difference between consecutive reorientation angles being $15°$ approximately 0.33, or one-third, of roots start closer to a different reorientation angle than intended.

In order to compare behaviour in a truly angle-dependent way, we need to ensure that each root is correctly categorised by starting angle. Non-gravitropic behaviours such as waving and skew can cause significant variation in angle before reorientation (Fig. 4.2). The obvious method is to simply take roots which start more than some distance from the target angle and relabel them as the appropriate category. However this approach is flawed, as when comparing means and variances it is important not to conflate roots on different physical plates. While all care was taken to ensure that the experimental conditions were consistent between experiments some variation is inevitable. This does not pose a significant problem to determining the mean behaviour as one would expect any variations in behaviour to balance out, however when looking at higher moments of root populations (such as the variance) we cannot rely on differences between experiments to cancel out. If we were to combine similar distributions with slightly different means we would expect the variance of the resultant distribution to increase. Because of this we cannot simply group roots together but must treat each plate independently, when re-categorising roots with initial angles outside the ac-

ceptable range we would have to "split" each plate into components based upon the root starting angle. As in each plate the starting angles are not uniformly distributed by splitting them in this way we will end up a much larger range of roots per plate, a hypothetical plate of 20 roots could be split into a group of 19, and a group of 1 given an unfortunate distribution of initial angles. This presents difficulties when comparing results of such disparate sizes, and makes the results highly sensitive to outliers.

An alternative to simply splitting the roots is to set some minimum "sub-plate size", where if enough roots from a single plate would be re-categorised they are, but if the number falling into the same category is below some minimum the roots are instead discarded. This ensures that each root in the resultant data-set is categorised correctly and that each plate contains a reasonable number of roots but at the expense of throwing away data. With this method there is some necessary trade-off between similarity of plate size (and thus comparability), and number of roots discarded.

A third alternative which seeks to equalise plate size and correctly categorise initial root angle is to sort the starting angles of each root on a plate. The roots are then grouped with their neighbours into sub-groups of a given size. A plate of 30 plants with a wide range of starting angles could become 6 sets of 5 roots, each with a much smaller initial angle distribution. These sub-groups can then be categorised based on the average starting angle of the group. Using this method most roots will be correctly categorised, and each group of roots will be at a roughly equal size, allowing meaningful comparison between groups. The main advantage of this method is that no data is discarded.

While we have used the latter method of categorising roots there is no clear answer to how best to to balance the competing demands of 1. Accurately classifying starting angles, 2. Keeping plate sizes roughly equal allowing for accurate comparisons, and 3. Discarding the minimum data possible. The results of this re-categorising can be seen in table 4.1 and Figure 4.3
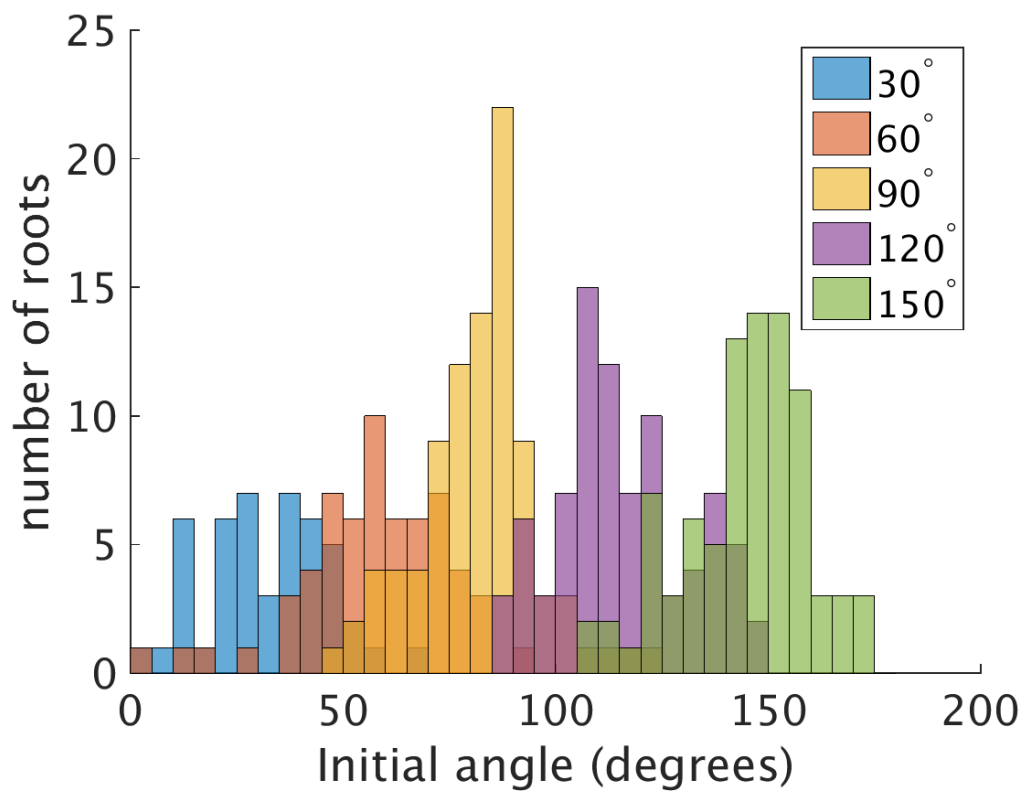
Figure 4.1: The distribution of initial root angles based on the reorientation angle. The large overlaps between reorientation populations make categorising by reorientation angle problematic.
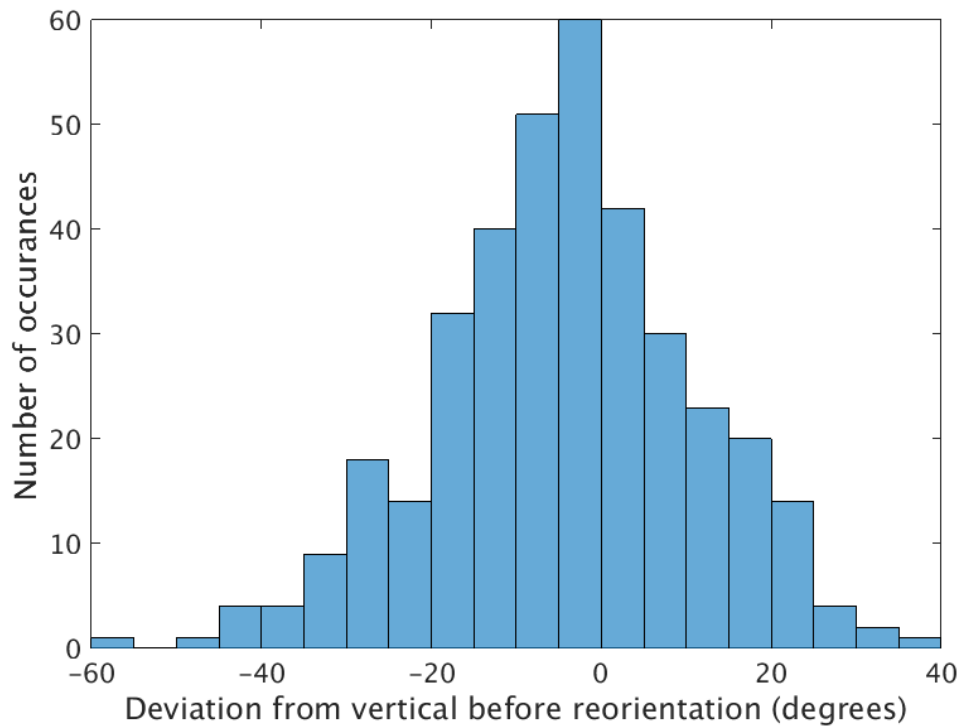
Figure 4.2: The pre-reorientation distribution of initial root angles, variation in response can be caused by processes such as waving and skewing.
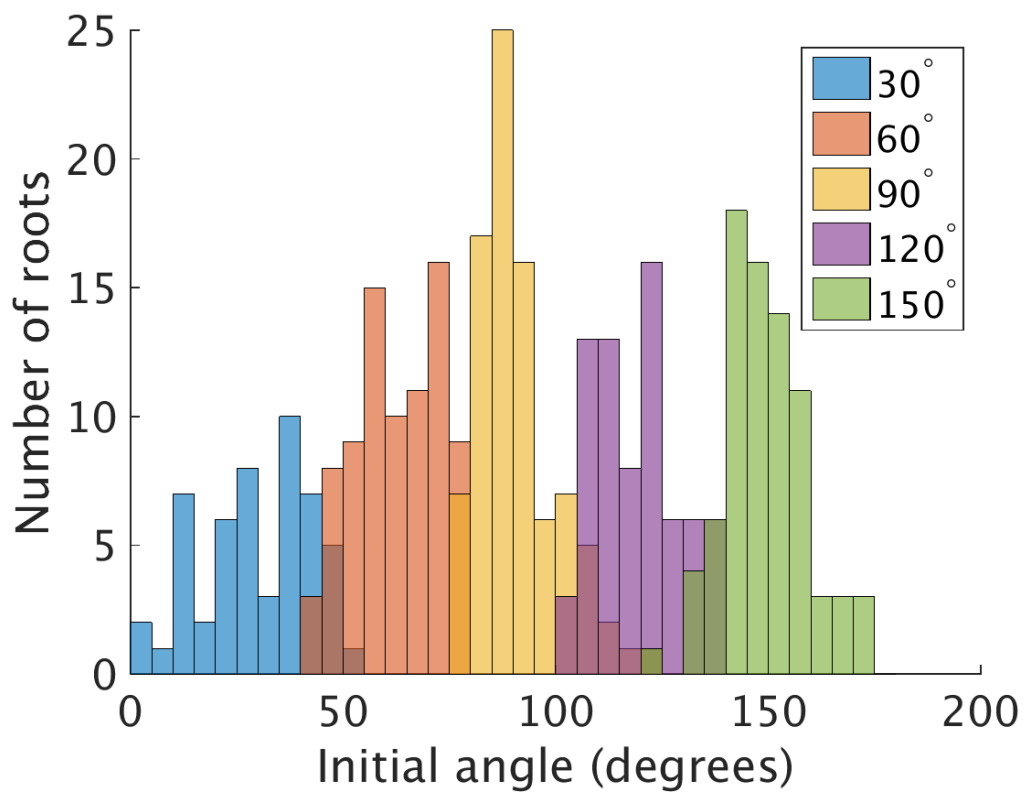
Figure 4.3: The distribution of initial root angles after re-categorising. While there is still some overlap between populations it is minimal, while experimental batch size has been normalised (not shown) and the total number of roots has been conserved.

4.2.2   Graviresponse is noisy

It is initially difficult to determine the nature of gravitropic behaviour from the reorientation kinetics alone. Figure 4.4 shows the raw angle over time traces for roots reoriented to 90°. As can be seen in the figure the response is highly variable, with the fastest roots reaching the vertical in under 4 hours while the slowest are still at angles above 60° when the experiment ends at 6 hours after reorientation. This gives the fastest roots an average angular velocity approximately 3 times higher than the slowest. Similarly when looking at the bend rate as a function of angle the results are equally noisy (see Figure 4.4) with a significant fraction (approximately 30%) of measurements indicating upwards bending. When fitting to the raw bend rate data the Sine Law is able to account of just under 8% of the observed variation in response (least-squares fit to $y = c \cdot sin(\theta), r^2 = 0.078$). It is tempting to dismiss this range of bend rates as individual variation, with individual roots following relatively smooth paths through the cloud of measurements, however this is not the case. Figure 4.4 shows the paths of 3 individuals through angle/bend space, not only are these paths non-smooth, but there appears to be greater within root variation than between root variation. While individual measurement error may account for some of this variation in individually measured bend rates, it cannot explain the large range of responses seen in angle over time.

Given this variation in response it is not possible to distinguish between different models of gravitropic response, such as the Sine Law, or the root-tan model presented in section 1.3.1 (see Figure 4.4). One solution to the problem of fitting to noisy data is angle binning, Figure 4.4 shows the reorientation data from Figure 4.4 averaged over 1°,2°,5°, and 10° bins. It is clear that even with small bin sizes the noise can be reduced to reasonable levels. However while this allows for more accurate analysis we are merely hiding the variability, any model which seeks to capture root behaviour must still take it into account.
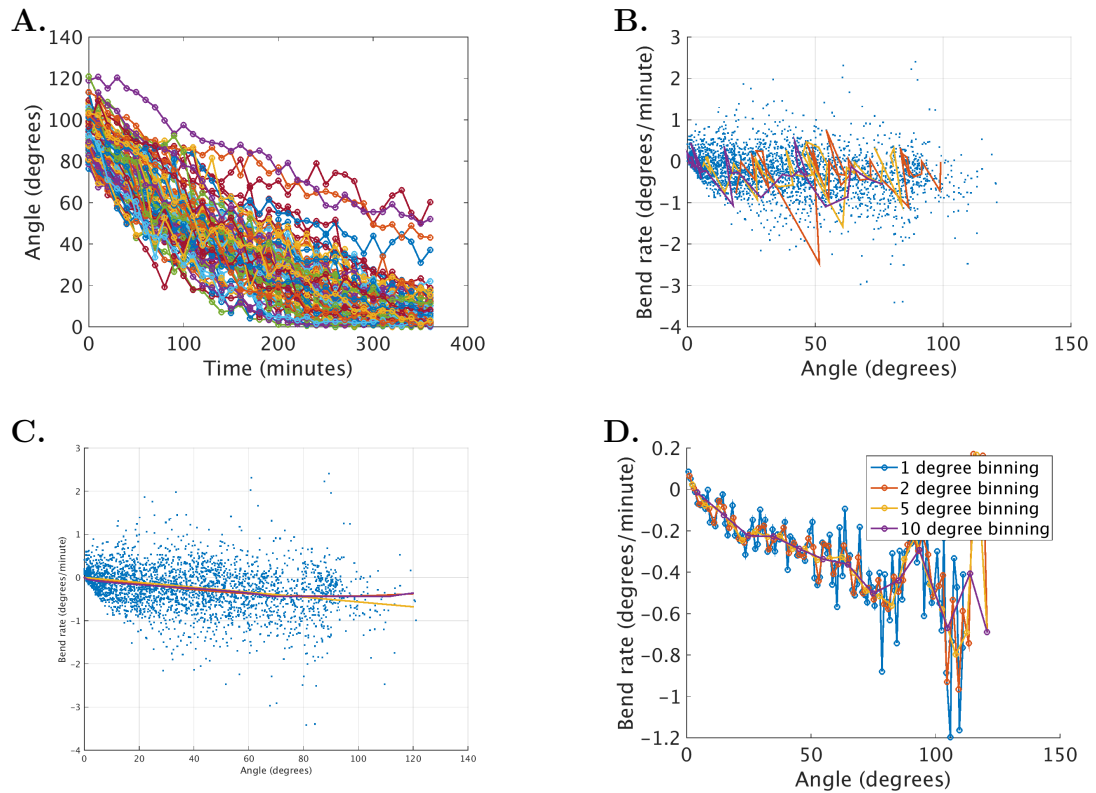
Figure 4.4: **A.** Raw angle against time traces for 90° reoriented roots, measured at 10 minute intervals. **B.** Example angle/bend-rate traces for 90° reoriented roots. **C.** It is impossible to distinguish between possible models based of the raw reorientation data. 3 models are presented here: Sine Law, the root-tan model, and a simple linear fit. **D.** By using spatial binning it is possible to dramatically reduce the level of noise. 4 bin sizes are shown, 1°,2°,5°, and 10°. Over this range of bin sizes the underlying structure does not change dramatically. 87 roots have been used for this analysis but where binned the number of points per bin varies.

4.2.3 Graviresponse is not time-dependent

Establishing what determines root behaviour at any point is crucial to understanding and accurately modelling gravitropic response. The degree to which the behaviour is angle and time-dependent, as well as the presence of hysteresis (where current behaviour depends upon previous stimuli) not only has implications for model development but also for our understanding of non-vertical GSA maintenance. Here we refer to responses which vary over a longer time period as being time dependent, in this context this means a response which occurs on the order of 10 minutes or more. An example would be if roots were unable to continue bending when constrained at a given period for a significant amount of time. Hysteresis is a similar concept but refers to the effect of a roots history over a given time scale. An example of hysteresis in response would be if a root at 90° behaved differently depending on whether it had initially been reoriented to 90° or was in the process of bending down from 120°. To determine the level of time-dependence we can compare the behaviour of roots at the same angle at different times after reorientation, and to determine hysteresis we can compare the behaviour of roots at the same angle but after different initial reorientations. Figure 4.5 shows the mean bend rate as a function of angle for the 90° reorientation kinetics during 6 different time periods since reorientation. It is clear from this figure that over the time period of the experiment there is no significant difference in behaviour between roots at the same angle ($p \approx 0.22$, 2-way ANOVA with angle and time since reorientation as independent variables). While only data from 90° reorientations has been presented here in order to control for the effects of hysteresis, this does limit the amount of data at certain angles and time combinations. For example, there are few roots around 90° after 5 hours. If we expand the data set to include all the reorientation data from the 30°-150° range we can see that even over a large range of reorientation angles there does not appear to be any difference in behaviour due to time since reorientation (Figure 4.5, $p \approx 0.4$, 2-way ANOVA with current angle and initial reorientation angle as independent variables). If the behaviour of a stimulated root displays hysteresis we would expect to observe a change in behaviour dependent on the roots recent history. Unfortunately our control over a root's path once reorientation

has begun is limited, making it hard to precisely control the history of a root for any given measurement. We can get some control over the history of a root by varying the reorientation angle. By comparing the behaviour of roots reoriented to a given angle with those passing through that angle from a higher reorientation we can determine whether having been at a higher angle some time previously influences current behaviour. Figure 4.5(c) shows the bend rate as a function of angle grouped by the initial reorientation angle. It is clear from this that the initial reorientation angle does not affect the behaviour of a root at a given angle. Taken together this shows that over the given time scales time-dependent effects and hysteresis do not play a significant role in gravitropic behaviour. From a modelling perspective we can assume that a root's current angle is likely the sole determiner of its behaviour. Mechanistically, this suggests that the processes involved act on a time scale significantly faster or slower than that measured. Slower time scales are unlikely to have a noticeable effect on any observed behaviour in primary roots as the time scale would have to be significantly longer than the course of a gravitropic response, however we cannot rule out possible effects of long term variations on GSA maintenance in non-vertical organs. It seems clear that over small enough intervals time-dependent effects will be important simply due to the physical limits of the system, we can however rule out the long time impact of these limits.

4.2.4 Graviresponse is angle-dependent

While we can see from our analysis of bend rates that gravitropic behaviour is angle-dependent ($p \leq 0.01$, 2 way ANOVA with current angle and time since reorientation as independent variables) the relationship between angle and gravitropic response is not clear. While we could assume a Sine Law relationship, a visual inspection of the data shows it contains many of the same features that have previously caused problems for the Sine Law, such as a greater than 90° maximum bend rate (see section 1.3.1). In order to accurately predict root behaviour, as well as shed light on the mechanisms behind such behaviour, we need to determine the nature of the angle/bend-rate relationship. We have chosen to
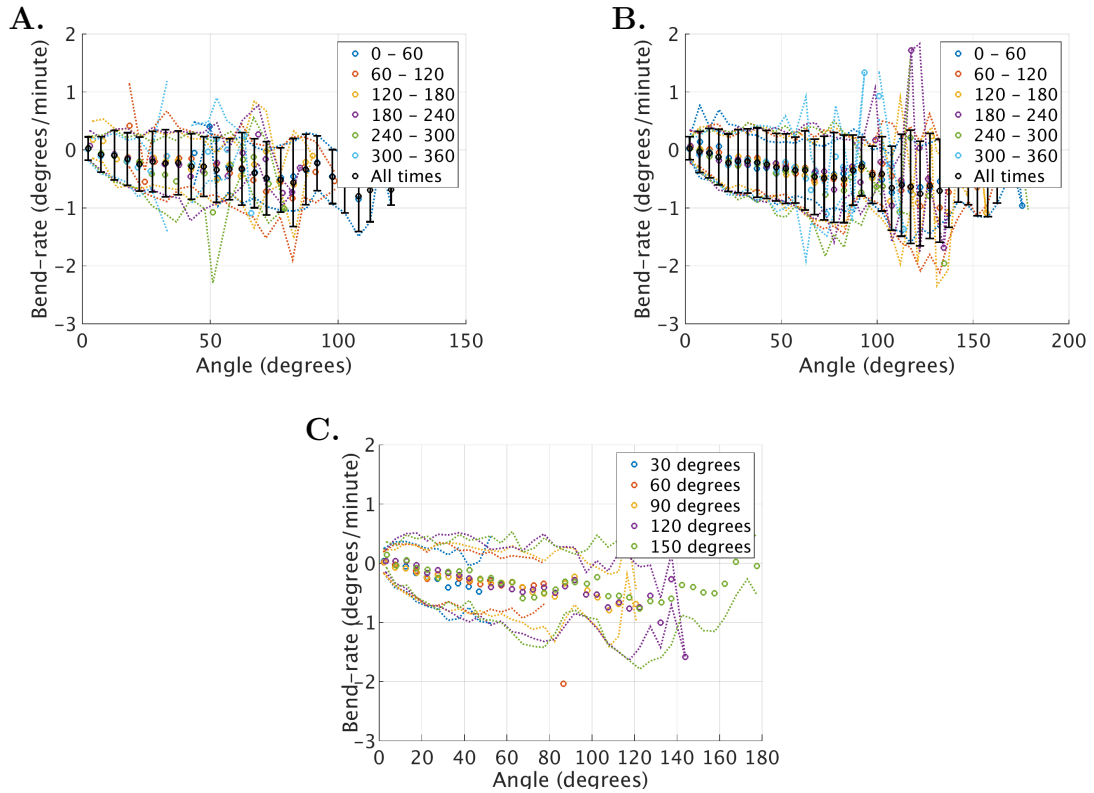
Figure 4.5: **A.** Binned bend rate as a function of angle for 90° reoriented roots. There is no difference in behaviour due to time since reorientation ($p \approx 0.2$, 2-way ANOVA, with current angle and time since reorientation as independent variables). N = 87, error-bars show standard deviation as the number of measurements per bin varies. **B.** Binned bend rate as a function of angle for all reoriented roots (30° - 150° reorientations). There is no difference in behaviour due to time since reorientation ($p \approx 0.4$, 2-way ANOVA, with current angle and time since reorientation as independent variables). N = 368, error-bars show standard deviation as the number of measurements per bin varies. **C.** Binned bend rate as a function of angle grouped by initial reorientation angle. There appears to be no significant difference between behaviours at the same angle based on the starting angle of the root. N = 368, error-bars show standard deviation as the number of measurements per bin varies.

Model	r^2	$p(Gaussian)$
Sine Law	0.885	0.05
root-tan	0.883	0.23
linear fit	0.862	0.15

Table 4.2: Goodness of fit statistics for all binned reorientation data below 90°, Based off 11341 measurements from approximately 305 roots.

compare 3 models of angle-dependent behaviour. The first is the Sine Law which has historically been used to describe this behaviour. The second is a root-tan model based on a geometric relationship between statolith position and bend rate. Lastly is a simple linear fit, while this has no mechanistic basis at the current time it is the simplest model of root behaviour which may be able to describe the increased bend rates seen above 90°. When determining the degree to which a model agrees with the data we are taking two factors into account. Firstly, the variation between the model and the data should be small compared to the variation in the data, this is captured by the r^2 statistic. Secondly, if the model is correct we could reasonably assume that errors due to random noise would be normally distributed and show no positive or negative bias. To test this we are using a second measure of goodness of fit, which is the probability the residuals come from a Gaussian distribution with a mean of 0. Even after reducing the variation in response by angle binning it is difficult to distinguish between the 3 models. Figure 4.6 shows the best fit (LSQ) of the 3 models to the 90° reorientation data. The difference between the three models is small for the $\leq 90°$ range of angles. This is mirrored in the r^2 values which show that all the models explain a large but similar amount of the observed response, although at these small angles the error in the root tan model can most easily be explained as noise (table 4.2).

The difference between the Sine Law and the root tan model remains small even at high angles while a linear fit continues to describe the response at angles above 90°. At angles of up to 130° (the approximate angle of maximum bending) the linear fit provides a significantly better fit to the data than the other two models (Figure 4.6). Although none of the models residuals can be confidently put down to noise, a linear fit continues the capture response well, with an r^2 of approxi-

Model	r^2	$p(Gaussian)$
Sine Law	0.567	0.004
root-tan	0.572	0.0002
linear fit	0.795	0.03

Model	r^2	$p(Gaussian)$
Sine Law	0.46	0.049
root-tan	0.47	0.0016
linear fit	-0.14	0

Table 4.3: Goodness of fit statistics for all binned reorientation data below 130°. Based off 12720 measurements from 345 roots.

Table 4.4: Goodness of fit statistics for all binned reorientation data at all angles. Based off 13194 measurements from 368 roots.

mately 0.8 (table 4.3). This may be due to hidden dependencies between points. While the angle/bend rate values are treated as independent, as the responses are calculated from the same time series data; a single angle measurement in the time series will contribute to the bend rates in multiple angle bins. This has the potential to interfere with statistical tests that assume independence between samples.

Due to the reduction in bend rate as the roots reach the vertical at 180° when the entire data set is included the root-tan model can best describe the data however the difference between the Sine Law and the root tan is negligible (Figure 4.6, table 4.4). Overall it is hard to determine a single best description of the data. While a linear fit appears to work best for angles below approximately 130°, the commonly found angle of maximum bending, it is incapable of dealing with the decrease in bend rate above this angle.

Given a model of bend rate we can normalise our observed values by the model, this should allow us an alternative visualisation which makes it easier to determine the deviations from the models. This is equivalent to calculating the value of the "c" proportionality coefficient required to make each point fit the model (see section 1.3.1, Eq. 1.3), this should be the same if a single model is to fit the full range of behaviour and so we should see a constant value. Note this is only possible for the Sine Law and the linear fit models, it cannot be done for the root tan model as the model has an extra degree of freedom which we cannot separate out the response. Fig. 4.7 shows the values obtained from this normalisation. In both cases similar features of the data are apparent. Neither model is able to fit the higher angles, although the linear model fares significantly better. The point
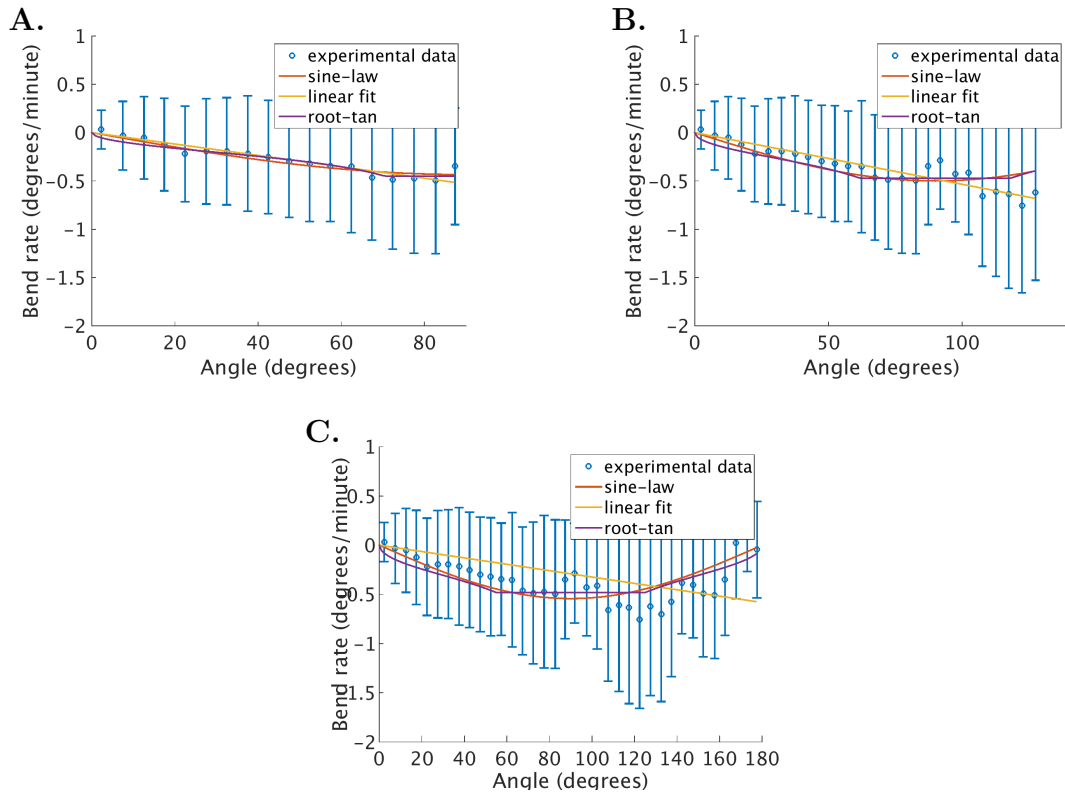
Figure 4.6: **A.** Comparison of angle-dependent models for all reorientation data at angles below 90°. Based off 11341 measurements from approximately 305 roots binned into 5° bins. Error-bars show standard deviation as the number of measurements per bin varies.. **B.** Comparison of angle-dependent models for all reorientation data at angles below 130°. Based off 12720 measurements from approximately 345 roots binned into 5° bins. Error-bars show standard deviation as the number of measurements per bin varies.. **C.** Comparison of angle-dependent models for all reorientation data. Based off 13194 measurements from 368 roots binned into 5° bins. Error-bars show standard deviation as the number of measurements per bin varies..

at which the failure becomes apparent is higher ($\approx 130°$ compared to $\approx 90°$ for the Sine Law) and the deviation is more consistent, showing a clear linear decrease in the fit parameter. The Sine Law deviations however are much more numerous and less self consistent. The second feature of note is the deviation around $25°$. In both normalisations there is a sharp increase in response around $25°$, although this is transitory it will likely have knock on effects when fitting to response as a function of time. Lastly and perhaps more subtly is the dip in response rate around $90°$. While in absolute terms this is small, it is significant and like the $25°$ deviation is likely to have knock on effects when fitting to behaviour over time. This normalisation allows us to check for auto-correlations within the data, giving us a new method for determining time-dependent effects over a range of time scales simultaneously. Figure 4.7 shows the mean auto-correlation values for the individual roots over the time period of the experiment. For each individual we have calculated the time-series $t_i = \frac{\delta\theta}{sin(\theta)}$, and $t_i = \frac{\delta\theta}{\theta}$. By calculating the auto-correlation between terms in this sequence time-dependent or periodic effects should become apparent. As our series is taken from the difference between samples along a time series we would expect unbiased measurement errors to produce a negative auto-correlation over the time scale of a single sample, as can be seen here. Beyond this however there is a negligible relationship between normalised bend rates at time periods above 10 minutes, indicating that at most periodic or time-dependent effects appear to account for less than 1% of the observed response.

Overall, the evaluation of the 3 models of gravitropism presented here is a mixed bag. No model is able to adequately explain the response over the full range of angles tested. At low angles, the 3 models are at a practical level indistinguishable. The only model able to describe the response above the horizontal is a linear relationship between angle and bend rate, but this too fails above approximately $130°$. Traditionally, modified Sine Laws have been presented to better describe observed behaviour, often adding an extra parameter to shift the point of maximum bending to this point, however this technique presents methodological flaws covered later (see section 4.3). Considering the physical system involved it does not seem surprising that as a root-tip approaches $180°$ the ability to produce a
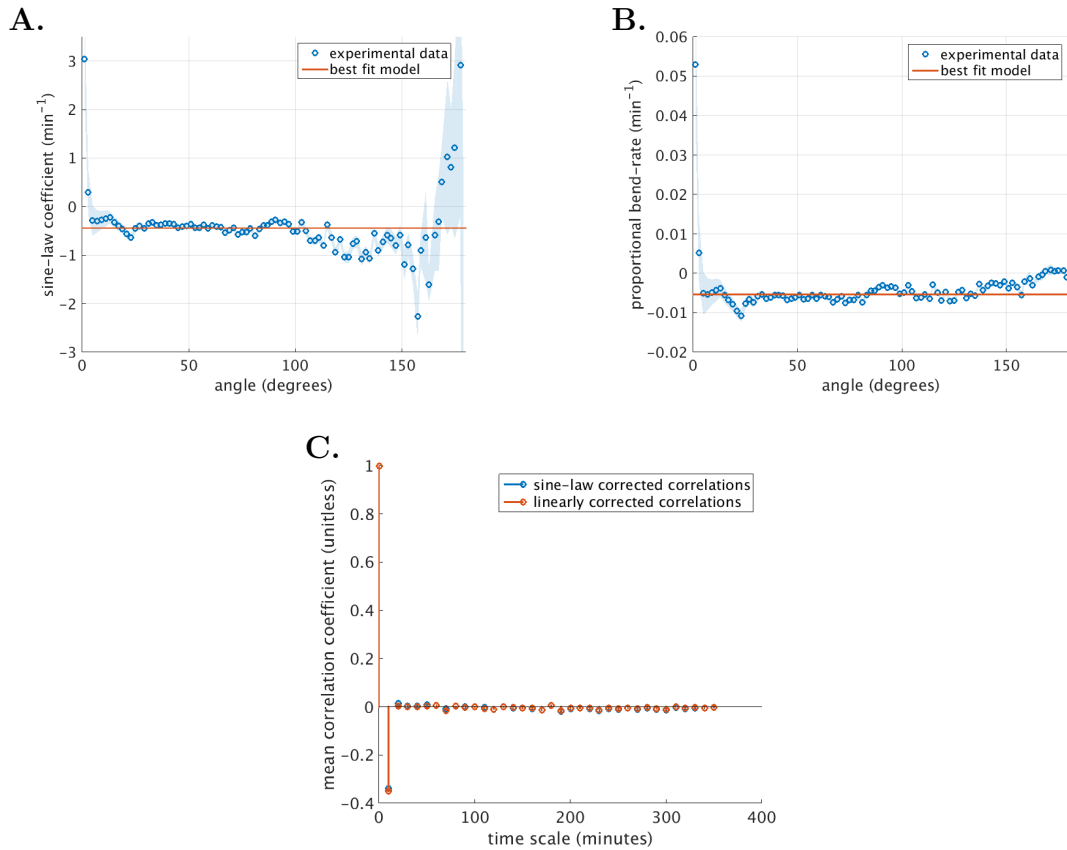
Figure 4.7: **A.** Sine-law coefficients required to fit the data over the full range of angles measured. A best fit model is provided for comparison. Some outliers have been omitted for clarity. Based off 13194 measurements from 368 roots binned into 2° bins. Shaded regions show standard error. **B.** Proportional bend rate (equivalent to a linear coefficient) required to fit the data over the full range of angles measured. A best fit model is provided for comparison. Based off 13194 measurements from 368 roots binned into 2° bins. Shaded regions show standard error. **C.** Mean auto-correlations for bend rates normalised according to the sin-law or a linear fit. Both models show some degree of negative auto-correlation over the 10 minute time period. It is not clear whether this is a feature of the response or is a result of measurement error. There is no meaningful correlation over periods above 10 minutes. Based off 13194 measurements from 368 roots.

gravitropic response is reduced. Determining a downward face of the cell is likely to be increasingly difficult and inaccurate as both the cells lateral faces become parallel to the direction of gravity (at 180° it is no longer meaningful to consider either a "downward" face). It is certainly plausible that instead of a continuous decrease in the magnitude of gravitropic perception, 130° marks the point at point at which the root-tip has difficulty determining the lower side wall. Below this point a linear relationship between angle and response performs significantly better than the alternatives. Looking at the proportional bend-rates (Figure 4.7 there appears the be a very consistent deviation from the linear model, unlike that seen by the Sine Law. This may indicative of a reasonable model choice albeit with incorrect parameters, in this case the higher angle response may be linearly decreasing at this point. Despite its limitations I would argue that a linear relationship between angle and bend-rate is the best description of the data presented here however, like all the models presented, it is clear it is only able to describe a section of the angles over which response occurs.

4.2.5 Maximum bending occurs at 130°

Given the success of a linear model in describing the angle-response data below the point of maximum bending it is useful to determine, as well as possible, an exact angle of deviation from the model. This will allow us to more accurately determine the limits of the model as well as its accuracy within the applicable range of angles. Additionally having an accurate angle of deviation may provide insights into the mechanism behind the response. Visually the response above 130° appears to decrease at a constant rate becoming close to 0 at 180° This suggests a possible model able to describe bending across the full range of angles and, more importantly here, to determine the point of maximum response with a high degree of accuracy. We can do this by creating a piece-wise linear function with a single knot. Effectively we can use 2 linear fits with the stipulation that below the intersection of the fits we use one fit, and above it we use the other. We can then perform a LSQ fit using any of the standard methods to determine the best fit parameters and thus the point of maximum bending. In order to

simplify the fitting process and reduce the parameter space the function has been reformatted to Equation 4.1, where g_1 is the gradient of the low angle section, θ_{max} is the point of maximum bending, and g_2 is the gradient of the high angle section.

$$\frac{\delta\theta}{\delta t} = \begin{cases} g_1 \cdot \theta & \theta \leq \theta_{max} \\ g_1 \cdot \theta_{max} + g_2 \cdot (\theta - \theta_{max}) & \theta > \theta_{max} \end{cases} \tag{4.1}$$

The result of fitting to this bi-linear model is shown in Figure 4.8.

Care must be taken when interpreting the results of this model. While it does produce good results, fitting the observed data well over the entire range of angles this is to be expected given the increased degrees of freedom over the models tested previously (the bi-linear fit has 3 DoF, compared to 2 for the root-tan model, and 1 for both the Sine Law and the standard linear fit). It is difficult to say how much the improvement is simply down to the extra flexibility allowed by the model. However it does allow us the determine the point at which the linear model diverges from the observed responses, at 131.5°. This appears to be largely invariant to the size of the angle bins used, varying by less than ±1° over bin sizes ranging from 1° to 10°. Additionally as the lower portion of the function is largely independent of the upper portion we can be confident that the fit produced is an accurate representation of the bending below the turning point and is not biased by the inclusion or exclusion of data to either side. As such this technique is used only to determine the range in which we can be confident about the linearity of response, and the magnitude of the proportionality constant.

4.3 Discussion

As discussed previously, root gravitropism kinetics have largely been described in the context of the Sine Law, however there are a number of problems with this model that have yet to be addressed. The most striking of these is the maximum bend-rate appearing above the horizontal as is predicted, but other
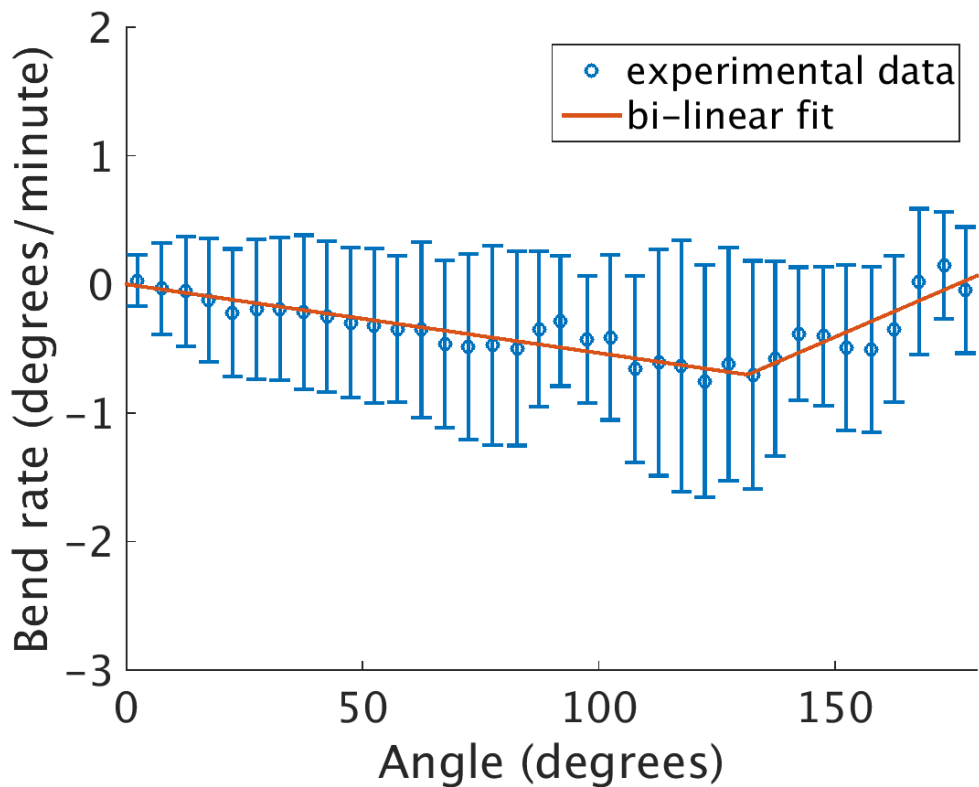
Figure 4.8: A two part piece-wise linear fit, or bi-linear fit, to reorientation kinetics across all tested angles. This fit predicts a maximum bending angle of 131.5°. This fit can explain a large proportion of the observed response ($r^2 \approx 0.70$), and the residuals are normally distributed around the model ($p \approx 0.18$) as would be expected due to noise. Based off 13194 measurements from 368 roots binned into 5° bins. Error-bars show standard deviation as the number of points per bin varies.

problems arise when trying to reconcile the mechanistic basis of the model with our growing understanding of graviperception. The Sine Law is based on the presumption that the force of gravity acting across the organ determines the magnitude of response. Experiments in hypergravity, such as on centrifuged roots, do not show positive a relationship between strength of gravitropic stimuli and response (Fitzelle and Kiss, 2001) as would be expected. Added to this is recent work showing that the statocytes themselves do not in fact act as force sensors (Chauvet et al., 2016). It has also been shown that the magnitude of the auxin gradient across gravistimulated roots follows a linear model, at least up to 120° (Sageman-Furnas, 2016). More circumstantially is the successful prediction of graviproprioceptive response in a wide range of shoots using a linear model of response (Bastien et al., 2013), although in this case linearity was used as a simplified model and no claims as to its accuracy were made.

Relatively little is known about gravitropic behaviour from a systems point of view such as the effects of time-dependent vs angle-dependent behaviour and the role of hysteresis. While there is evidence that gravitropic behaviour is angle-dependent, such as the continuous bending seen on ROTATO (Mullen et al., 2000), time-dependent models have also been proposed for the mechanism behind the response (Band et al., 2012). Determining these dependencies is vital to our understanding of lateral root behaviour. Our current understanding of GSA maintenance in lateral roots being caused by an AGO is dependent on a smooth angle-dependent response over the range of GSA's observed. While the AGO model requires angle dependence for GSA maintenance over long time periods, time-dependent effects and hysteresis cannot be ruled out, and may play a part in response as a root returns to its GSA.

In order to determine the factors involved in gravitopic response we have performed large scale reorientation kinetics experiments over a range of angles form 30° to 150°. When comparing reorientation rates there appears to be no difference between responses at the same angle but at different times since reorientation. This supports the previous work seen on ROTATO which suggests that gravitropic responses can be maintained at a constant level for wide ranges of time since reorientation. Moreover this demonstrates that angle is the determining factor in

response even during changing gravitational stimuli, something not demonstrated on the ROTATO system. Analysis of bend rate as a function of angle does not show the presence of hysteresis over the time scales tested further supporting angle as the key factor in response. Additionally by looking at the auto-correlation between normalised bend rates as a time series we can determine that magnitude of time-dependent any hysteric effects independently of the specific time since reorientation and across a wide range of time scales. While this detected evidence of short term correlations of the same frequency as the sampling, this is to be expected when analysing the differences between measurements taken with some independent error. Beyond this we found no significant time-dependent effects, however we can only test for effects over the time period of the measurement. We cannot therefore rule out any effects faster than the sampling frequency of 10 minutes, or longer than the measurement time of 6 hours (such as would be caused due to root waving).

Across all of our analysis we see a consistent maximum response at around 130°. Similar results have been widely reported in the past (Audus, 1964; Galland, 2002; Larsen, 1969; Mullen et al., 2000) with the maximum response often found in the region of 120° to 130°. Our data shows this is not simply a transient effect as could be caused by higher angles allowing faster statolith movement away from the previous lower face of the cell. The consistency of this result across different times and histories strongly indicates that this is a real and persistent phenomenon.

This high angle of maximum response was a motivating factor in the comparison between different models of response. While there appears to be no simple model that accurately describes behaviour at all angles however there are a few conclusions that can be drawn from the comparisons. At no point does the Sine Law perform significantly better than a linear fit (or the more complicated root tan model). At low angles the models are practically indistinguishable. While the Sine Law is often the go-to model when looking at reorientation kinetics this may be not be the most appropriate model. The Sine Law has been approximated by a linear model (Bastien et al., 2013) with good results, but rather than simply being a simplification, a linear model may in fact be more accurate and

apply over a wider range of angles than the Sine Law. Given the evidence cited previously that statocytes do not appear to act as a force sensor, and that auxin asymmetry correlates directly with stimulation angle (see section 6.4.4) it seems likely that this is a direct result of the gravitropic mechanisms and not simply the result of a poorly realised response. Moving to a piece-wise linear fit allows us a highly accurate measurement of the maximum bending angle and provides an extremely good fit to the observed response, however it does not seem right to propose this as a description of gravitropic response without further insight into the mechanisms behind it.

The cause of the maximum bend response at 130° is not currently known. If we assume a linear model where the statocyte is acting as an angle sensor then we may able to gain insights from looking at statolith behaviour. Using physical models of statocytes it has been found that the maximum number of statoliths in contact with a lateral cell face occurs at around 130°. This physical model was subject to limitations however. The number of "statoliths" in contact with the lateral face was counted when they were at equilibrium. In the root tip statoliths do not settle into a stable equilibrium, instead showing saltatory movements which would be expected to distribute the statoliths more even throughout the cell. While this may indicate that around 130° is the point at which the initial movement of statoliths after a reorientation would produce the maximum response, if this was the cause of the maxima in bend rate we may expect the effect to be transitory as the statoliths are more evenly distributed throughout the cell. Another possible explanation for the maxima is that after 130° it becomes difficult to distinguish the lower face as statoliths start to rest against both sides of the cell. However if this the case one would expect the effect to be symmetrical around the horizontal which is not the case. Some mechanism is needed to break the symmetry of the response and as of yet this is not known, although there is preliminary data to suggest that the cell geometry may be able to break this symmetry.

While it is possible to compare models after a significant amount of noise reduction has been done, even with large datasets (over 10,000 data points were collected for this analysis) the data remains too noisy to fully determine the behaviour. The variability in response is huge throughout the dataset, and while

some of this may be attributable to errors in measurement and variability in experimental conditions this cannot account for the range of responses observed. This is not necessarily surprising as there is evidence that noise may be significant in the mechanisms behind gravitropic behaviour, either due to errors in the detection of a weak signal or in a more active role such as stochastic resonance acting to boost the signal. Given a typical statoliths mass the force of the statolith resting on a membrane is of the same order as thermal noise within the cell Björkman (1989). Although it is unclear how much of a role resting force has to play in statolith position detection (certainly the statocyte as a whole does not seem to sense force as discussed above) this certainly opens the possibility of highly noisy response. This is potentially compounded by the saltatory movement displayed by statoliths even when at rest (section 1.2.3). Taken together this suggests that whether the gravitational signal is encoded in statolith position or in resting force, in either case the resulting signal is likely to be either incredibly weak or highly variable. Given this it would actually be surprising if the response was not highly variable. This variation in response has a number of implications. Firstly it demonstrates the need for a large dataset as collected here, even then it may not possible to fully understand the data without extensive analysis. Secondly when developing a model of gravitropic behaviour it may not be sufficient to simply capture the mean response, if the behaviour can be treated as a stochastic process it may be possible to capture other features of the response such as the higher order moments of a responding population. If so this could give us valuable insight into the mechanisms behind the behaviour as well as providing a valuable tools when analysing mutant phenotypes.

Chapter 5

A computer vision system for root angle analysis

5.1   Introduction

Given the noisiness inherent in gravitropic response (see section 4.2.2) the need for large data-sets is paramount. While we have collected data from a large number of root reorientations over a broad range of angles the analysis is very time-consuming which limits the size of the data-set obtainable. Given a 6 hour measurement time, sufficient to record a full bend after a typical 90° reorientation, and a sampling frequency of ten minutes, of the order of time a bend event may be detected, each root requires 37 measurements. Our primary dataset contains 368 roots, with over 500 roots measured initially, some of which had to be discarded due to experimental problems (roots burrowing into the growth medium, growing into other roots, poor imaging conditions, etc). In total over $13,500$ measurements are included in the final dataset, with over $20,000$ being made in total. Manual measurement on this scale is incredibly time consuming and is the bottleneck when producing large datasets. Even at 10 minute measurement frequencies the amount of data to be analysed is large, however in order to truly capture response we would ideally like to measure at intervals smaller than re-

sponse can occur. Given some reasonable limits on response given by statolith sedimentation time and auxin transport rates (see section 6.2.1) we can estimate that response may be able to occur in as little as a few minutes. Ideally we would like to be able to measure response on the scale of one minute. This is not currently practical given the time limits imposed by manual measurements. For the final dataset we have collected, over $130,000$ measurements would have to be made; an order of magnitude more than was practical.

By automating the image analysis we should be able to drastically reduce if not remove entirely the measurement bottleneck, as well as increase the sampling rate. There exist freely available computer vision systems for use analysing root data, such as the popular RootNav (Pound et al., 2013), however to date these systems all rely on manual annotation for each image analysed. While this is well suited to single images of individual plants it does not scale well to time-lapse image series where the amount of annotation would be large.

This chapter covers the adaption of the ROTATO computer vision system covered in chapter 3 to large scale data collection and analysis, and to produce a system able to analyse large time-lapse image sequences with minimal human interaction, along with the difficulties this entails.

5.2   Imaging setup

Good image quality is key to accurate image analysis. In order to reduce possible interference by phototropic responses the decision was made to do all imaging under near infra-red lighting. This not only removes phototropism as a confounding effect but should allow direct comparison between roots imaged using this system and those imaged on ROTATO (see section 3.2.1 for more details on the use of NIR).

In order to allow for flexibility in lighting modular lighting boards were designed, each containing 2 LEDs outputting NIR light at a wavelength of 940NM. Each board runs the 2 LEDs in parallel off a pair of rails which allow multiple boards
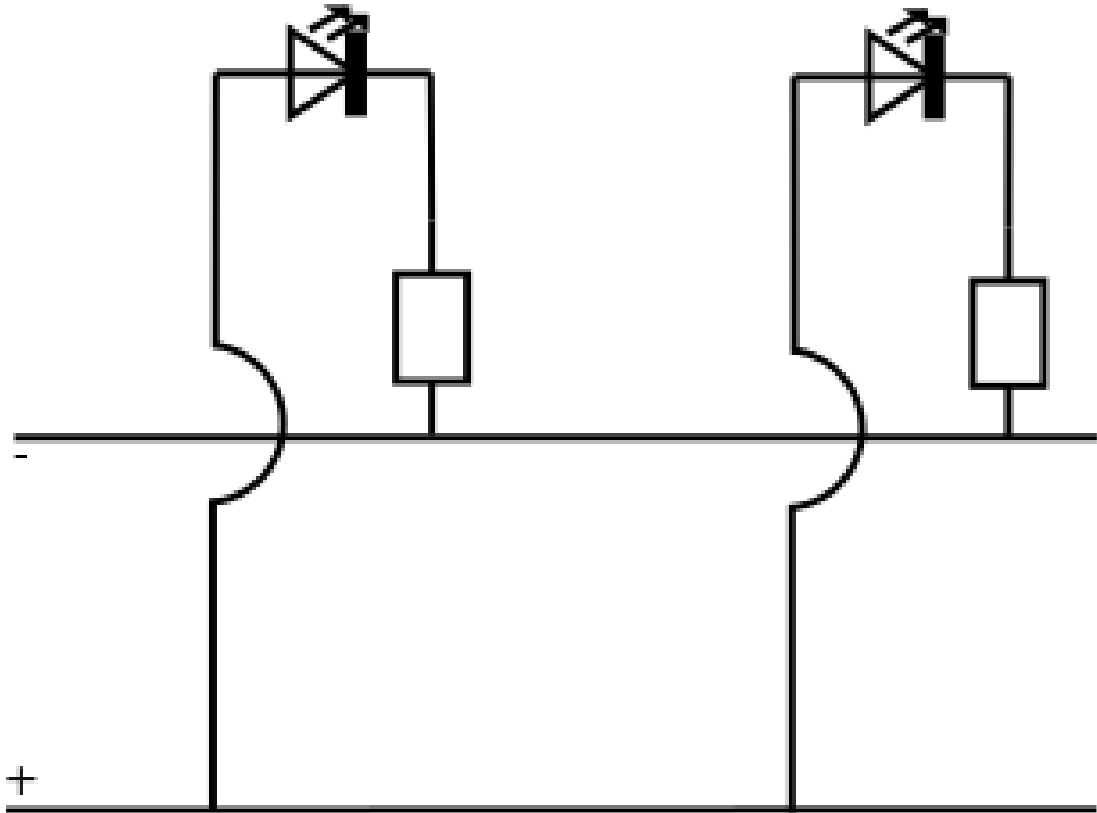
Figure 5.1: The circuit diagram for the near infra-red LED modules. The two power rails can be connected to other modules allowing each LED to be run in parallel.

to be daisy chained together. This design allows multiple boards to be easily connected or disconnected from the system with minimal effort, as each LED in the chain runs in parallel this can continue until the power supply reaches capacity. Given the low draw from the LED's in practise there is no upper limit to how many units can be connected. The circuit diagram for the LED modules is given in Figure 5.1. LED modules were placed to ensure even illumination of the plate from multiple directions where possible. Due to space and temperature constraints front lighting was used rather than back lighting. While back lighting would produce a clearer image the amount of lights required to produce even illumination over the area of the plate could cause the plate to overheat.

5.3 Computer vision techniques

Rather than create a new system for analysis of multiple roots the computer vision method from the ROTATO system was adapted for plates containing multiple roots, this allowed code reuse and simplified debugging and testing.

Like the ROTATO vision system the computer vision system has the following steps.

1. The image is converted to grayscale by taking the green colour channel.

2. Background normalisation is performed by taking the difference between each pixel and its local neighbourhood.

3. The image is thresholded.

4. Morphological closing is done to fill in gaps in the root.

5. Skeletonisation is performed and skeleton end-points are used to get tip position.

6. Tip angle is measured, either from the skeleton or the tip area.

As multiple roots are present in the image and there is no reliable automated method of distinguishing roots of interest from other objects in the image (whether that's other roots or non-root features) manual selection of root tips is needed. When a set of time-lapse images is selected the first image is loaded. The user is then prompted to select the root tips of interest using the mouse. Each time a subsequent image is analysed the tips are matched to the closest selected positions, and the root tip position is updated. This allows the system to track the movement of a root tip throughout the time-lapse.

5.3.1 Challenges

Some of the challenges presented by automated root tracking have been covered previously (section 3.3.3) however tracking multiple roots presents some new dif-

95

ficulties not present in the ROTATO system.

The most obvious problem is in matching multiple root tips to their previous positions. In the current system a simple nearest neighbour method is used to match tips to their previous positions. This is surprisingly robust, although a maximum distance threshold is put in place to ensure that the tip position does not change if the tip is lost or if two roots collide.

Possibly the largest challenge to accurate analysis is the limited resolution available for whole plate imaging. As shown in table 3.1 decreased resolution necessarily leads to a reduced accuracy in angle detection, with the current imaging system the length of the tip to the beginning of the elongation zone is approximately 12 pixels, in practise using an ideal root this gives us an accuracy of $\pm 2.5°$, see Figure 5.2. However this assumes an ideal root and perfect segmentation, due to the relatively low resolution of the images even small errors in segmentation can significantly affect the angle detected. Even errors in the ideal segmentation due to rotation of the image are sufficient to produce significant deviations in the detected angle.

A more unexpected problem lies in the depth of field used when imaging whole plates. The low depth of field of the microscope used to image single roots on the ROTATO system has the beneficial side effect of blurring out any background features, such as irregularities in the backing material and condensation on the plates lid. Unfortunately when imaging the whole root the depth of field is sufficient to keep these unwanted features sharply in focus. When features such as condensation overlap with the root tip it becomes extremely difficult to correctly determine the root outline, and as such the root tip angle.

5.4 Results

The vision system was tested on the same data-set presented in chapter 4, consisting of 368 roots reoriented to angles between 30° and 170°. Over the data-set as a whole we see similar average bend rates in the automated analysis as we do

A.

B.
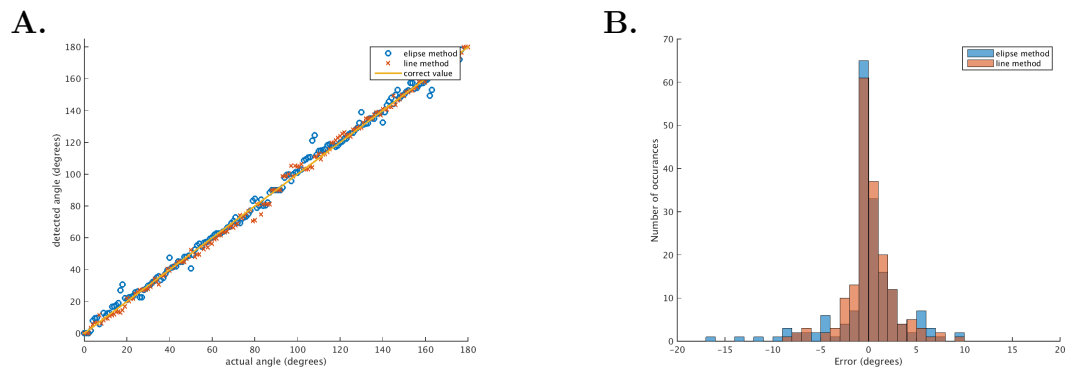
Figure 5.2: **A.** Accuracy of angle detection for an ideal root. A virtual root was created and rotated to a given angle, this was then compared to the value returned when the root was passed to the computer vision angle detection system. Two angle detection methods have been tested, on an ideal root using the centre line of the root is superior to using the outline to determine angle. This is not always the case when the root is not well formed. **B.** Error in the angle detection for an ideal root. A virtual root was created and rotated to a given angle, this was then compared to the value returned when the root was passed to the computer vision angle detection system. Two angle detection methods have been tested, on an ideal root using the centre line of the root is superior to using the outline to determine angle, with a mean error of 2.5° compared to 3.8°. Both methods appear to follow a heavy tailed distribution with generally good accuracy and infrequent but very poor outliers.

97

in the manual, with a bend rate of approximately $-0.0062 \cdot \theta$ ($\frac{\circ}{minute}$) compared to $-0.0053 \cdot \theta$ ($\frac{\circ}{minute}$) for the manual measurements below $130°$ (see Figure 5.3).

Interestingly we do not see a decrease in bend rate above $130°$. This could be a consequence of the noisiness of the automated results. It is clear when looking at the distribution of bend rates (Figure 5.3) than while the mean bend rate may be similar we are seeing a much broader distribution when using the automated angle detection. If we are seeing an increase in the noise of measurements this may mask the decrease in bend rates seen at higher angles. As the data at high angles is relatively sparse a large proportion of the measurements at higher angles may be due to peaks in the noise around lower angled roots. Regression to the mean would then cause a disproportionately high number of large bends to be reported.

A large part of the increased range of bend rates seen may be down to a combination of increased measurement rate and relatively low resolution images. Due to the large number of roots being measured simultaneously each root takes up significantly less space in the image. Although the images themselves are high resolution (36MP, 7360x4912), the typical length from root tip to differentiation zone is only around 12 pixels. Using an ideal root segmentation we are only able to accurately identify the root tip angle to within approximately $2.5°$, giving us a lower bound on noise of at least that. This combined with the lower noise reduction during normalisation due to a higher measurement frequency (for more details see section 6.4.2) could explain the apparent increase in the variation in bend rates.

When comparing measurements at the level of individual plates the results are highly variable. Due to the timing involved much of the data set was collected before the vision system was developed. In many cases the images produces were, while good enough for manual measurement, not of sufficient quality to allow automated angle measurement. Reasons for this include inconsistent or dim lighting conditions, imperfectly focused images, and objects such as condensation on the plate. Fig. 5.5 demonstrates some untrackable images. Of the 33 plates analysed 11 were not able to be analysed, of the remaining 22 plates not all roots
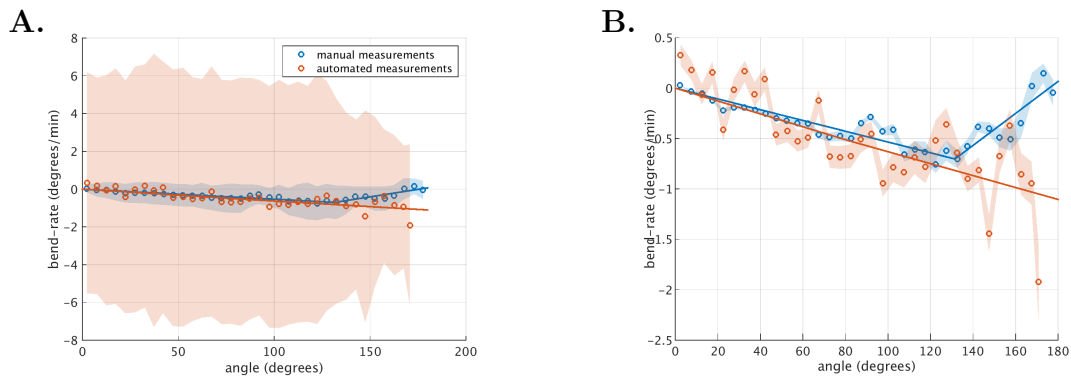
Figure 5.3: **A.** Angle against bend rate for roots reoriented to between 30° and 170°. Shaded areas show standard deviation. Based off 13194 manual measurements and $\approx 130{,}000$ automated measurements from 370 roots. **B.** Angle against bend rate for roots reoriented to between 30° and 170°. Based off 13194 manual measurements and $\approx 130{,}000$ automated measurements from 370 roots. Shaded areas show SEM but the number of points per bin varies.

were able to be tracked, in total including the discarded plates 25% of roots could not be analysed.

However when sufficient care is taken to ensure good image quality, as shown in Figure 5.6 and 5.7, the results closely match the manual data (Figure 5.8). In general however there is a tendency to overestimate the angle compared to the manual measurements (Figure 5.8), particuarly in cases where the image quality is marginal. This is especially clear when looking at the mean angle of the experimental groups. Fig. 5.4 shows the mean angle over time for the roots grouped by initial reorientation angle (excluding plates with no successful measurements), it is clear that the automated system is not able accurately measure root angle when run on the dataset as a whole.

5.5   Discussion

While the system is able to produce good results under ideal conditions, and with good image quality, it is not robust enough to automate the analysis of the
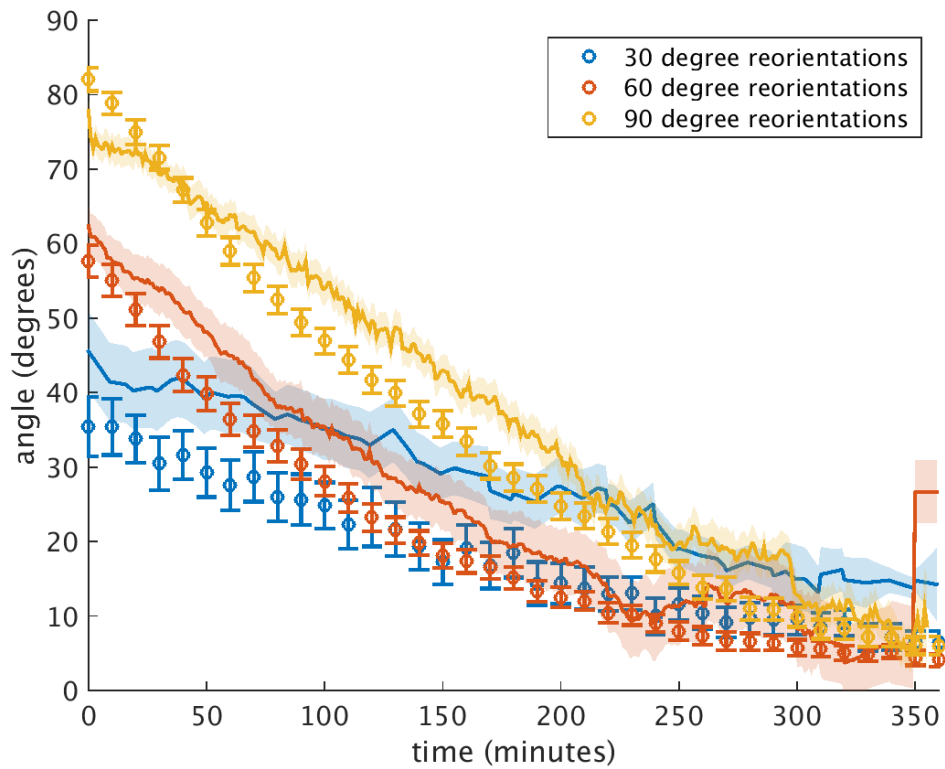
Figure 5.4: Mean angle over time for 30°, 60°, and 90° reorientations. Points represent manual measurements and lines automated measurements. Only plates that were both manually measured and successfully automated are included in this comparison. N = 237 automated roots, 296 manually measured roots, error bars and shaded regions are SEM.
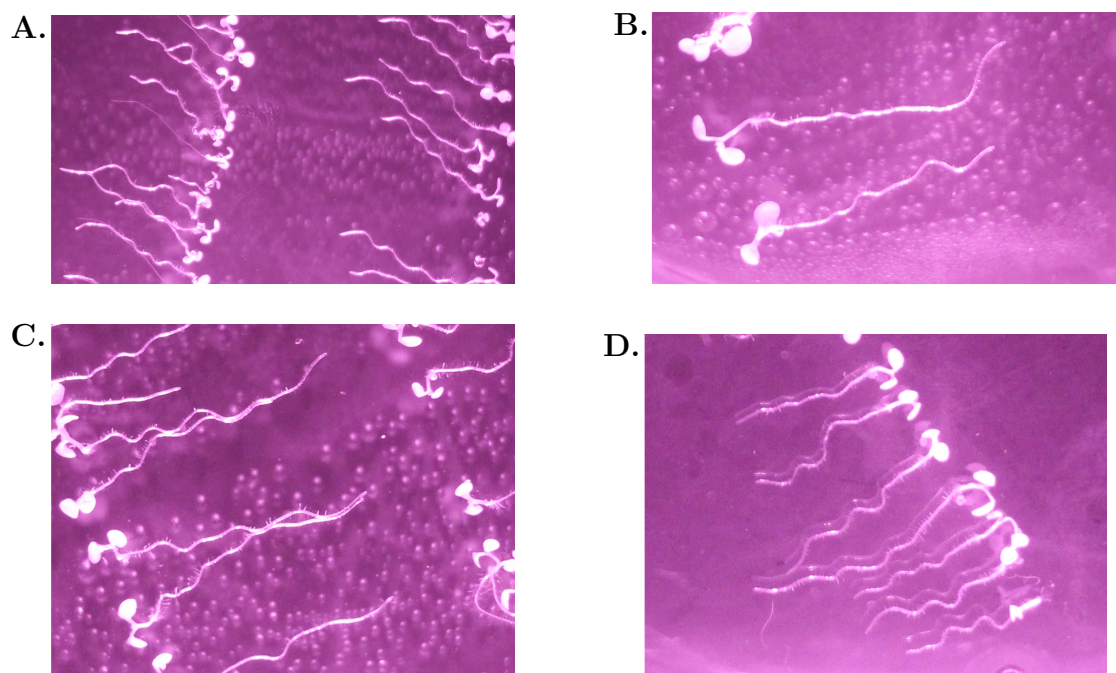
Figure 5.5: Examples of poor images. In sub-figures **A**-**C** condensation makes the roots difficult to track. In **D** The lighting has caused reflections from the plate lib to be visible, this obscures the roots, creates false roots, and makes tracking impossible.
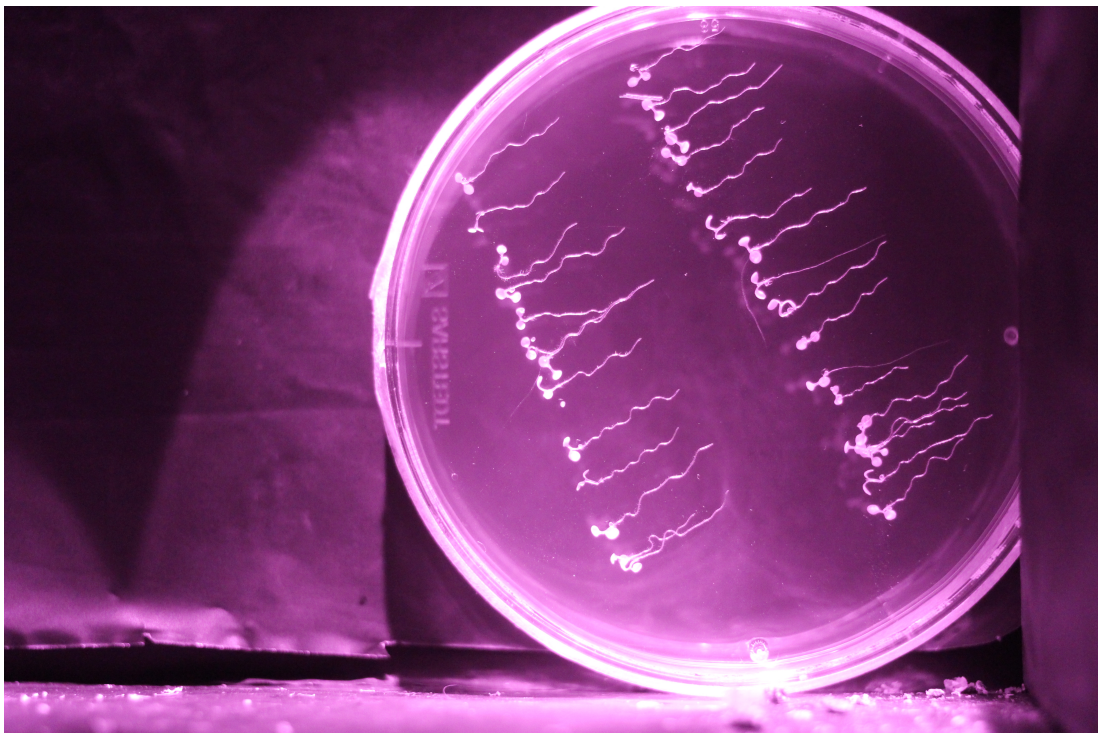
Figure 5.6: A clear image allows for accurate image analysis. The the roots are of high contrast and sharply in focus, there are no other objects or condensation on the plate. While the lighting is not uniform it is locally consistent.

Figure 5.7: These roots contrast sharply with the image background and maintain good contrast along the entire length of the root. Additionally the background is uniform and relatively clear.
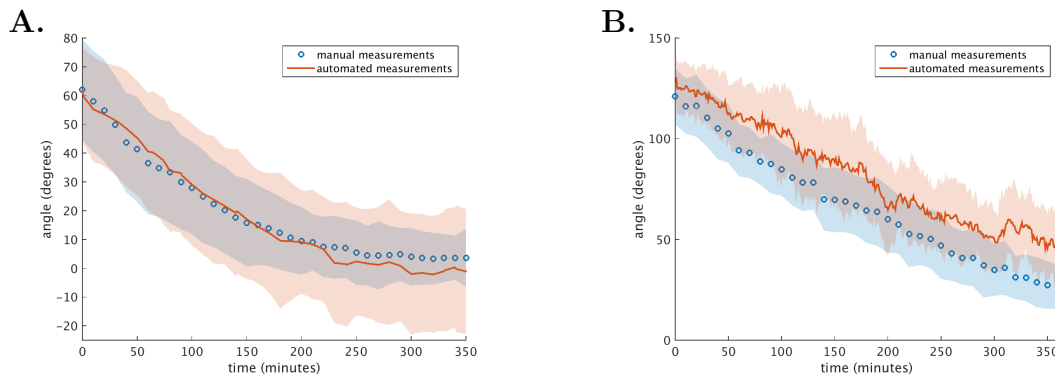
Figure 5.8: **A.** On good quality images the automated results agree well with the manual measurements. Points and line show the mean value from a single experiment, the shaded region shows standard deviation. N = 23. **B.** There is a tendency to overestimate the angle compared to manual measurements, this can be due to loss of contrast as the root approaches vertical causing the tip to be lost. Points and line show the mean value from a single experiment, the shaded region shows standard deviation. N = 28.

existing dataset. There are a number of problems when analysing whole plate images rather than the single root images of the ROTATO system.

1. Low contrast around the root tip can lead to loss of the tip, producing erroneous high angles to be reported.

2. Small roots limit the angular resolution of the tip detection.

3. Condensation and other features on the plate can obscure the root tip, or be erroneously identified as the root tip.

4. Collisions between roots can cause the root tip to be lost.

These problems are mostly able to be mitigated if sufficient care is taken to properly prepare the system before imaging, however for more reliable results changes to the physical setup would be beneficial.

In the initial experimental setup the lighting was placed above and slightly in front of the plate. This top lighting reduced glare as opposed to front lighting, and the oblique angle of the lighting produced more even illumination than was possible
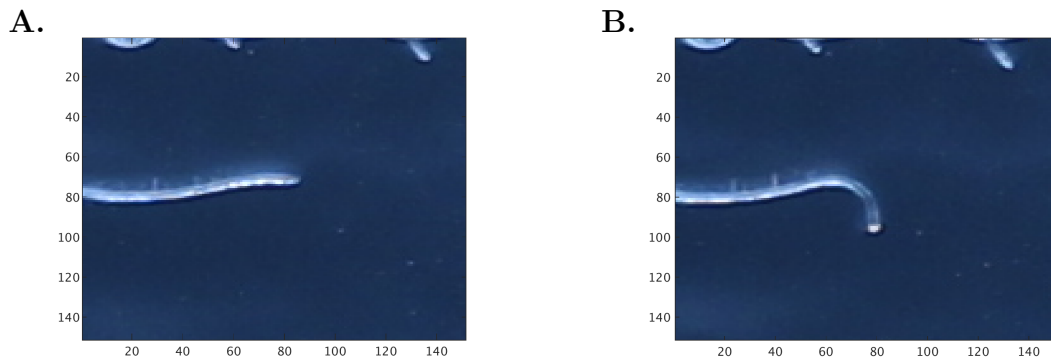
Figure 5.9: **A.** At initial reorientation the root is near horizontal with uniform contrast along its length. **B.** Over time as the root tip approaches the vertical contrast is lost. In this case there is an area of low contrast just behind the root tip, this makes analysis difficult as the tip risks being lost.

using the same lights in a back-lighting setup. However as the light was coming from the top it highlighted horizontal objects which lie perpendicular to the path of the light. While this allows for good detection of roots near the horizontal which contrast strongly with the background, as the root tip approaches the vertical the contrast decreases. This is illustrated in figure 5.9, where a root which is clearly defined near the beginning of a time-lapse series loses contrast as it approaches the vertical. This can be compensated for by reducing the detection threshold, either globally or locally in the region of the tip, but this comes at the cost of over-segmentation. In later experiments the position of the lighting was adjusted to produce more even illumination at all angles. While this mitigated the problem by increasing contrast at lower angles not all roots were sufficiently illuminated to produce reliable segmentation. The system as a whole could be dramatically improved by the introduction of back-lighting which can produce very high contrast images reliably and at all angles. Preliminary tests demonstrate that with good back-lighting such images can be produced (Figure 5.10) implementing such a system would require a significant rebuild to the physical system. Nevertheless it promises a dramatic improvement in image quality and measurement accuracy.

Figure 5.10: A backlit image can produce extremely good contrast and consistency, this allows highly accurate analysis.

While the size of the root in the image limits the accuracy possible when measuring tip angle, this is unlikely to cause systematic errors as seen in the results. However it still would be beneficial to increase the resolvable accuracy as this would allow for more accurate bend rates to be measured. This is particulary important given the high measurement frequency desirable in a system such as this. While increasing the resolution would help improve the accuracy, this is secondary to the problems involved in accurately segmenting the roots at the existing resolution.

As mentioned previously good sample preparation is key to good automated analysis. As the vision system is fundamentally based on detecting light objects on a dark background, the presence of foreign light objects causes serious problems (Figs. 5.11,5.12). At a software level these can be mitigated by a post-processing step. The system is capable of reliably filtering out many sources of error by removing small connected regions from the segmented image (see Figure 5.13), when these objects overlap with the root tip they become very difficult to separate from the root, as shown in figure 5.14. While this problem is easy to solve once it has been identified it does present serious difficulties when analysing older images which may have been taken before the problem was apparent.

As tip detection is performed by looking for the endpoints of a root skeleton, collisions between roots can cause the tip to be lost. If a root collides with another root the skeletons of the two roots become joined, as shown in figure 5.15. While realistically it may not be valid to measure the behaviour of roots after they collide with each other, in order to discard such roots they need to be accurately identified. Identification of collisions is normally caught by setting limits on the distance a root tip can move between consecutive images. As root growth is slow we not expect a tip to change position by a significant amount in the time between images, when roots collide the root tip may no longer be detected and it is likely that the nearest detected tip is far away relative to the distance a root may grow between images. This method is not infallible however as collisions can occur near the tips of two roots. Even when a collision is successfully detected it represents a loss of data as that root can no longer be accurately measured, both due to the limits of the vision system and due to change in response caused
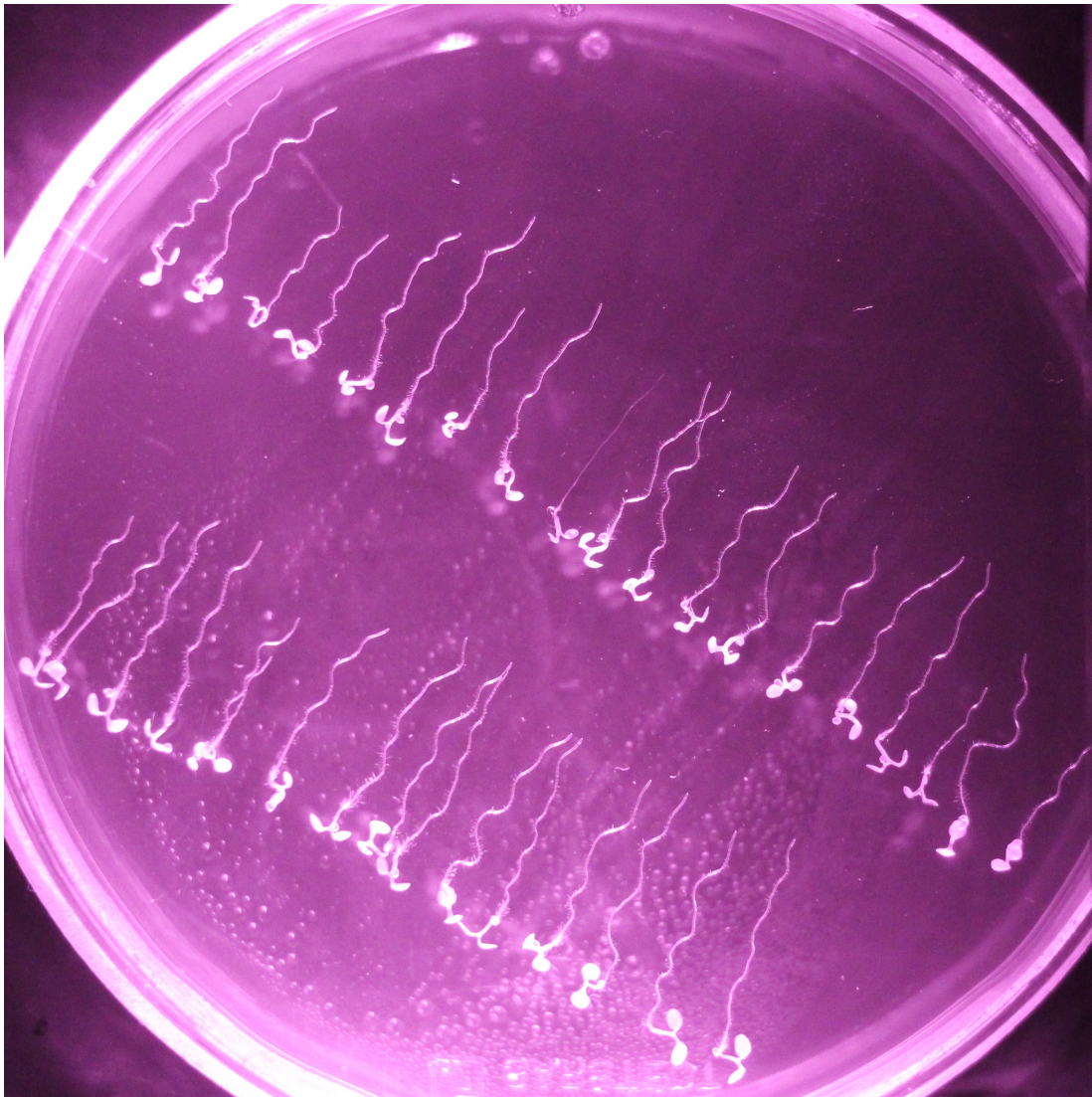
Figure 5.11: There is heavy condensation in the lower portion of the plate. This can be erroneously identified as belonging to a root (subfigure 5.12).
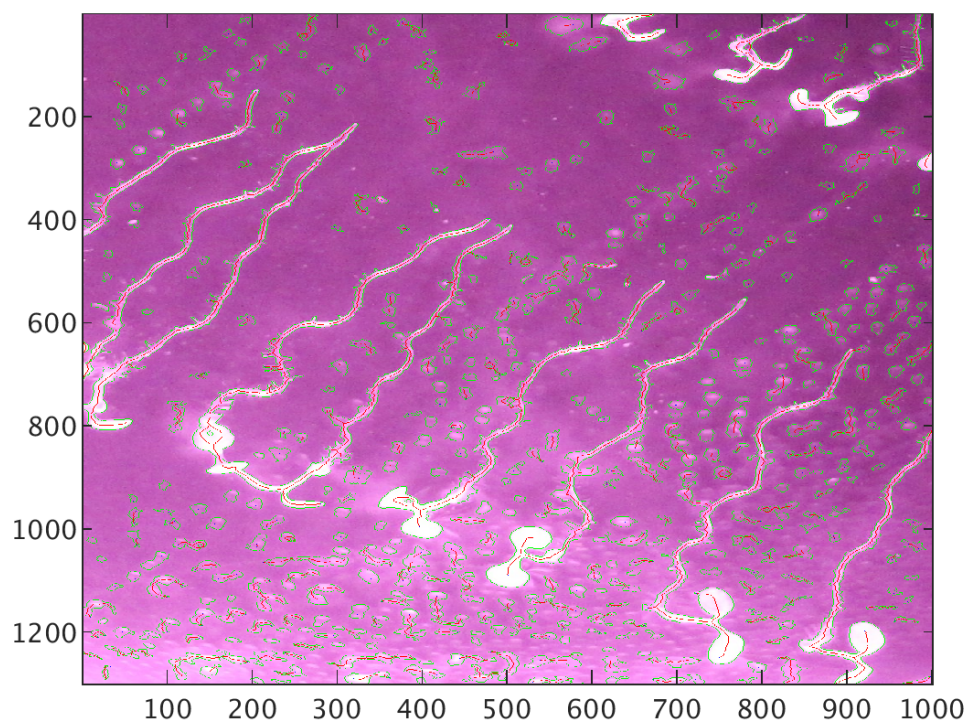
Figure 5.12: Unless post-processing is performed condensation will cause false positives when identifying roots. Root outlines are shown in green, and centre-lines in red.
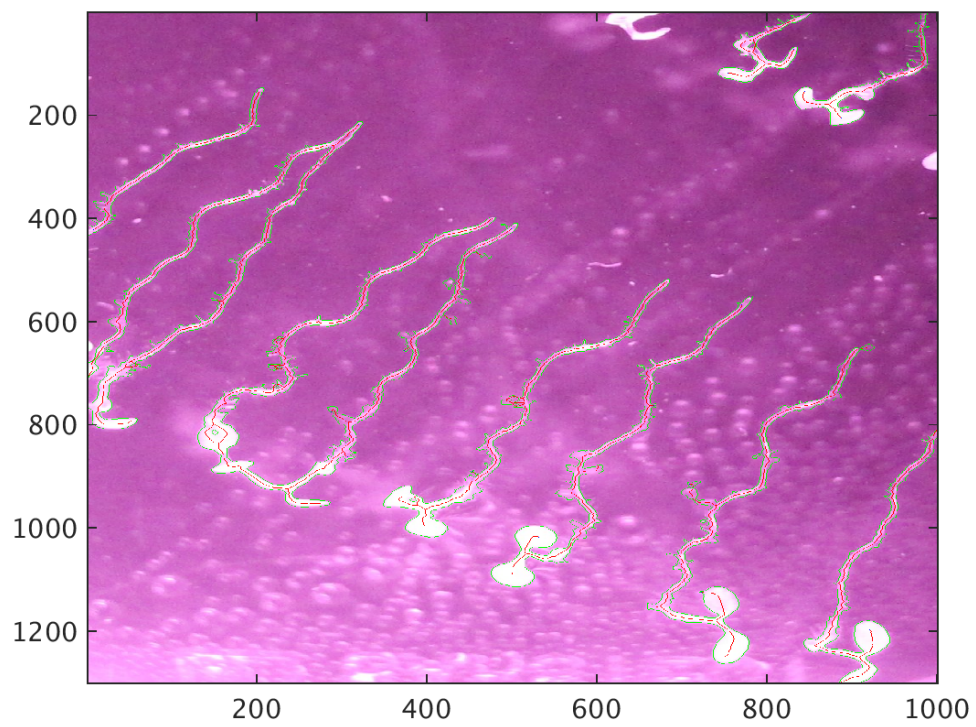
Figure 5.13: After post-processing almost all erroneous detection's have been removed, however condensation close to the root can still disrupt the segmentation (centre and bottom right). Root outlines are shown in green, and centre-lines in red.
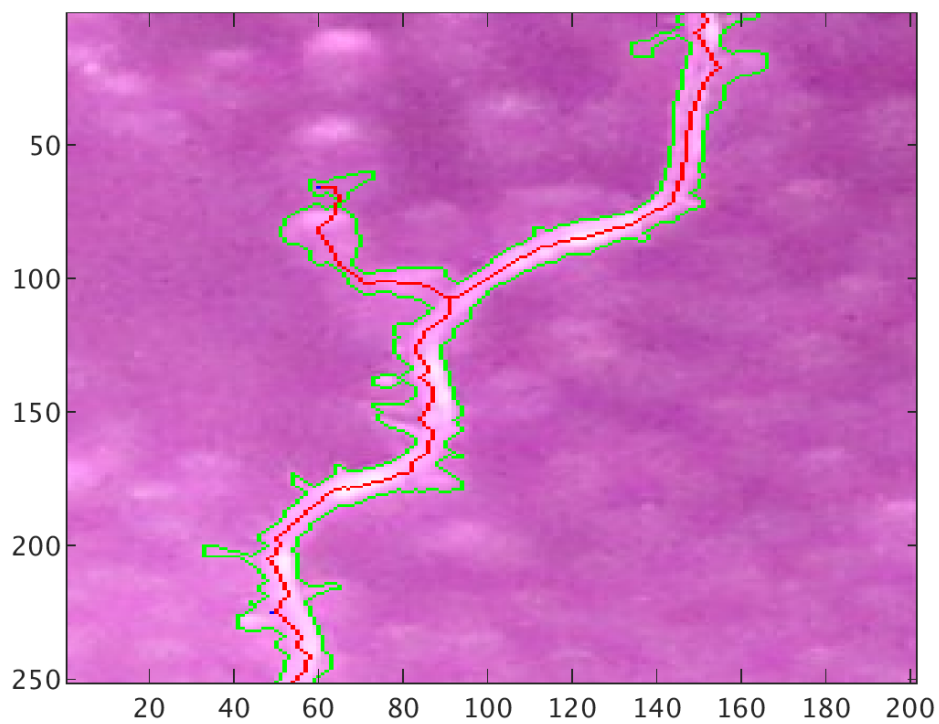
Figure 5.14: Condensation near a root has been misidentified as part of the root (the upper left branch of the segmentation). In this case it will not affect the tip angle as the error occurs far from the root tip (not shown). Root outlines are shown in green, and centre-lines in red. Two false root tips have been identified in blue.
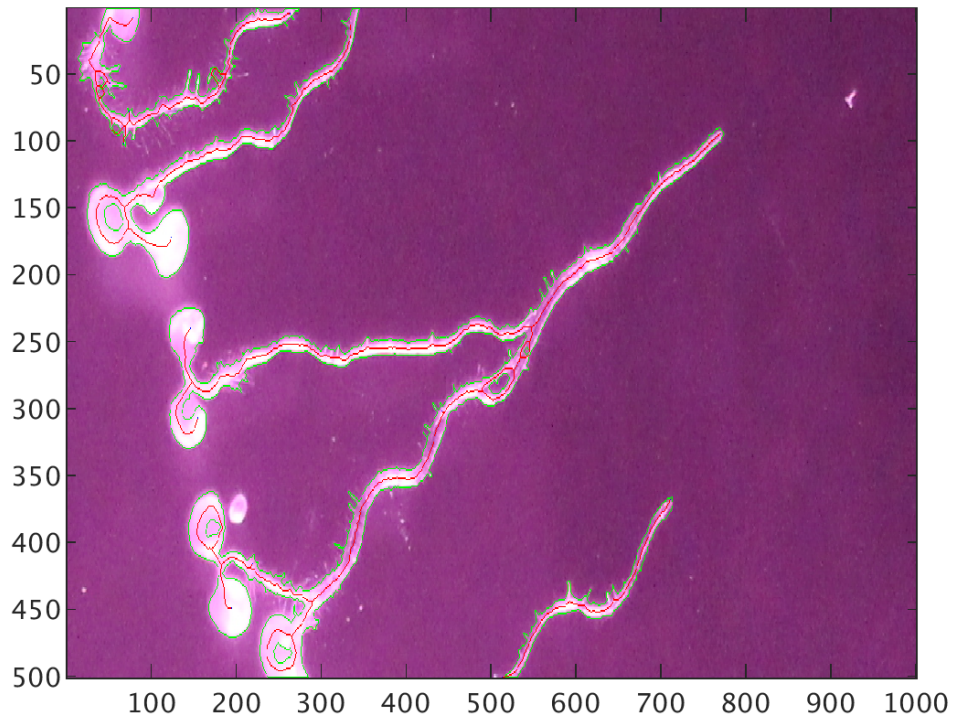
Figure 5.15: Collisions between roots can cause the root tip to be lost. Here three roots have collided causing their skeletons to become joined. Only the longest root is able to be measured. Although it is not necessary or desirable to measure tip angle after collisions, they can cause problems for the tracking system.

by the collision. This problem can be avoided by placing fewer individuals on a plate however this limits the amount of data produced in a single experiment.

Chapter 6

A stochastic model of root gravitropism

6.1   Introduction

Previous attempts to describe gravitropic behaviour have produced models able to describe the expected behaviour of a root or shoot but have not attempted to explain the variation in individual response. As shown earlier, individual root responses can be highly variable and this variation cannot be simply attributed to individual variation alone (section 4.2.2). In this chapter we present a stochastic model of gravitropic behaviour, building on the results obtained in chapter 4. Using this model we are able to describe gravitropic response at the population level; capturing the mean and variance of reorientated roots, both over time and instantaneously, as angle-dependent behaviour. Unlike previous models we are able to place limits on the processes involved in generating gravitropic response such as the time-scales of detection and bending. We hope that this will then be useful in identify a mechanistic basis for behaviour at the organ scale.

6.2 A minimal stochastic model

6.2.1 Model outline

A minimal stochastic model can be built from the following assumptions:

1. Angle-dependent behaviour can be accounted for at the tissue level without explicitly modelling each process involved.

2. Gravitropic behaviour is inherently stochastic.

3. Gravitropic behaviour is angle-dependent.

We have chosen a discrete model where during a given period of time a root has some probability of making a bend. Implicit in this assumption is that there is a complementary probability of the root not bending during this time period. During the course of a gravitropic response we see periods of bending and non-bending that occur on a far faster time scale than could be accounted for by root waving. While it is possible that there is some complicated function which determines the occurrence of bending and non-bending periods during a gravitropic response there is no clear evidence that this is the case. Indeed we have seen no time-dependent patterns in gravitropic response that may indicate periods of bending and not bending occur on a given timescale as might be expected if this was down to some deterministic phenomena.

Given the lack of evidence of time-dependent behaviour and the clear influence of root tip angle on a roots bend-rate we treat the root as having a probability of bending dependent on the roots angle. We assume a linear relationship between bend probability and angle for a number of reasons. Firstly at low angles ($\leq 90°$) a linear model performs as well as other models tested such as the Sine Law (see section 4.2.4). Secondly and perhaps most importantly a linear model provides significantly better predictions for the range of angles between $90°$ and the point of maximum bending at approximately $130°$. Lastly at angles above $130°$ we have seen good results when using a bi-linear fit (section 4.2.5). While we must be careful when using the bi-linear fit due to the reasons outlined previously, it is a

powerful tool when used to determine the limits within which a linear model can be applied.

In order to keep the model tractable we are assuming that when a bend occurs it is of a given size. This assumption has largely been made in order to simplify the model, it being the minimal assumption necessary to produce predictive results. However given our understanding of the mechanics of bending this assumption is reasonable. If, as has been suggested, elongation rate follows a sigmoidal pattern (see section 1.2.2) in response to auxin concentration we can approximate this using a step function (Cleland, 1972) which produces 2 discrete growth rates. We would expect straight growth when both the upper and lower side are growing at the same rate, and for bending to occur when the sides are growing at different rates. As we have two growth rates there is only a single positive magnitude of growth rate difference, over a given time-step this should produce a bend of a known side dependent on the difference between the two possible growth rates.

Given these assumptions we have formulated a discrete model with the following parameters.

1. δt = The time step during which a bend may occur, conceptually equivalent to the time a bend event takes to unfold. Measured in minutes.

2. Δ = The size of a single bend event in degrees.

3. p = The proportionality coefficient giving the probability of bending at a given angle. $P(bend) = p \cdot \theta = \frac{\lambda \delta t}{\Delta}$, where $\lambda = \theta'$.

By assuming our bend probability is directly proportional to the current angle we set the GSA to 0 (as $p \cdot 0 = 0$). This limits the applicability of the model to primary organs where the GSA is equal to 0. In order to describe non-vertical growth either this assumption would have to be modified or another source of bending, such as from the AGO, would have to be included. We have neglected to include upwards bending in the model despite seeing cases of upwards bending in the data. This is done partly for simplicity, but also because it is not clear whether upwards bending in roots with a GSA of 0 is due to gravitropic behaviour, or other non-gravitropic responses such as waving or skewing. In roots left at the

GSA, root waving will produce both upwards and downwards (when the root is not vertically downwards already) bending, we would expect this to explain at least some of the upwards bending observed after reorientation. We also cannot discount mechanical effects from root-gel interactions as a source of upwards bending. While is is clear that for roots with a non-vertical GSA upwards bending would have to be included, as when reorientated these roots are able to bend upwards to their GSA, but in this case it is safe to put them aside. While we would expect some latency in response we have treated this as sufficiently small to be discarded. In this respect our model is similar to the Sine Law which assumes instantaneous response. As long as the time-step used is sufficiently large to account for the delay in detection and auxin transport this seems reasonable.It has been shown that gravity perception is extremely fast with presentation times of as little as 10 seconds in Arabidopsis (Kiss et al., 1989). Given a distance from the columella to the elongation zone of approximately $500\mu m$ (Verbelen et al., 2006), and an auxin transport velocity of about $8mm/hour$ (Kramer et al., 2011) we would expect a lower bound of around 3-4 minutes for the response time, plus the time for cellular elongation to occur.

6.2.2 Expected behaviour

From the parameters above we can calculate the mean response of a root over both time and angle. Given a root at angle θ and time t, the probability of bending in time δt is equal to $p \cdot \theta$. If a bend occurs the angle at time $t + \delta t$ is equal to $\theta_t - \Delta$, otherwise the angle is equal to θ_t. The mean angle at time $t + \delta t$ is then given by Equation (6.1), if we approximate this to a continuous model the mean bend rate is given by (6.2). It is immediately obvious from (6.2) that the bend-rate is proportional to the angle as would be expected from a linear model. Given a continuous model we would then expect the mean angle to follow the exponential decay given by Equation (6.3), which follows naturally from Equation 6.2.

However as we are working with discrete time we can obtain the equivalent to equation (6.2) by following the steps in equation (6.4). This results in the geo-

metric decay shown in Equation (6.4).

In practice with a small Δ, both the continuous and discrete solutions given by equations (6.3) and (6.5) produce very similar results. Given a Δ of 10° and a probability of bending equal to 1 at 180°, equations (6.3) and (6.5) differ by less than 0.5° at the most divergent (see Figure 6.1). This makes the exponential decay given by equation (6.3) a very useful approximation of the predicted model mean. As all three parameters can be combined into a single parameter grouping, by fitting λ we are able to constrain the parameter space available to the model, which proves to be useful when model fitting. This reduces our mean response to a single parameter model similar to the unmodified Sine Law, however unlike the Sine Law this is able to explain bending above 90° without requiring additional parameters.

Unlike the exponential approximation we cannot reduce the geometric equation to a single parameter model, as we would expect the mean behaviour to approximate the exponential model we are not able to extract the model parameters δt, Δ, and p from the mean behaviour although we can constrain the parameter values such that $\lambda = \frac{\Delta \cdot p}{\delta t}$ where λ can be obtained from the mean response. In order to estimate the model parameters we must look at other properties of the distribution of root angles over time, particularly the variance.

$$\overline{\theta}_{t+\delta t} = \overline{\theta}_t - \Delta p \cdot \overline{\theta}_t \tag{6.1}$$

$$\frac{\delta \overline{\theta}}{\delta t} = \frac{(\Delta \cdot p) \cdot \overline{\theta}}{\delta t} \tag{6.2}$$

$$\lim_{\delta t \to 0} \overline{\theta}_t = \theta_0 \cdot e^{-\lambda t}, \quad \lambda = \frac{\Delta \cdot p}{\delta t} \tag{6.3}$$
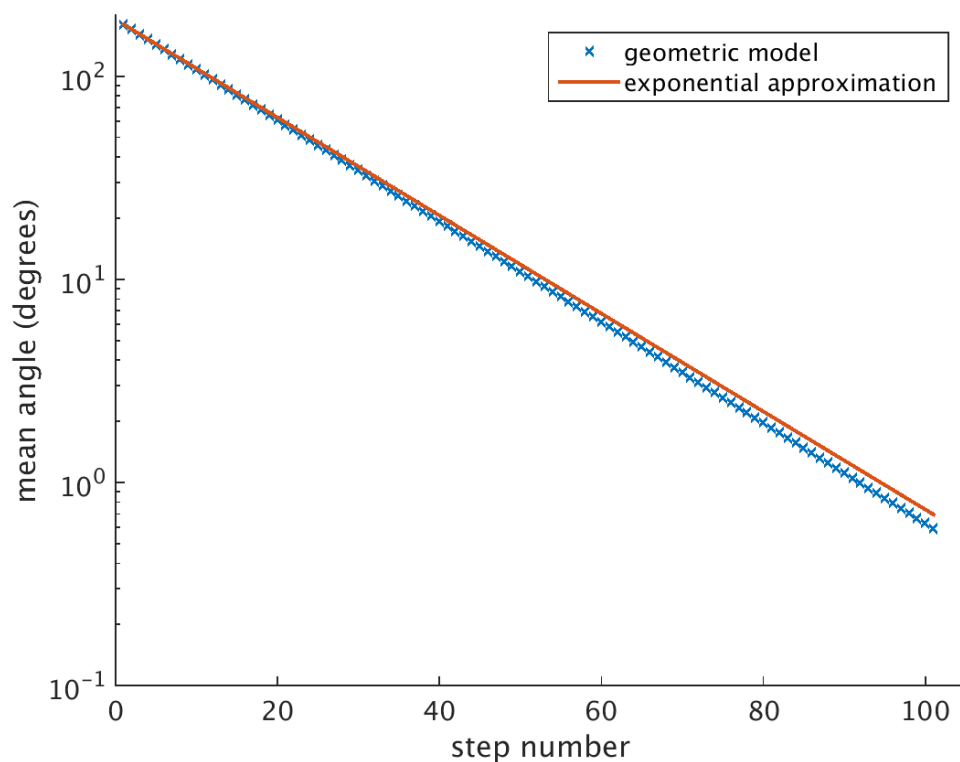
Figure 6.1: Comparison between the geometric and exponential approximation with reasonable test parameters ($p = \frac{1}{180}, \Delta = 10$). The difference is less than 0.5° at the greatest point.

$$
\begin{aligned}
\overline{\theta}_{t+\delta t} &= P(\neg\text{bend}) \cdot \overline{\theta}_t + P(\text{bend}) \cdot (mean\theta_t - \Delta) \\
&= (1 - p \cdot \overline{\theta}_t) \cdot \overline{\theta}_t + (p \cdot \overline{\theta}_t) \cdot (\overline{\theta}_t - \Delta) \\
&= (1 - p \cdot \Delta) \cdot \overline{\theta}_t \quad (6.4)
\end{aligned}
$$

$$
\overline{\theta}_t = \theta_0 \cdot (1 - p \cdot \Delta)^{\frac{t}{\delta t}} \tag{6.5}
$$

6.2.3 Angle-dependent variation

At any given angle we would expect there to be a probability $p \cdot \theta$ of bending. Over small changes in angle where we θ and thus $P(bend)$ are can be treated as constant. Bend decisions can then be treated as independent. In this case over a given amount of time t, N independent bend decisions could be made. This situation is analogous to independent coin tosses, in that the number of bend decisions made will follow a binomial distribution. The variance in response over a given time frame, t, is then given by the binomial variance equation (Equation 6.6).

If we take the Equation (6.6) and consider a single step of the model, we arrive at Equation (6.7) which represents the variance in the bend-rate of a root. It is clear from this formulation that the bend size, Δ, is the most significant contributor to the predicted variance, as for any θ where $(P = p \cdot \theta, \quad 0 \leq P \leq 1)$, then $P \cdot (1 - P)$ is bounded at 0.25 where $P = 0.5$. As the bend size is unbounded it will therefore be the largest contribution to the angle-dependent variance for any $\Delta > 0.5°$. As the angle over time is given by the integral of the bend-rate over time given some initial condition, we can see that the bend size Δ is also the primary contributor to the variance as a function of time. Equation 6.7 gives us the variance in response per time-step, in practise we will normalise bend rates to degrees per minute to give comparable values to measurement data.

While we can approximate the bending over small numbers of steps as binomial, as each bend results in a change in the probability of bending the resulting distribution is not binomial (Butler and Stephens, 1993). When fitting over time we cannot make this approximation and the variance must be calculated numerically as shown in section 6.2.4.

$$\sigma_\theta^2 = \Delta^2 \cdot P \cdot (1 - P) \cdot N, \quad N = \frac{t}{\delta t}, \quad P = \theta \cdot p \tag{6.6}$$

$$\sigma_\theta^2 = \Delta^2 \cdot (\theta \cdot p) \cdot (1 - \theta \cdot p) \tag{6.7}$$

Given some error ϵ in measurement we would expect to see the variance given by equation (6.8), as we normalise by dividing by the time-step . Over large measurement times our measurement error tends towards zero, however in order to assume a binomial distribution of bends we are assuming a constant probability of bending and so this only holds given a small change in angle. Clearly we cannot then just use a long measurement time to reduce the effects of error, neither can we necessarily assume that over small time scales the correspondingly small angle changes will be significantly greater than the error in measurement. This problem can be addressed by simulations where we would expect that over longer time periods the error in recorded bend rate will match that observed in the data, but over short measurement periods we would expect greater than predicted variation.

$$\sigma_\theta^2 = \Delta^2 \cdot P \cdot (1 - P) + \epsilon^2 t, \quad P = \theta \cdot p \tag{6.8}$$

6.2.4 Variation in response

While the expected behaviour and instantaneous variance are straightforward to calculate, the variance over a large number of steps is much more difficult. Previously we have made the approximation that the probability of bending remains roughly constant. This allows us treat the distribution of bends as binomial which greatly simplifies things. However as each bend changes the changes the probability of future bends we cannot treat each bend decision as independent. By treating the model as a Markov chain we can calculate the probability of any given number of bends occurring in a given number of steps.

The change in probability, P, after a single bend is equal to Δp. For a root with a starting probability of bending P_0, and a change in probability δP the probability of making N bends, where $N \leq \frac{P_0}{\delta P}$, in M steps is given by Equation (6.9). The angle after N bends is then equal to $\theta_0 - \Delta \cdot N$. This allows us to calculate the expected probability distribution for a root's position after a given amount of time, and so calculate the mean and variance of a population starting from a given angle. The mean angle given by this method is identical to that given by

Equation (6.5).

If we treat each root as an infinite population of roots all at the same initial angle, we can describe the proportion of roots at each angle obtainable by the model as a vector of 0's with a 1 at the point in the vector corresponding to the starting angle. As the model does not include upwards bending the starting angle is the maximum achievable angle and can be set to the first position in the vector. Our starting population is then represented by the vector $1, 0, 0, \cdots$, corresponding to the vector term in Equation (6.9). At any angle the root can either bend by Δ or not bend, therefore after each step there are 2 possible angles the root can occupy. The proportions of the population after the first step will consist of $p \cdot \theta_0$ which have bend and are now at the angle $\theta_0 - \Delta$, and $1 - (p \cdot \theta_0)$ which are still at the initial angle. After each new step, or given some other distribution of angles, the proportion of roots at a given angle is equal to the proportion of roots previously at that angle which did not bend (the previous proportion multiplied by $(1 - p \cdot \theta)$) plus the proportion of the roots at just above the angle in question which have now bent down (the previous proportion at $\theta + \Delta$ multiplied by $1 - p \cdot (\theta - \Delta)$). Each row of the matrix term in Equation (6.9) represents these proportions at a given angle. Each time we multiply the initial population distribution vector by the matrix take a single step through the model updating the population distribution as we go. As each row in the matrix represents an angle differing the Δ and we have set the first row to represent the angle θ_0 we can set each θ in the matrix to $\theta_0 - (r \cdot \Delta)$, where r is the row number (counting from 0).

To simplify the calculation given by Eq.6.9 we can do the matrix multiplications first by raising the matrix term to the power M then multiply by the initial distribution. As we started with a distribution vector with only a 1 in the first position this is equivalent to taking the first row of the final matrix. In fact each row in the matrix represents the distribution after a different number of steps, for efficiency we can calculate the final matrix once to obtain the full distribution over each step from 0 to M.

The advantage of calculating the expected distribution numerically is that when dealing with populations of roots at different starting angles we can calculate

the distributions of each root simultaneously and then combine the results into a single distribution. This allows us to easily model the behaviour of real root populations rather than using an idealised model of the population starting with a single starting angle.

$$
P(N|M) = \begin{bmatrix} 1 \\ 0 \\ 0 \\ \vdots \end{bmatrix} \cdot \begin{bmatrix} 1 - p \cdot \theta_0 & p \cdot \theta_0 & 0 & \cdots & \cdots \\ 0 & 1 - p \cdot (\theta_0 - \Delta) & p \cdot (\theta_0 - \Delta) & 0 & \cdots \\ \vdots & \ddots & \ddots & \ddots & \vdots \\ \cdots & \cdots & \cdots & 0 & 1 - p \cdot (\theta_0 - N \cdot \Delta) \end{bmatrix}^M
$$

(6.9)

6.3   Numerical methods

6.3.1   Parameter estimation and model fitting

We can constrain the parameters by making use of the exponential approximation for the mean angle given in Equation (6.3). As the mean angle depends on the parameter group $\frac{\Delta \cdot p}{\delta t}$, while the variance depends primarily on Δ we have chosen to group the parameters into the 2 groups Δ and $\frac{p}{\delta t}$ for fitting, by setting δt to a known value we can reduce the fitting to only p and Δ. Initial values are then given for both p and Δ. Next the value λ is calculated. As we expect angle to be the determining factor in gravitropic behaviour, λ is calculated by fitting to the binned $(\theta, \delta\theta)$ values as shown in section 4.2.2. As we are assuming a linear relationship between angle and bend-rate we know the model will not hold above the angle of maximum response. Therefore a bi-linear fit is used (section 4.2.5) whereby the gradient of the fit below the angle of maximum response is equal to λ. This results in a λ of 0.0059 $°/min$, for comparison we are also able to estimate this value from the proportional bend-rates $\left(\frac{\delta\theta}{\theta}\right)$, or a fit over time. At low angles however fitting over time becomes less reliable as both measurement error and natural variation make a proportionally greater contribution to the

Method	$\lambda(°/min)$
bend-rate (bi-linear)	0.0059
bend-rate (linear, $\theta \leq 90$)	-0.0057
proportional bend rate (median)	-0.0058
mean over time (4 hours)	-0.0057
mean over time (6 hours)	-0.0061

Table 6.1: Comparison of the parameter group $\lambda = \frac{\Delta \cdot p}{\delta t}$ obtained via different methods. A bi-linear fit to bend-rate as a function of angle is used for model fitting.

resulting fit. In fact as the probability of bending approaches 0 the relative variance, given by the coefficient of variation for a single time step approaches infinity (Equation 6.10) making estimation of mean increasingly difficult. Because of this we get more accurate results only fitting to the first 4 hours of response where the mean angles are greater. The resulting values are given in table 6.1.

$$\frac{\sigma}{\mu} = \sqrt{\frac{1-p}{n \cdot p}} \tag{6.10}$$

Given a λ and initial values for both Δ and δt we can then set p subject to Equation (6.11). This ensures the model is able to fit the mean bend-rate and angle of the data over time. We then perform a least-squares fit on the parameter Δ, which minimises the difference between the expected variance given Δ and the observed variance. When doing this we update the probability p such that λ remain constant. Determining a suitable δt is difficult as we have no way of directly measuring it. The final value of Δ puts an upper bound on the value as if the time-step is too large the probability must become greater than 1 at high angles if λ is to be maintained at the measured value. There must also be a lower bound given by auxin transport speeds and the speed of response, but we are not able to quantify this accurately. It appears however, that the size of δt affects the magnitude of finite data effects. While this is difficult to quantify as, by their nature, finite data effects disappear when large amounts of data is tested, we have set δt at 7 minutes. This is sufficient time for the physical processes involved to occur, is below the upper bound set by Δ and λ, and appears to produce good

fits to the data.

$$p = \frac{\lambda \cdot \delta t}{\Delta}; \quad\quad\quad (6.11)$$

When fitting to multiple experimental batches, we cannot simply combine both sets of roots into a single experiment. Due to unavoidable differences in conditions it is possible that some batches may display different behaviour to others. We would expect over a large number of experiments that both faster and slower behaviour will be present and that the mean behaviour will be unaffected, the increase in sample size will also compensate for any small variations. However if we combine experimental batches with differing means we will increase the variance of the resulting set. When fitting to multiple experimental batches the fit is performed so as to minimise the sum of the squared residuals over all batches.

The final fitted parameters for our dataset are as follows.

- $\delta t = 7$ minutes

- $p = 0.0049$

- $\Delta = 8.4°$

This gives a λ of 0.0059.

6.3.2   Model alignment

When comparing the behaviour of different root populations with differing starting angles it is useful to have a method of comparing these different experiments to a single unified model. While this can be done by looking at the response as a function of angle, as done in chapter 4, the binning process weights different angles differently depending on the number of measurements taken at that angle. This can be problematic for visualisation as the weighting is not easily determined from the figures. Additionally, as the raw data is taken in the form of angle measurements over time, a time-dependent visualisation is in some ways

more natural than an angle-dependent visualisation.

Assuming no time-dependence or hysteresis in the system (as shown in section 4.2.3) we would expect a root behaving at angle θ to display the same behaviour no matter its time since reorientation or original reorientation angle. We can then treat a root reorientated to angle θ and at time 0 the same as a root reorientated to $\theta + \delta\theta$ and at some time t. In effect, each root can be treated as enacting a portion of the response of an ideal root originally reorientated to $180°$ (excluding roots reorientated to above $130°$)), and whose behaviour is given by Equation (6.12). For any set of measurements in the form (θ, t), we can then choose some offset t_{offset} such that we minimise the difference between the measured results and the ideal path. Given a least squares fit we aim to minimise the equation given in Eq. 6.13. We are effectively shifting each set of measurements along in time in order to align them with the expected exponential as well as possible. When λ is known this sum can be minimised by any standard solver, we have implemented a modified Newton's method for this, when λ is not known however it can be estimated from the angle-dependent bend rate. As we are fitting over time more accurate fits for λ are often obtained by running a second pass after the initial alignment and fitting the exponential equation (6.12) to the newly aligned measurements, from this we can obtain a second estimate of λ and re-fit the alignments.

While this method is a good visualisation tool it does include the addition of a degree of freedom for every set of measurements aligned and so should not be solely relied upon.

$$\theta_t = 180 \cdot e^{\lambda \cdot t} \tag{6.12}$$

$$\sum_{i=0}^{n} \sqrt{(\theta_i - 180 \cdot e^{\lambda \cdot (t_i - t_{offset})})^2} \tag{6.13}$$

6.4 Results

The model as described is sufficient to predict properties of the distribution of root populations over time, such as the mean angle and variance. We also can simulate populations where appropriate for verification.

6.4.1 Root tip angle distribution

Geometric fits to 90° reorientation data show good agreement above approximately 20° in all cases, however there is some deviation below this point with the experimental data showing faster bending than predicted as shown in Figure 6.2. Despite this deviation at low angles the model is able to describe the data well ($r^2 \approx 0.99$).

While the mean angle is relatively stable the variability of the variance is significantly greater. Simulations show the variance has a consistent index of dispersion of ≈ 0.5 over the time period of the experiment and given the same starting population as seen experimentally. Nevertheless we are able to provide good fits to the experimental conditions in two out of the three cases tested, with the third showing greater than predicted variance (Figure 6.2). Given the sample sizes used and the high predicted variation in the variance it is actually unlikely that the observed variance would closely fit the expected in all cases. While more accurate estimates of the variation in response could be obtained with larger sample sizes we are unable to combine sets of roots as unlike the mean the variance is not stable.

Comparisons of descriptive properties of the root populations are important for both verification and model fitting, but we are not limited to testing the mean and variance alone. By simulating the root behaviour we can compare the observed distribution of angles with that predicted by the model. Figure 6.3 shows the observed distribution of the roots analysed in figure 6.2 compared to simulated roots. Root angles were linearly interpolated to the measured times. While comparisons were performed for all times measured only measurements taken

every 2 hours are shown here. We see very good agreement between the observed and the simulated results at early time points, however at long times (and thus low angles) we see a more sharply peaked distribution than predicted. This may be due to the overshooting present in the model which is not observed in this set of experimental data (though has been reported previously). We cannot see any significant statistical difference between the simulated and observed results at any time points ($p > 0.05$, two-way t-test using the Bonferroni correction for multiple comparisons).

While the model is able to predict both the mean and variance of roots reorientated to the horizontal we should be capable of predicting behaviour at all angles below the angle of maximum bending at 130°. Fig. 6.4 shows the geometric fits to a total of 368 roots reorientated to angles between 30° and 150°. In order to ensure accurate comparisons between different starting angles and consistency with values used for variance fitting, individuals were re-categorised depending on their actual starting angle after reorientation as described in section 4.2. As expected, reorientations to above 130° show very poor fits to the model. At low angles below approximately 20°, we see similar deviations in the 60° data as we saw previously with the 90° reorientations. The only exception at low angles is the 30° reorientation data which shows good agreement with the model. An overview of the observed behaviour across the full range of angles can be gained by aligning the observed values to a single model as shown in figure 6.5. Although this alignment adds a significant extra degree of freedom to model it allows for good visual analysis.

6.4.2 Angle-dependent variation

As predicted by equation (6.8), the variation in angle-dependent response is greater than that predicted by the model (Figure 6.6), although of the same order of magnitude with the mean standard deviation being approximately 25% larger than predicted. When comparing with simulations we see the expected increase in angle-dependent variation over ten minute measurements but not over thirty minute measurements.
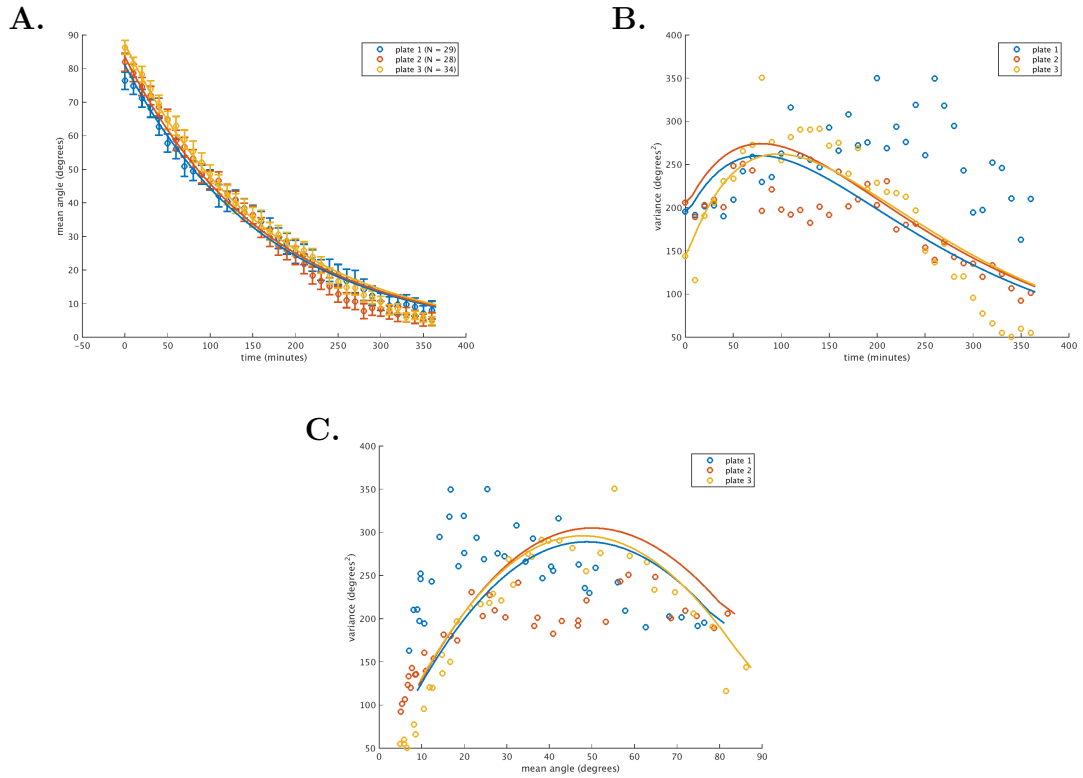
Figure 6.2: **A.** Example model fits for the mean angle of 90° reorientation kinetics. Each plate has been fit separately to avoid biasing the variance (shown in **B**). Fits are geometric given by Equation (6.5), where $p = 0.0049, \Delta = 8.4°, (\lambda = 0.0059)$. **B.** Example model fits for the variance of 90° reorientation kinetics. Each plate has been fit separately to avoid biasing the variance. Fits are calculated from the expected distribution given the individual root starting angles, where $p = 0.0049, \Delta = 8.4°, (\lambda = 0.0059)$. **C.** Example model fits for the variance as a function of the mean for 90° reorientation kinetics. Each plate has been fit separately to avoid biasing the variance. As the behaviour is angle-dependent measuring the variance as a function of angle is more robust than fitting over time.
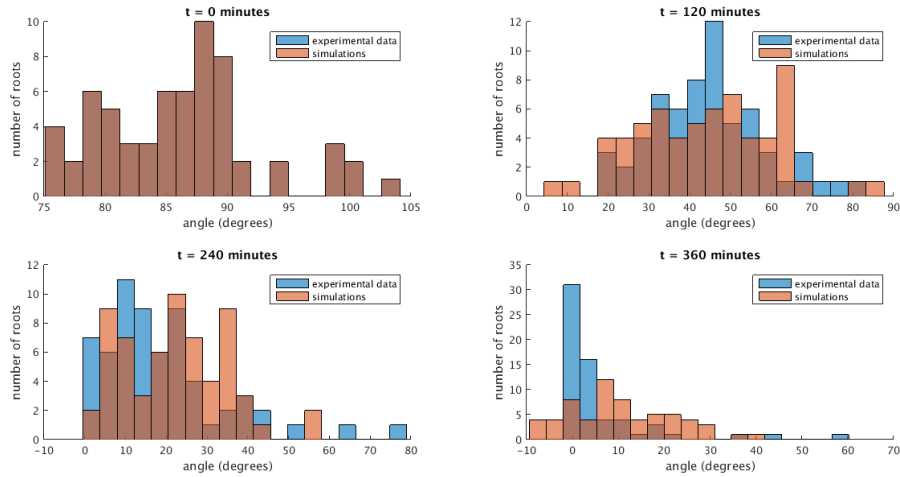
Figure 6.3: Comparisons between the observed root-tip angle angle distribution and simulated results for 91 roots over the course of a 6 hour kinetics experiment. Simulated angles were linearly interpolated at the time points shown. N = 91.
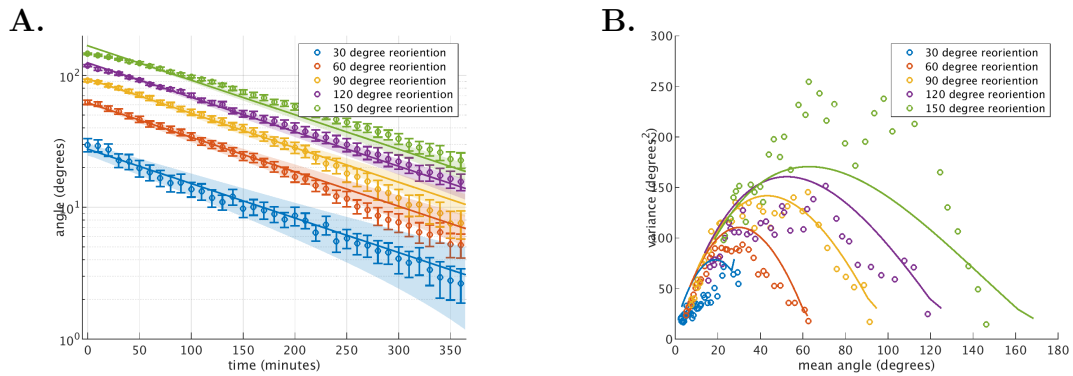
Figure 6.4: **A.** Example model fits for the mean angle of all reorientation kinetics. Mean values are the mean of each plate mean for plates reorientated to the given angle. Fits are geometric given by Equation (6.5), where $p = 0.0049, \Delta = 8.4°, (\lambda = 0.0059)$. Error bars show SEM. N given in table 4.1. **B.** Example model fits for the variance as a function of angle for all reorientation kinetics. Mean values are the mean of each plate variance for plates reorientated to the given angle. Fits are calculated from the full distribution given using the method outlined in section 6.2.4, where $p = 0.0049, \Delta = 8.4°, (\lambda = 0.0059)$. N given in table 4.1

Figure 6.5: Means of $30°, 60°, 90°, 120°$, and $150°$ reorientation kinetics aligned to a single model. Roots with initial angles significantly above $150°$ have been grouped separately. Good fits are seen from approximately $130°$, although some groups ($60°$ and $90°$) display deviations at angles below approximately $20°$. N given in table 4.1

6.4.3 Finite data effects
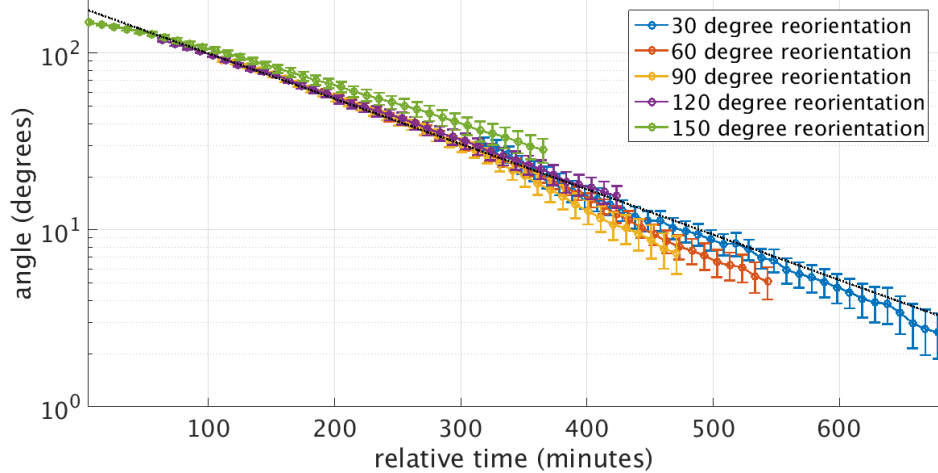
It is noticeable from the aligned angles over time (Figure 6.5) that the $60°$ and $90°$ reorientations bent faster than predicted at low angles; below roughly $20°$. It is not clear however whether this is due to the nature of the response or is a result of having finite data. If we look at the probability of making N bends after a number of steps sufficient to reduce the mean angle to some small value (as calculated in Equation (6.9)) we can see the resulting distribution displays visible kurtosis, with the probability of over-bending by a large number of steps being greater than that of under-bending by an equivalent number. While we would expect that with a large enough sample the expected number of bends made would be as we predict, with a small sample we might expect to see a greater chance of over-bending rather than under-bending. This is testable in simulation, where we do in fact see similar over-bending to that seen in experimental results, albeit not to the same degree. Figure 6.7 shows an example simulation run over 100 roots, roughly the number gathered in the data set, while we do not see deviations as large as seen in the experimental data the same trend is present,
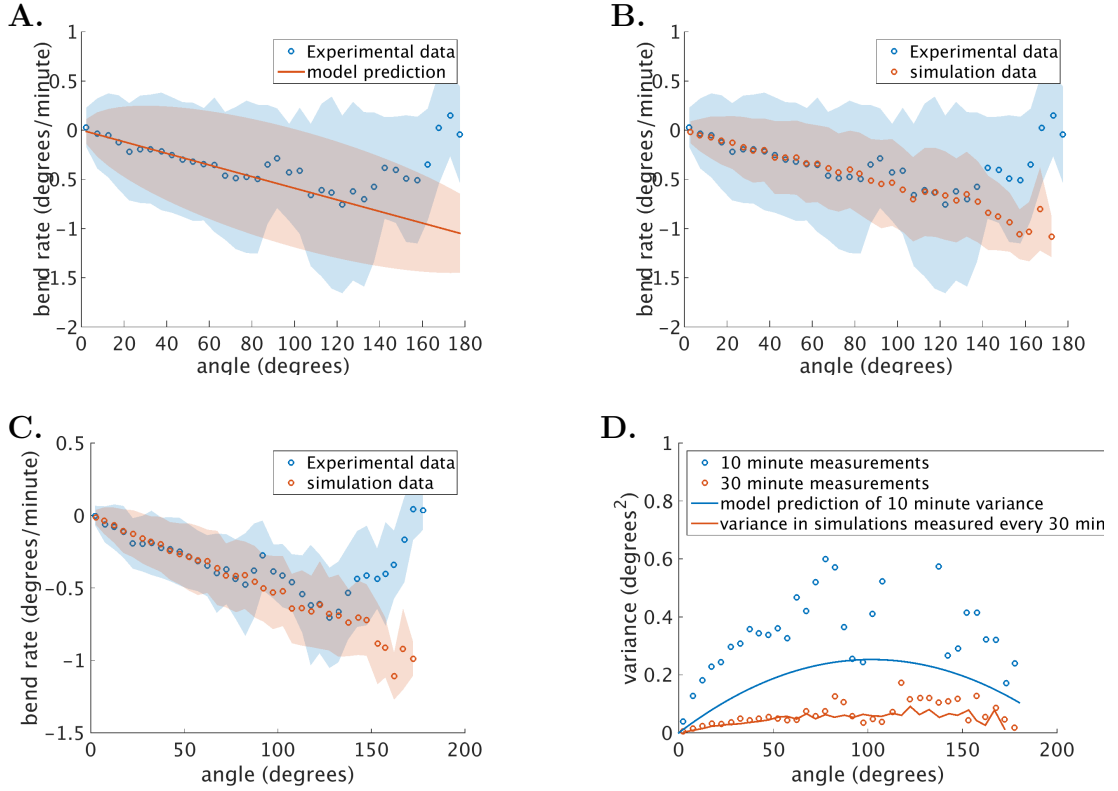
Figure 6.6: **A.** Predicted instantaneous angle-dependent behaviour compared to observed behaviour. Model predictions were calculated from Equation (6.6) where $p = 0.0049$, $\Delta = 8.4°$, ($\lambda = 0.0059$) and assuming no error. Error bars show standard deviation. As expected we see slightly over the predicted variation in response. Based off 13194 measurements from 370 roots binned into 5° bins. **B.** Predicted instantaneous angle-dependent behaviour compared to observed behaviour. Model predictions were based on simulations measured every 10 minutes, where $p = 0.0049$, $\Delta = 8.4°$, ($\lambda = 0.0059$). Error bars show standard deviation. As simulations do not display measurement error or individual differences we would expect less variation in simulation than observed. Based off 13194 measurements from 370 roots binned into 5° bins. **C.** Predicted instantaneous angle-dependent behaviour compared to observed behaviour over a 30 minute time-scale. Model predictions were based on simulations measured every 30 minutes, where $p = 0.0049$, $\Delta = 8.4°$, ($\lambda = 0.0059$). Error bars show standard deviation. Over these time scales we would predict measurement errors to be negligible meaning we see good agreement between simulation and experiment. Based off 4398 measurements from 370 roots binned into 5° bins. **D.** Angle-dependent variance for data measured at 10 minutes and 30 minutes compared to predictions. The 10 minute data is more variable than expected which can be accounted for by measurement error, model predictions are based of Eq. 6.6. The 30 minute data fits the predictions well, over 30 minutes we cannot assume bending is binomial so simulations have been used to calculate the variance.

131

suggesting at least some of the deviation observed may be explained by finite data effects. Figure 6.8 shows the mean of 1000 runs of the model at 30°, 60°, 90°, and 120° with the experimental data for comparison. While this approximately ten times the sample size gathered experimentally there is still some deviation from the expected angle below roughly 10°. As expected this deviation increases as we increase Δ due to a variations from the expected number of bends resulting in larger effects. It also decreases with larger sample sizes, again as expected. Unfortunately at low angles the gravitropic response is weaker compared to other behaviour such as root waving and skewing, this makes it increasingly difficult to accurately measure the gravitropic behaviour at low angles. While the reason for the low angle deviation from the model is not clear it seems likely that it is a combination of finite data effects and other behaviour obscuring the gravitropic response.

6.4.4 Auxin concentration after reorientation

The model presented here provides a good description of gravitropic root behaviour but does not explain the mechanism behind this behaviour. Further, while we have shown the response can be described by a stochastic model we do not know the source of the variation within responses. It is possible (and indeed seems likely) that the statocyte is a noisy angle sensor. If this is the case we would expect to see considerable variation in auxin concentration in the flanks of a gravistimulated root as a result of the noisy output from the columella. It is also possible that cellular elongation is not a consistent process in which case we would expect less variation in auxin concentration as the variation in response would occur in the response to auxin not the perception of gravity.

R2D2 is a ratiometric auxin reporter containing a stable RFP and an auxin degradable YFP which allows for auxin levels in vivo to be assessed (Liao et al., 2015). R2D2 measurements were obtained from the post-columella epidermis of roots after 40 minutes of gravistimulation at angles between 0° and 120° (Sageman-Furnas, 2016). By comparing RFP and YFP we are able to infer relative auxin levels on both the upper and lower side of the root. While this gives consistent
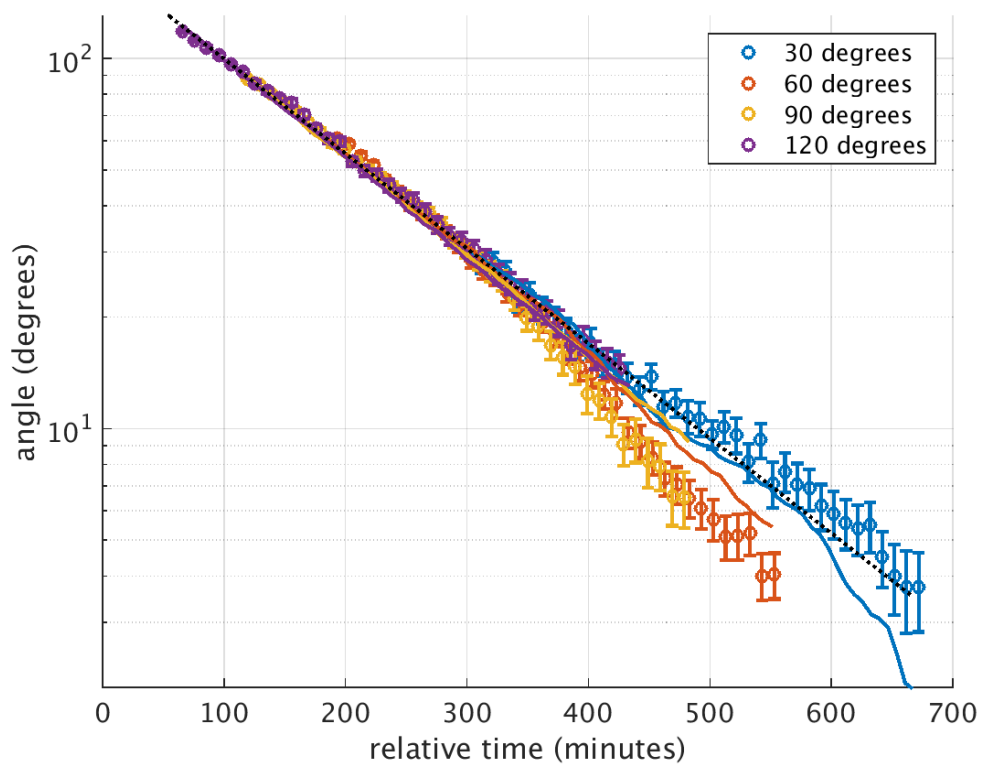
Figure 6.7: Means of 100 simulated roots at 30°, 60°, 90°, and 120° using the experimentally determined bend size of 8.4°. 100 roots is of the same order of magnitude as the data collected (52-87 roots), while the low angle deviation is not as great as is seen in the data a similar trend is present.
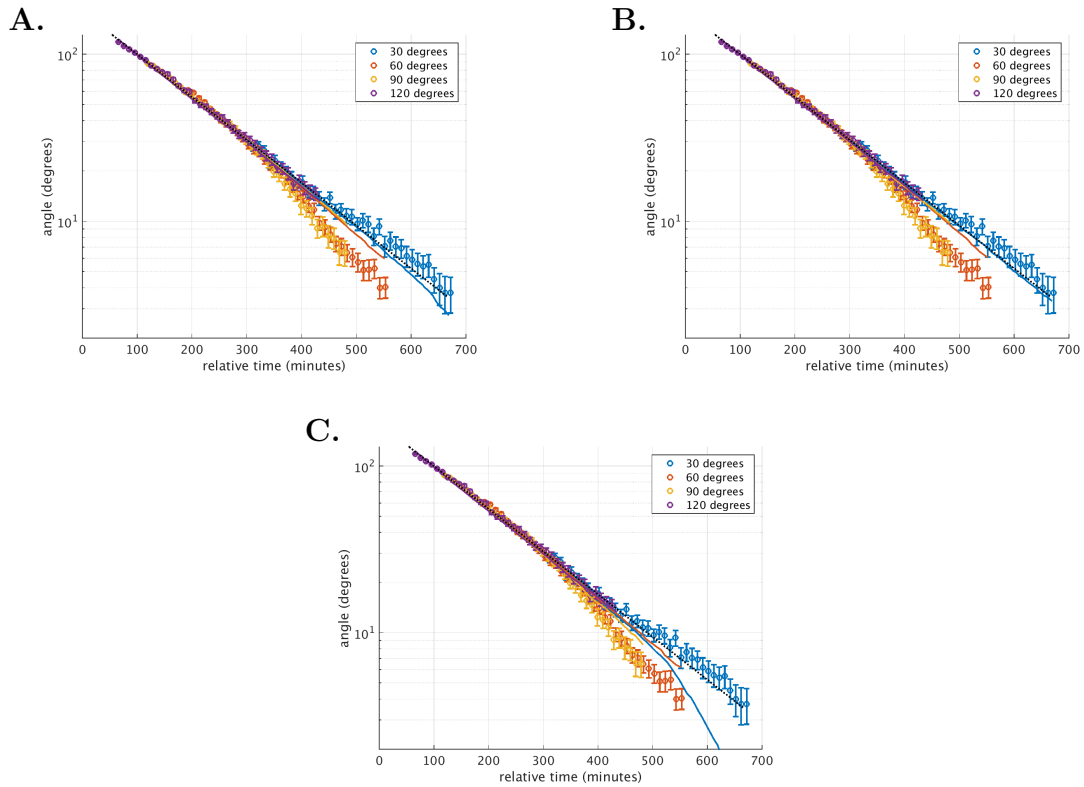
Figure 6.8: **A.** Means of 1000 simulated roots at 30°, 60°, 90°, and 120° using the experimentally determined bend size of 8.4°. Simulations are shown with lines, experimental data with circles. At low angles simulated results tend to bend more than expected. This effect increases with higher Δ and decreases with higher sample sizes. **B.** Means of 1000 simulated roots at 30°, 60°, 90°, and 120° using a bend size of 10°. Simulations are shown with lines, experimental data with circles. At low angles simulated results tend to bend more than expected. This effect increases with higher Δ and decreases with higher sample sizes. **C.** Means of 1000 simulated roots at 30°, 60°, 90°, and 120° using a bend size of 20°. Simulations are shown with lines, experimental data with circles. At low angles simulated results tend to bend more than expected. This effect increases with higher Δ and decreases with higher sample sizes.

auxin levels we are not able to determine the exact auxin concentration in absolute terms, nor do we know the concentration necessary to induce a response in the elongation zone. If we make the minimal assumption that bend probability is proportional to the auxin asymmetry, then we can find some conversion factor c such that $P(bend) = c \cdot Auxin$. This allows us to fit the model to the measured R2D2 fluorescence despite not having a well defined conversion between fluorescence and auxin concentration. We can obtain a value for c by fitting the probability of bending as predicted by the model on the data-set collected previously to the mean R2D2 asymmetry at the measured angles, as shown in figure 6.9. While this does not allow us to predict the measured mean asymmetry we can then use the conversion factor obtained here to predict the expected variance in auxin levels, shown in figure 6.10. Unfortunately with the limited data available we are not able to determine whether the variation observed is sufficient to explain the variation in response. While it appears that the variance is of the same order of magnitude as expected we see lower than expected variation at low angles, and higher than expected at high angles. Additionally the shape of the variance as a function of angle is not convex as would be predicted. However as we have shown previously the measured variance itself is very susceptible to noise, and with the small sample sizes available ($12 \leq N \leq 14$) this cannot be ruled out.

Interestingly while the ratio of auxin asymmetry at a given angle is reasonably consistent (at least after 40 minutes of gravistimulation) the magnitude of auxin on the upper and lower sides of the root is not. Figure 6.11 shows the upper and lower auxin levels for individual roots. The absolute auxin concentration can vary by up to a factor of 4 within a single reorientation angle but the $\frac{lower}{upper}$ ratio remains constant.

6.5 Discussion

Historically, models of gravitropic behaviour have focused on the expected behaviour, with the Sine Law and its variants presenting a deterministic prediction
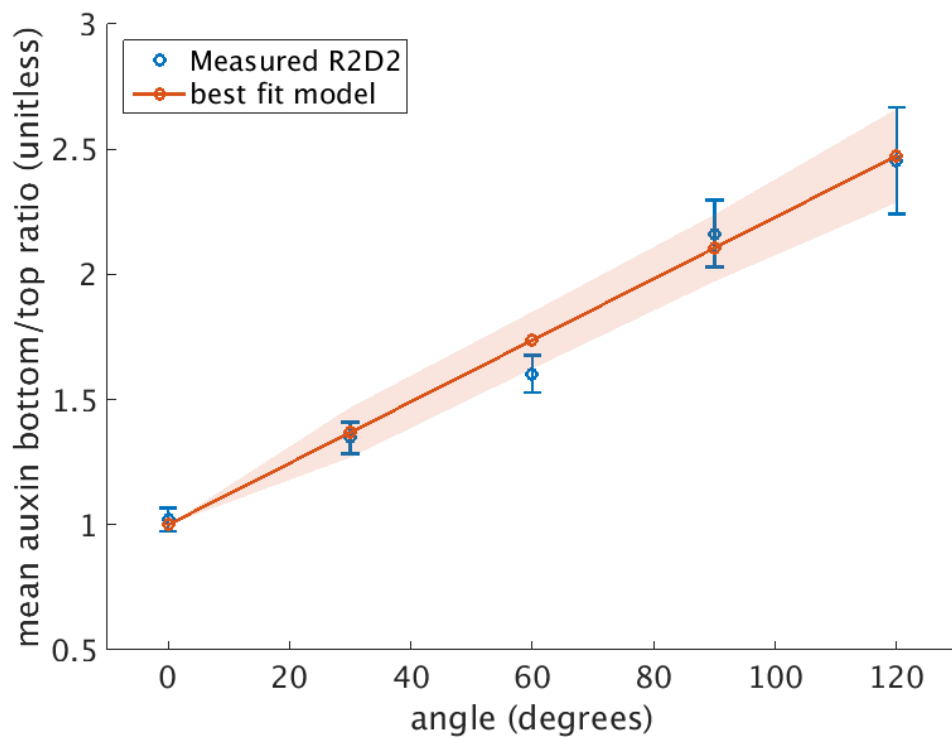
Figure 6.9: Mean auxin asymmetry 40 minutes after gravistimulation. The model fit shows a LSQ fit to the experimental data. The is a linear relationship between angle and auxin asymmetry up to 120° as predicted by the model. $N \geq 13$, error bars and shaded region show SEM.
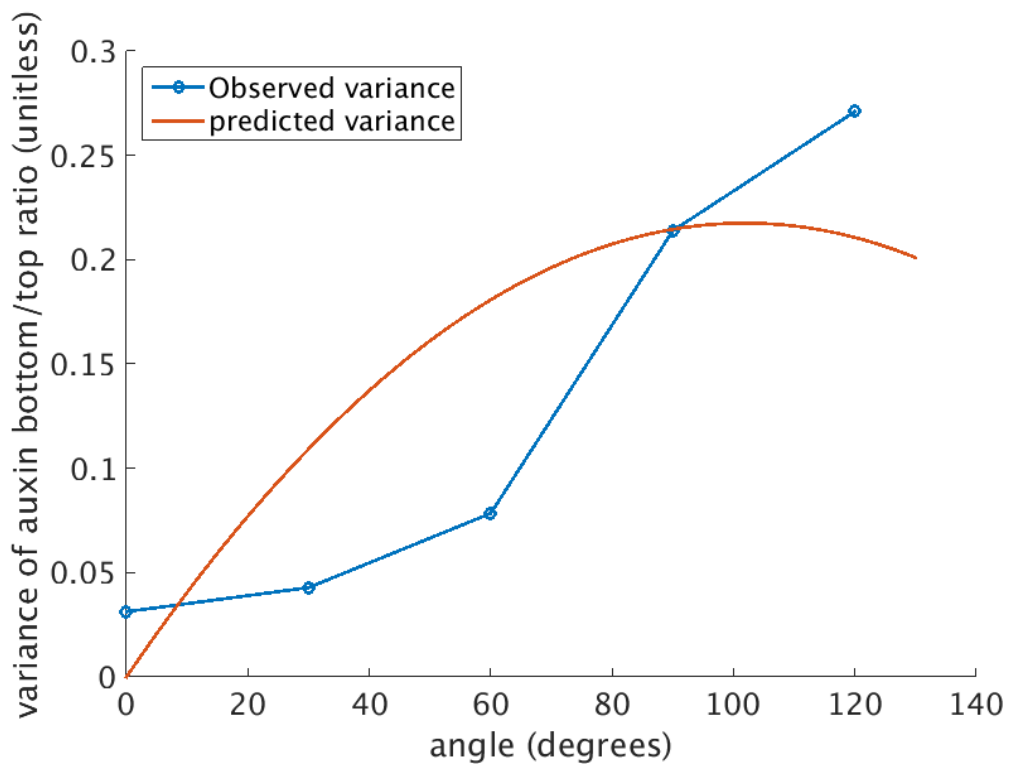
Figure 6.10: Variance in observed auxin asymmetry 40 minutes after gravistimulation. Model fits are based of the expected instantaneous variance scaled by c. While the variance of of the correct order of magnitude it is not possible to determine whether it is sufficient to explain the variation in response. $N \geq 13$
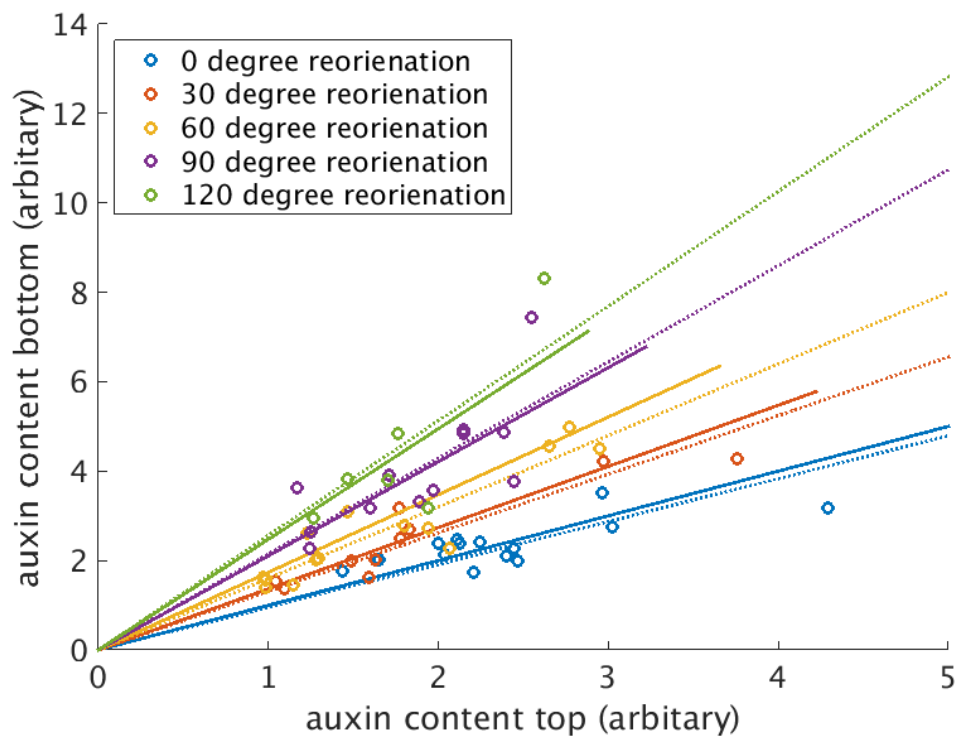
Figure 6.11: Individual upper and lower side auxin concentrations 40 minutes after gravistimulation. While there is considerable variation in absolute concentrations the ratio of $\frac{lower}{upper}$ is consistent with a linear model. Circles represent individuals, solid lines represent the predicted ratio based on the fit shown in figure 6.9, dotted lines represent the best fit to the data at the given angle.

of the gravitropic response. Implicit in this is the assumption that the mechanisms behind the gravitropic response are also deterministic, or at least sufficiently consistent that they can be treated as such, and that the variation in population response is down to individual differences. However there is evidence at both the mechanistic level and the behavioural level that the gravitropic response itself is a stochastic process. Statoliths display erratic saltatory movements, possibly making the generation of a consistent signal difficult, and there is evidence that increasing thermal noise is able to increase the gravitropic response. Added to this the relative weakness of the gravitational signal compared to the background noise within a cell would make accurate measurements difficult, although stochastic resonance may be able to boost the detection.

By treating gravitropic response as a stochastic process we are able to predict the population level behaviour of reorientated roots below 130°. Given reorientations of 90° we are able to predict the mean and variance of root populations (Figure 6.2). While predictions of the variance over time are not always reliable (Figure 6.2) this may be down to the high degree of variability in the variance, which is predicted to be greater than in the mean response (see section 6.4.1). Despite this we are able to predict the variance against angle more reliably (Figure 6.2). This is likely to be due to the lack of time-dependence in the response; as gravitropic response is fundamentally an angle-dependent process we would expect angle-dependent analysis to produce more reliable results. This holds over a range of angles with a single model able to predict both the mean angle variance of root populations reorientated to between 30° and 120° over the course of 6 hours (Fig. 6.4).

Although the model produces good fits up to 130°, we are not able to capture the behaviour above this point, this is especially obvious when the data is aligned a single model as shown in figure 6.5. This demonstrates the difficulties in fitting to data over time, as even once the high angle populations have on average moved to below the cut-off point of 130° the population still contains roots above this angle, skewing the results. Instead angle-dependent analysis provides a better description of the behaviour, with the model able to capture both the mean and variance in response up to 130°. It is true that we see greater variation than

predicted in the experimental data (Figure 6.6), however this is to expected given the limitations in measurement accuracy when measuring small responses over a fast time scale. If larger measurements are used, measuring every 30 minutes as opposed to 10, we see good agreement between experimental and predicted behaviour (Figure 6.6).

At very low angles we see considerable variation in response, with some experiments bending faster than predicted. While we cannot fully explain this effect it is likely to be due to finite data effects. Similar responses are seen in simulations although not at the magnitudes observed experimentally (Figure 6.7). Unfortunately at low angles it becomes increasingly difficult to separate the weak gravitropic response from the background behaviour of the root, which may explain some of the discrepancy.

We have had some success describing the behaviour stochastically, but it is not clear at what point the variation in the response originates. While the statocyte seems like a good candidate, given the aforementioned sources of noise within the cell; we cannot confirm whether the output of the columella as measured by the auxin concentration in the flanks is sufficiently variable to explain the response. By relating the observed auxin concentration to the probability of bending we can make tentative predictions for the expected variation, but we do not have a clear enough understanding of the dynamics of the R2D2 reporter to give accurate predictions. Nevertheless the observed variation in auxin concentration is of the correct order of magnitude to explain the variation in response, and so this cannot be ruled out.

The fact that we are able to describe the response using a discrete model suggests that the response to a gravitropic signal is non-linear, indeed the cellular response to auxin has been shown to be sigmoidal making a discrete step function an appropriate description. If this is the case we would expect relatively consistent bending (the consistency depending on the steepness of the sigmoid) to occur when the auxin concentration reaches some critical threshold. It remains to be seen whether this is achieved when natural noise on top of a angle-dependent baseline exceeds this threshold, or whether it is the result of large scale changes

in concentration which are triggered irregularly. While we have assumed instantaneous bends at discrete time points it is clear that the physical process of bending occurs over time. However the fact that response can be described well with a time step of 7 minutes suggests that this is sufficient time for bending to occur. As the response has been shown to depend on the current angle this must be sufficient for the angle to be detected a gravitropic signal to pass from the columella to the elongation zone. This requires a number of process to occur for which we can estimate the times required. Statolith sedimentation and the initial perception of a gravitropic stimulus has been shown to occur on the order of 30 seconds. While we do not have accurate figures for the auxin transportation time from the columella to the elongation zone, given rough auxin transport rates (Kramer et al., 2011) and the distances involved this is likely to be around 3 minutes. This suggests that the response to a change in auxin concentration occurs over the time scale of a 3-4 minutes. Further work is necessary to confirm this estimate.

Chapter 7

General discussion

Over the course of this project a ROTATO system has been developed allowing roots to be constrained at a given angle with respect to gravity for prolonged time periods (chapter 3). While the hardware used was not sufficiently reliable, the software developed has proven to be robust and portable; and is now being used successfully elsewhere. The computer vision system developed for the ROTATO has been adapted for large-scale automated analysis of multiple roots (chapter 5). Although older data-sets were not able to be automated this provides a platform for future work to be analysed in greater detail than was possible previously.

In depth analysis of a large data-set of reorientation kinetics has been performed, with an emphasis on determining the factors that contribute to gravitropic response at the behavioural level, and over which time-scales (chapter 4). Gravitropic response was found to be angle-dependent, with time-dependent effects being negligible and no evidence of hysteresis at the time-scales studied. Gravitropic response was found to be highly variable, with mean bend-rates increasing linearly up to 130°.

Based on the analysis performed in chapter 4, a minimal stochastic model was developed which is able to predict gravitropic response at the population level as well as providing mechanistic insight into the processes and time-scales involved in a gravitropic response (chapter 6).

7.1　The ROTATO system

When attempting to understand tropic behaviour is is important that one is able to accurately control the stimulus under study. Due to the nature of gravitropic behaviour, and the impracticality of changing the magnitude or direction of gravitational field the plant is experiences, the ROTATO system, in which roots can be constrained at a given angle with respect to gravity, promises to be a valuable tool for understanding gravitropic behaviour in more detail than is currently possible. Although at least one other ROTATO is known to exist (Mullen et al., 2000) the details of it's construction are not currently publically available.

The ROTATO system described in chapter 3 consists of a software system to identify, track, image, and adjust, roots as well as a set of physical hardware capable of making the required measurements and adjustments. The two components have been designed to be easily separable so that new ROTATO systems can be built with different hardware as required. This has been demonstrated successfully as the software outlined in chapter 3 has now been ported to the original hardware used in Mullen *et al.* and is performing well. While specific details will depend upon experimental conditions and equipment, the ROTATO software is able to accurately track roots position and angle to within $\pm 1°$ for prolonged periods. When conditions are good this has shown itself to be extremely reliable, however as is often the case when dealing with objects in the real world conditions are often far from perfect. There are known problems when the growth media if not consistent, such as when bubbles are present, which have been shown to reduce to accuracy significantly. While it is possible that alternative computer vision techniques, such as a level-set method, could deal with such problems it is likely that any such system will fail on occasion. Given this there are a number of simple steps that can be taken to produce good results. Firstly plates can be screened before being placed on the ROTATO system allowing obvious problems to be caught. Secondly experiments can be monitored in real time to ensure problems are caught promptly, often a simple adjustment of the lighting or camera position can prevent loss of accuracy occurring. Due to the slow growth rate of most plant roots, combined with measures in place to ensure that individual

errors do not significantly affect the root tip angle, it is often possible to see a problem coming well before it occurs making even infrequent checks sufficient. With this in mind, the software is capable of performing its job well and will hopefully be of considerable use in the future.

The results obtained from the ROTATO system are inconclusive and of unknown accuracy. While the tip angle measurements themselves can be verified, the behaviour observed is not as expected or previously reported (Mullen et al., 2000). Like previous studies we see continuous consistent bending at the population level, but the rates of bending do not match those previously observed. Specifically, while there is an upwards trend in bend-rates, with higher angles producing higher bend-rates, at 60° we observed faster bending than at 90°. While the exact angle of maximum bending is disputed most estimates put it between 105° and 130°, indeed in free response experiments we observe maximum bend-rates at around 130° (see chapter 4). There are two immediately obvious possible sources of error. Firstly this could simply be down to natural variation in response, it is possible that the results obtained are accurate and that the sample size is simply too small detect the increase in response between 60° and 90°. The second possibility is a failure of the controlled conditions. While the ROTATO system was in a controlled environment with the temperature maintained at 20° it has been known for the temperature regulation to fail. As the experiments themselves are time consuming the data was collected over the course of a few months, it is possible that over this time there were large enough changes in conditions to affect the results. The last possibility is a problem with the ROTATO hardware itself. While we are able to verify the accuracy of the software from the stored images produced during the experiment, we are not easily able to verify the accuracy of the stage response while an experiment is in progress. If the reported adjustments do not match the actual adjustments the results obtained will be incorrect. While we have not detected any significant error in adjustments under test conditions the possibility cannot presently be discounted.

7.2 Automated analysis is necessary for high throughput measurements

Given the inconsistency in gravitropic response, even between plants under identical conditions, large sample sizes are necessary to accurately measure the expected behaviour. This is especially important when higher order moments, such as the variance, are being measured as they can be more prone to error than the mean response. In order to measure fast responses high frequency measurements are also necessary, although this comes with drawbacks in the accuracy of measurement. Currently the bottleneck when collecting large amounts of data from kinetics experiments is the time required to manually analyse the images produced. An automated system would allow significantly larger numbers of plants to be analysed, and at higher measurement frequencies than is currently possible.

The automated analysis method discussed in chapter 5 provides a good platform for moving towards completely automated analysis. Under the correct conditions properties such as the mean and variance of root populations can be measured showing good agreement with manual measurements. However the system is not currently able to accurately measure root tip angles under poor conditions. This is certainly an area where more advanced computer vision techniques would be appropriate, as unlike the ROTATO system mentioned above it is not always practical to manually verify measurements and adjust the conditions during the course of the experiment. While the accuracy of the measurements is limited by the resolution of the images produced, better imaging conditions should also allow for much more accurate automation. Preliminary test images obtained using back-lighting show very good image conditions, with consistent background and excellent contrast maintained throughout. It is likely that the current vision system would be able to produce good results under these conditions, however the analysis of the data collected during the course of this project cannot be automated unless significant improvements are made to the vision system.

7.3   Root gravitropism is angle-dependent

To date there has been little effort to characterise gravitropic behaviour as a dynamic system. While the assumption has generally been that behaviour depends up on angle (tip angle in roots), the time scale of sensing and response has not been carefully considered beyond presentation time assays. There have not been any extended attempts to study hysteresis at the behavioural level, some models have alluded to hysteresis to explain low angle bending (Band et al., 2012). By analysing response as functions of both time and angle we are able to determine that time-dependent effects are negligible or non-existent over the time scales of a response. We were also unable to see any evidence of hysteresis in gravitropic behaviour. This is not to say that time can be disregarded in all models of gravitropism. Clearly, cellular process such as statolith sedimentation, PIN localisation, and auxin transport take time to happen. Additionally, any behavioural response times will be limited by factors such as auxin transport velocity (Kramer et al., 2011) and the distance between the root tip and the elongation zone (Verbelen et al., 2006). We can however say that these processes are relatively fast, at least compared to the scale of a full gravitropic response which can take many hours. Therfore, under free response conditions, the angle which is being responded to is not going to be significantly different to the current angle.

Detailed analysis of a large number of roots has allowed us to more accurately analyse behaviour as a function of angle than has been seen previously. By binning responses by angle we are able to look at behaviour over very small angle ranges. Although this approach does lose us some accuracy in individual measurements compared to looking at the population level mean angles and bend-rates, this is more than compensated for by ensuring that we are not grouping together roots at vastly different angles. When looked at this way we see what appears to be a linear relationship between angle and bend rate up to around 130°. Similar angles of maximum bending have been observed previously with measurements typically ranging between 120° and 135° (Audus, 1964; Larsen, 1969). More interesting is the shape of the response. This binning approach is, to my knowledge, unique in that it allows a much higher angular resolution

of measurements than is normally obtained. It perhaps for this reason that we are able to distinguish between a Sine Law like response and a linear response, certainly the differences are subtle and unlikely to be noticeable without a large data set and careful testing. Adoption of a linear model has significant advantages over a modified Sine Law. Firstly the Sine Law relies on an assumption about the mechanism behind graviperception, specifically that it is dependent upon the force of gravity acting across the organ. Modifications to the Sine Law which are able to accurately capture the angle of maximum response are forced to abandon this mechanistic justification. It is possible that such modifications could be explained by the shape of the collumella. Statocytes are not perfectly square, at least in Arabidopsis. This causes the lateral cell wall to be at a different angle to the centre line of the root. If it was the force acting on the lateral cell wall we could then explain maximum bending at angles above 90°. However while this may be able to produce maximum bending angles above 90° the statocyte does not appear to be sufficiently rhomboid to explain the increase in bending up to 130°. In fact there is recent evidence that it is angle not force which is detected by the statocyte (Chauvet et al., 2016), if this is the case then a linear relationship is the more parsimonious model of behaviour. This is convenient as it allows us to model behaviour even when measurements are taken at few discrete angles, as is common when studying gravitropic behaviour, without fear of over-fitting to our data as may occur with modified Sine Laws. Mathematically, the behaviour produced is also easier to deal with than ad-hoc modified Sine Laws, producing an expected exponential decay in tip angle. In fact the assumption of linearity has been made in the past to produce more mathematically tractable models (Bastien et al., 2013).

For all it's advantages, a linear model cannot explain the observed decrease in bend rate above 130°. While it makes intuitive sense that as a root approaches vertical it becomes harder to determine its lower side, higher angle behaviour remains to be properly characterised. While one may naively expect bending to decrease above the horizontal, in order for a non-90° maximum bending angle there needs to be some mechanism to break the 90° symmetry. Some initial geometric models of cell geometry suggest the shape of the statocytes may be

sufficient to break the 90° symmetry. However this remains to be shown.

It is striking that there is considerable variation in gravitropic response even within an individual responding root (see section 4.2.2). While it is possible that this is merely due to the interaction between gravitropic and non-gravitropic behaviour, such as root waving, this explanation seems unlikely because most non-tropic behaviour in Arabidopsis is not large or fast enough to explain the variation, with waving having a period of around 20 hours (Simmons et al., 1995).It is because of this that we conclude that the gravitropic behaviour itself is best described stochastically. Stochastic processes in gravitropism have been suspected before (Ma and Hasenstein, 2007; Meroz and Bastien, 2014) at the cellular level but gravitropism is normally treated deterministically. It is not clear at what point in the gravitropic process the stochasticity occurs, however there are a number of promising options. It is possible the graviperception is subject to noise. It is known that statoliths display saltatory movements although the effect this has on gravitropic response is not clear (Hejnowicz and Sievers, 1981; Leitz et al., 2009), however these relatively large random movements may well introduce a level of stochasticity into the auxin signal output by the cell. It has been suggested that due to the weakness of the gravity signal noise amplification may be necessary for sensitive graviperception (Hasenstein, 2011). Given this statolith dynamics and the initial phases of signal transduction are a natural place to look for the source of variation in gravitropic response. In this case we can consider the statocytes/statoliths as noisy sensors which give rise to noisy responses. It is also possible that the response to auxin of the cells in the elongation zone is not consistent. While there has been work to determine a dose response curve for auxin concentration (Cleland, 1972) it is not clear how consistent the response is. In this respect it is possible that the motors which drive the gravitropic response are themselves noisy.

7.4   The stochastic model of root gravitropism

Treating gravitropic behaviour as a stostastic process allows us to create powerful models capable of predicting not just the average response but the expected distribution of responses seen in a population. This provides a useful tool not just for model verification but for exploring new phenotypes, as variation in response can now be studied explicitly. For example by using a stochastic model it would be possible to determine whether differences in response are due to real changes in gravitropic response or due to variation in starting angles caused by a root waving phenotype. If the model parameters can be accurately mapped to biological processes it would allow the causes of similar behaviour, such as a change in graviperceptive sensitivity or auxin sensitivity, to be disentangled.

While we have tried to produce a minimal model of gravitropic behaviour there are a number of assumptions which have mechanistic implications. The assumption of linearity is supported by the idea that statoliths do not in fact act as force sensors, as discussed previously (section 7.3). While we have seen no time-dependent effects in our analysis, the fact that a time-independent model can capture the behaviour is encouraging. Although it has not been possible to fully pin down the best time-step to use for the model, we have had good results with a δt of 7 minutes. This is reasonable given that gravity perception can occur in as little as 10 seconds (Kiss et al., 1989) and rough estimates at the delay due to auxin transport are of the order of a few minutes (see section 6.2.1), but the response time of cellular elongation is not known. Given a δt of 7 minutes we would expect the response to be fast with elongation occurring within a couple of minutes of a change in auxin concentration. This is certainly a subject that would be interesting to investigate in depth as there is a lack of information on the specifics of elongation kinetics.

The model presented in this thesis is only relevant to primary roots with a vertical GSA. Analysis of lateral root kinetics reveals both similarities and differences in response. At angles up to 130° the response in primaries appears linear, as does the response in laterals but with an offset causing upwards bending below the GSA and downwards bending above the GSA (Fig. 7.1). This is supported by the
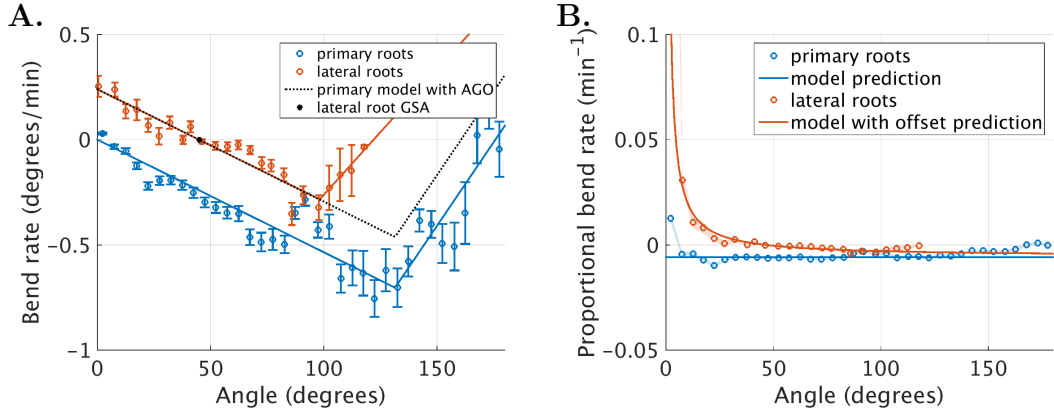
Figure 7.1: **A.** A comparison between bend rate in lateral and primary Arabidopsis roots. At low angles the lateral roots (red) appear to behave similarly to primary roots (blue) with the addition of an offset. The black dashes show the addition to an offset to the primary root fit sufficient to obtain the observed GSA, the angle-dependent behaviour is very similar between the two models as shown by the similarity in gradient. N = 111 lateral roots, 370 primary roots binned into 5° bins. Fits are bi-linear. **B.** The proportional bend-rate for primary and lateral roots. In laterals the proportional bend rate appears to be hyperbolic as is consistent with a constant offset. The measurements for this data were obtained from Ryan Kaye.

proportional bend rate which appears to fit a hyperbolic model as would occur given a constant offset (Fig. 7.1). This is as expected given previous work identifying an anti-gravitropic offset (Roychoudhry et al., 2013). Crucially however the gradient of the response is the same in both lateral and primary roots, suggesting that the gravitropic mechanisms are shared in both laterals and primaries and that our model may be able to be adapted for lateral roots. Interestingly the point of maximum bending has shifted to around 90° in lateral roots. The reasons for this are unknown, and as we do not know what determines the point of maximum bending in primaries it is hard to suggest a cause for the shift. It would be interesting to see how the model can be adapted to include an AGO, and whether this would shed any light on the problem. It is worth considering that the difference between the maximum bend angle in primaries and laterals is around 40°, very close to the lateral root GSA (approximately 45° based off the fit in this dataset) although it is not clear whether the two are related.

While we have assumed for this model that the gravitropic response is stochastic, it is possible that the root growth itself is a stochastic process. This could be due to either stochastic cell division in the root apical meristem, or to noisy cellular elongation in the elongation zone. As gravitropic response relies on differential growth, stochastic growth underlying a deterministic gravitropic process could be expected to produce stochastic behaviour. If this is the case the model presented here may be generalisable to root growth under other conditions. High resolution (both spatial and temporal) measurements of root growth in non-gravistimulated roots would allow the variation in growth rate to be quantified, and a distinction between stochastic gravitropism and stochastic growth to be made.

7.5 Final comments

In this thesis we have presented in depth analysis of gravitropic behaviour in Arabidopsis with an emphasis on understanding what determines the magnitude of a gravitropic response. We have shown the importance of angle dependence when describing gravitropic behaviour as well as the inherently stochastic nature of the response. Additionally a minimal model has been proposed which is capable of describing the behaviour of populations under gravitational stimulus in greater detail than has been possible previously. However our understanding of gravitropic behaviour is still far from complete. Important questions remain to be answered such as what determines the angle of maximum response and why does it appear to be different in lateral roots? Any complete model of root behaviour will need to be extended to include other tropic behaviours, and it would be interesting to see whether other tropisms can be framed in a similar way. Non-tropic behaviours such as circumnutation and root waving have been modelled but their interaction with tropic responses has not been adequately addressed.

Root behaviour is often treated as purely the response to stimuli, such as gravity and light, but in soft herbaceous plants mechanical interactions with the environment are likely to play a large role in determining the final behaviour displayed. It would be interesting to see how behavioural models such as the one presented

here can be integrated with mechanical models, as this may allow for a better understanding or the underlying biological responses.

While this work was concerned with Arabidopsis, almost all species of plant (and fungi) display gravitropic behaviour, many of which have been previously shown to follow similar Sine Law like behaviour. There is still work to be done extending our model to other species and to organs with non-vertical GSA.

Plant behaviour is exceedingly complex and we have a long way to go before we are able to fully describe it, let alone fully understand the mechanisms behind it.

Bibliography

Audus, L. (1964). Geotropism and the modified sine rule; an interpretation based on the amyloplast statolith theory. *Physiologia Plantarum*, 17(3):737–745. 11, 13, 14, 67, 89, 146

Band, L. R., Wells, D. M., Fozard, J. A., Ghetiu, T., French, A. P., Pound, M. P., Wilson, M. H., Yu, L., Li, W., Hijazi, H. I., et al. (2014). Systems analysis of auxin transport in the arabidopsis root apex. *The Plant Cell*, 26(3):862–875. 9, 22

Band, L. R., Wells, D. M., Larrieu, A., Sun, J., Middleton, A. M., French, A. P., Brunoud, G., Sato, E. M., Wilson, M. H., Péret, B., et al. (2012). Root gravitropism is regulated by a transient lateral auxin gradient controlled by a tipping-point mechanism. *Proceedings of the National Academy of Sciences*, 109(12):4668–4673. 9, 68, 88, 146

Barbez, E., Dünser, K., Gaidora, A., Lendl, T., and Busch, W. (2017). Auxin steers root cell expansion via apoplastic ph regulation in arabidopsis thaliana. *Proceedings of the National Academy of Sciences*, 114(24):E4884–E4893. 5

Bastien, R., Bohr, T., Moulia, B., and Douady, S. (2013). Unifying model of shoot gravitropism reveals proprioception as a central feature of posture control in plants. *Proceedings of the National Academy of Sciences*, 110(2):755–760. 16, 88, 89, 147

Benková, E., Michniewicz, M., Sauer, M., Teichmann, T., Seifertová, D., Jürgens, G., and Friml, J. (2003). Local, efflux-dependent auxin gradients as a common module for plant organ formation. *Cell*, 115(5):591–602. 7

Björkman, T. (1989). Perception of gravity by plants. *Advances in Botanical Research*, 15:1–41. 91

Blancaflor, E. B. and Masson, P. H. (2003). Plant gravitropism. unraveling the ups and downs of a complex process. *Plant Physiology*, 133(4):1677–1690. 10, 17

Butler, K. and Stephens, M. (1993). The distribution of a sum of binomial random variables. Technical report, STANFORD UNIV CA DEPT OF STATISTICS. 119

Cannon, W. A. (1911). *The root habits of desert plants*. Number 131. Carnegie Institution of Washington. 1

Chauvet, H., Pouliquen, O., Forterre, Y., Legué, V., and Moulia, B. (2016). Inclination not force is sensed by plants during shoot gravitropism. *Scientific reports*, 6. 10, 67, 88, 147

Cholodny, N. G. (1927). *Wuchshormone und Tropismen bei den Pflanzen*. 6

Cleland, R. (1972). The dosage-response curve for auxin-induced cell elongation: a reevaluation. *Planta*, 104(1):1–9. 5, 115, 148

Cleland, R. E. (1987). Auxin and cell elongation. In *Plant hormones and their role in plant growth and development*, pages 132–148. Springer. 3

Corporation, N. (2012). *Piezo Motor Driven Components User's Manual*. Newport Corporation. 53, 54

Cosgrove, D. J. (1993). Tansley review no. 46. wall extensibility: Its nature, measurement and relationship to plant cell growth. *New Phytologist*, pages 1–23. 4

Cosgrove, D. J. (1997). Cellular mechanisms underlying growth asymmetry during stem gravitropism. *Planta*, 203(1):S130–S135. 5

Cosgrove, D. J. (2000). Loosening of plant cell walls by expansins. *Nature*, 407(6802):321–326. 5

Cosgrove, D. J. (2005). Growth of the plant cell wall. *Nature reviews molecular cell biology*, 6(11):850–861. 5

Cosgrove, D. J. (2015). Plant cell wall extensibility: connecting plant cell growth with cell wall structure, mechanics, and the action of wall-modifying enzymes. *Journal of experimental botany*, 67(2):463–476. 4

Darwin, C. and Darwin, F. (1880). *The power of movement in plants*. Appleton. 2

Digby, J. and Firn, R. (1995). The gravitropic set-point angle (gsa): the identification of an important developmentally controlled variable governing plant architecture*. *Plant, Cell & Environment*, 18(12):1434–1440. 17, 19

Dumais, J. (2013). Beyond the sine law of plant gravitropism. *Proceedings of the National Academy of Sciences*, 110(2):391–392. 12

Esmon, C. A., Pedmale, U. V., Liscum, E., et al. (2005). Plant tropisms: providing the power of movement to a sessile organism. *International Journal of Developmental Biology*, 49(5/6):665. 2

Fendrych, M., Leung, J., and Friml, J. (2016). Tir1/afb-aux/iaa auxin perception mediates rapid cell wall acidification and growth of arabidopsis hypocotyls. *Elife*, 5:e19048. 5

Feraru, E. and Friml, J. (2008). Pin polar targeting. *Plant Physiology*, 147(4):1553–1559. 6

Fitzelle, K. J. and Kiss, J. Z. (2001). Restoration of gravitropic sensitivity in starch-deficient mutants of arabidopsis by hypergravity. *Journal of Experimental Botany*, 52(355):265–275. 88

Fjell, I. (1985). Morphogenesis of the root cap in adventitious roots of salix viminalis. *Nordic journal of botany*, 5(6):555–573. 10

Fozard, J., King, J., and Bennett, M. (2012). Modelling auxin efflux carrier phosphorylation and localization. *Journal of theoretical biology*. 7

Galland, P. (2002). Tropisms of avena coleoptiles: sine law for gravitropism, exponential law for photogravitropic equilibrium. *Planta*, 215(5):779–784. 16, 67, 89

Grieneisen, V. A., Xu, J., Marée, A. F., Hogeweg, P., and Scheres, B. (2007). Auxin transport is sufficient to generate a maximum and gradient guiding root growth. *Nature*, 449(7165):1008–1013. 7, 9

Hager, A. (2003). Role of the plasma membrane h+-atpase in auxin-induced elongation growth: historical and new aspects. *Journal of plant research*, 116(6):483–505. 5

Hasenstein, K. H. (2011). Plant responses to gravity-insights and extrapolations from ground studies. *Gravitational and Space Research*, 22(2). 148

Hejnowicz, Z. and Sievers, A. (1981). Regulation of the position of statoliths inchara rhizoids. *Protoplasma*, 108(1):117–137. 148

Hillman, S. and Wilkins, M. (1982). Gravity perception in decapped roots of zea mays. *Planta*, 155(3):267–271. 10

Ho, M. D., McCannon, B. C., and Lynch, J. P. (2004). Optimization modeling of plant root architecture for water and phosphorus acquisition. *Journal of Theoretical Biology*, 226(3):331–340. 2

Honda, H. and Fisher, J. B. (1978). Tree branch angle: maximizing effective leaf area. *Science*, 199(4331):888–890. 1

Iino, M. and Carr, D. J. (1981). Safelight for photomorphogenetic studies: infrared radiation and infrared-scope. *Plant Science Letters*, 23(3):263–268. 31

Johnson, C. F., Brown, C. S., Wheeler, R. M., Sager, J. C., Chapman, D. K., and Deitzer, G. F. (1996). Infrared light-emitting diode radiation causes gravitropic and morphological effects in dark-grown oat seedlings. *Photochemistry and photobiology*, 63(2):238–242. 31

Kiss, J. Z., Hertel, R., and Sack, F. D. (1989). Amyloplasts are necessary for full gravitropic sensitivity in roots of arabidopsis thaliana. *Planta*, 177(2):198–206. 10, 116, 149

Kiss, J. Z., Wright, J. B., and Caspar, T. (1996). Gravitropism in roots of intermediate-starch mutants of arabidopsis. *Physiologia Plantarum*, 97(2):237–244. 10

Kleine-Vehn, J., Huang, F., Naramoto, S., Zhang, J., Michniewicz, M., Offringa, R., and Friml, J. (2009). Pin auxin efflux carrier polarity is regulated by pinoid kinase-mediated recruitment into gnom-independent trafficking in arabidopsis. *The Plant Cell*, 21(12):3839–3849. 7

Kramer, E. M., Rutschow, H. L., and Mabie, S. S. (2011). Auxv: a database of auxin transport velocities. *Trends in plant science*, 16(9):461–463. 116, 141, 146

Lam, L., Lee, S.-W., and Suen, C. Y. (1992). Thinning methodologies-a comprehensive survey. *IEEE Transactions on pattern analysis and machine intelligence*, 14(9):869–885. 49

Larsen, P. (1969). The optimum angle of geotropic stimulation and its relation to the starch statolith hypothesis. *Physiologia Plantarum*, 22(3):469–488. 13, 14, 67, 89, 146

Leitz, G., Kang, B.-H., Schoenwaelder, M. E., and Staehelin, L. A. (2009). Statolith sedimentation kinetics and force transduction to the cortical endoplasmic reticulum in gravity-sensing arabidopsis columella cells. *The Plant Cell*, 21(3):843–860. 148

Liao, C.-Y., Smet, W., Brunoud, G., Yoshida, S., Vernoux, T., and Weijers, D. (2015). Reporters for sensitive and quantitative measurement of auxin response. *Nature methods*, 12(3):207–210. 8, 132

Ljung, K., Hull, A. K., Celenza, J., Yamada, M., Estelle, M., Normanly, J., and Sandberg, G. (2005). Sites and regulation of auxin biosynthesis in arabidopsis roots. *The Plant Cell Online*, 17(4):1090–1104. 7

Lynch, J. (1995). Root architecture and plant productivity. *Plant physiology*, 109(1):7–13. 1

Lynch, J. and van Beem, J. J. (1993). Growth and architecture of seedling roots of common bean genotypes. *Crop Science*, 33(6):1253–1257. 1

Ma, Z. and Hasenstein, K. H. (2007). Noise amplification of plant gravisensing. *Advances in Space Research*, 39(7):1119–1126. 148

Marchant, A., Kargul, J., May, S. T., Muller, P., Delbarre, A., Perrot-Rechenmann, C., and Bennett, M. J. (1999). Aux1 regulates root gravitropism in arabidopsis by facilitating auxin uptake within root apical tissues. *The EMBO journal*, 18(8):2066–2073. 7

Meroz, Y. and Bastien, R. (2014). Stochastic processes in gravitropism. *Frontiers in plant science*, 5. 148

Metzner, P. (1929). Uber die wirkung der langskraft beim geotropismus. *Jahrb. Wiss. Bot.*, 71:325–385. 13

Michniewicz, M., Zago, M. K., Abas, L., Weijers, D., Schweighofer, A., Meskiene, I., Heisler, M. G., Ohno, C., Zhang, J., Huang, F., et al. (2007). Antagonistic regulation of pin phosphorylation by pp2a and pinoid directs auxin flux. *Cell*, 130(6):1044–1056. 7

Morita, M. T., Kato, T., Nagafusa, K., Saito, C., Ueda, T., Nakano, A., and Tasaka, M. (2002). Involvement of the vacuoles of the endodermis in the early process of shoot gravitropism in arabidopsis. *The Plant Cell Online*, 14(1):47–56. 12

Morita, M. T. and Tasaka, M. (2004). Gravity sensing and signaling. *Current opinion in plant biology*, 7(6):712–718. 10

Moulia, B. and Fournier, M. (2009). The power and control of gravitropic movements in plants: a biomechanical and systems biology view. *Journal of Experimental Botany*, 60(2):461–486. 11, 12, 13

Mullen, J. and Hangarter, R. (2003). Genetic analysis of the gravitropic set-point angle in lateral roots of¡ i¿ arabidopsis¡/i¿. *Advances in Space Research*, 31(10):2229–2236. 17

Mullen, J. L., Wolverton, C., Ishikawa, H., and Evans, M. L. (2000). Kinetics of constant gravitropic stimulus responses in arabidopsis roots using a feedback system. *Plant Physiology*, 123(2):665–670. 9, 13, 14, 27, 60, 88, 89, 143, 144

Nakahori, K., Katou, K., and Okamoto, H. (1991). Auxin changes both the extensibility and the yield threshold of the cell wall of vigna hypocotyls. *Plant and cell physiology*, 32(1):121–129. 4

Otsu, N. (1979). A threshold selection method from gray-level histograms. *IEEE transactions on systems, man, and cybernetics*, 9(1):62–66. 44

Palmieri, M. and Kiss, J. Z. (2005). Disruption of the f-actin cytoskeleton limits statolith movement in arabidopsis hypocotyls. *Journal of experimental botany*, 56(419):2539–2550. 11, 12

Pandey, D. K. and Chaudhary, B. (2016). A botanists cognitive view on plant growth: Cross-talk between developmental and sensitivity networks. *American Journal of Plant Sciences*, 7(15):2307. 30

Paul, A.-L., Amalfitano, C. E., and Ferl, R. J. (2012). Plant growth strategies are remodeled by spaceflight. *BMC plant biology*, 12(1):232. 20

Perbal, G., Jeune, B., Lefranc, A., Carnero-Diaz, E., and Driss-Ecole, D. (2002). The dose–response curve of the gravitropic reaction: a re-analysis. *Physiologia Plantarum*, 114(3):336–342. 3

Petrášek, J. and Friml, J. (2009). Auxin transport routes in plant development. *Development*, 136(16):2675–2688. 7

Pound, M. P., French, A. P., Atkinson, J. A., Wells, D. M., Bennett, M. J., and Pridmore, T. (2013). Rootnav: navigating images of complex root architectures. *Plant Physiology*, 162(4):1802–1814. 93

Robert, H. S. and Friml, J. (2009). Auxin and other signals on the move in plants. *Nature Chemical Biology*, 5(5):325–332. 7

Roux, S. J. (2012). Root waving and skewing-unexpectedly in micro-g. *BMC plant biology*, 12(1):231. 20

Roychoudhry, S., Del Bianco, M., Kieffer, M., and Kepinski, S. (2013). Auxin controls gravitropic setpoint angle in higher plant lateral branches. *Current Biology*, 23(15):1497–1504. 17, 18, 150

Roychoudhry, S. and Kepinski, S. (2015). Shoot and root branch growth angle controlthe wonderfulness of lateralness. *Current opinion in plant biology*, 23:124–131. 16

Sachs, J. (1882). Über orthotrope und plagiotrope pflanzenteile. *Arbeiten des Botanischen Instituts Würzburg*, 2:226–284. 12

Sack, F. D. (1991). Plant gravity sensing. *Int Rev Cytol*, 127:193–252. 10, 11

Sack, F. D. (1997). Plastids and gravitropic sensing. *Planta*, 203(1):S63–S68. 10

Sageman-Furnas, K. (2016). *Auxin-mediated Gravitropism of Arabidopsis thaliana*. PhD thesis, University of Leeds. 69, 88, 132

Saito, C., Morita, M. T., Kato, T., and Tasaka, M. (2005). Amyloplasts and vacuolar membrane dynamics in the living graviperceptive cell of the arabidopsis inflorescence stem. *The Plant Cell Online*, 17(2):548–558. 12

Sampedro, J. and Cosgrove, D. J. (2005). The expansin superfamily. *Genome biology*, 6(12):242. 5

Schneider, C. A., Rasband, W. S., and Eliceiri, K. W. (2012). Nih image to imagej: 25 years of image analysis. *Nature methods*, 9(7):671–675. 24

Schopfer, P. (2006). Biomechanics of plant growth. *American journal of botany*, 93(10):1415–1425. 4

Sievers, A. and Volkmann, D. (1977). Ultrastructure of gravity-perceiving cells in plant roots. *Proceedings of the Royal Society of London. Series B, Biological Sciences*, pages 525–536. 17

Simmons, C., Söll, D., and Migliaccio, F. (1995). Circumnutation and gravitropism cause root waving in arabidopsis thaliana. *Journal of Experimental Botany*, 46(1):143–150. 20, 148

Sukumar, P., Edwards, K. S., Rahman, A., DeLong, A., and Muday, G. K. (2009). Pinoid kinase regulates root gravitropism through modulation of pin2-dependent basipetal auxin transport in arabidopsis. *Plant Physiology*, 150(2):722–735. 7

Swarup, R., Kramer, E. M., Perry, P., Knox, K., Leyser, H. O., Haseloff, J., Beemster, G. T., Bhalerao, R., and Bennett, M. J. (2005). Root gravitropism requires lateral root cap and epidermal cells for transport and response to a mobile auxin signal. *Nature cell biology*, 7(11):1057–1065. 5

Thompson, M. V. and Holbrook, N. M. (2004). Root-gel interactions and the root waving behavior of arabidopsis. *Plant Physiology*, 135(3):1822–1837. 20

Tiwari, S. B., Wang, X.-J., Hagen, G., and Guilfoyle, T. J. (2001). Aux/iaa proteins are active repressors, and their stability and activity are modulated by auxin. *The Plant Cell*, 13(12):2809–2822. 8

Verbelen, J.-P., Cnodder, T. D., Le, J., Vissenberg, K., and Baluška, F. (2006). The root apex of arabidopsis thaliana consists of four distinct zones of growth activities: meristematic zone, transition zone, fast elongation zone and growth terminating zone. *Plant signaling & behavior*, 1(6):296–304. 116, 146

Vieten, A., Sauer, M., Brewer, P. B., and Friml, J. (2007). Molecular and cellular aspects of auxin-transport-mediated development. *Trends in plant science*, 12(4):160–168. 7

Went, F. W. (1927). *Wuchsstoff und wachstum*. De Bussy. 6

Zhang, N. and Hasenstein, K. H. (2000). Distribution of expansins in graviresponding maize roots. *Plant and Cell Physiology*, 41(12):1305–1312. 5

Appendices

Appendix A

An example ROTATO script

```
% sets up and runs 2 MATATO experiments in parallel

jitter = 0; % whether to jitter the root
constrain = 1; % whether to constrain the root
adjustTime = 60; % time in seconds between adjustments
micType = 'invMic'; % microscope type (determines default image analysis setting

% number of objects to run and which camera is attached to which stage
nMATS =2;
camIDs = [1 2];
stageIDs = [1 2];

% get time to run for
numSteps = input('Enter the length of time to run for (hours): ');
numSteps = round(numSteps*60);

% what sort of root is this?
lateral = input('Is this root a lateral (1 for yes, 0 for no)? ');

% make a connection to the controller.
```

```matlab
port = findMotorPort();
con = createConnection(port);

% instansiate MATATOs
MATATOs = {};
for i = 1:nMATS,
    MATATOs{i} = MATATOobject(jitter,constrain,lateral,micType,stageIDs(i),camID
end

% perform setup step
for i = 1:nMATS,
    MATATOs{i}.setup()
end

% run step loop
for i = 1:numSteps,
    tic;

    for j = 1:nMATS,
        MATATOs{j}.stepMATATO();

        MATATO = MATATOs{j};
        save(MATATOs{j}.saveName,'MATATO');
    end

    timeElapsed = toc;
    waitTime = max(0,(MATATOs{1}.adjustTime)-timeElapsed);
    pause(waitTime);

end
```

Appendix B

ROTATO experimental settings

The following table contains the standard experimental settings a ROTATO experiment. While these settings were used for the majority of experiments some computer vision were tweaked in order to ensure accurate angle detection. Internal settings, depreciated settings, and visualisation options are not included as they do not effect the results shown previously.

Setting	Value	Description
Adjustment time	60	The time in seconds between adjustments.
Adjustment number	361	The maximum number of adjustments made before stopping.
Maximum turn	2	The maximum turn allowed in a single step.
Minimum turn	2	The minimum turn allowed in a single step.
Constraint angle	X	The angle to constrain the root at, this varied depending on the experiment.
Constrain	True	Whether to constrain the root.
Jitter	False	Whether to add noise to the movement every step. This was used for testing only.
Lateral	False	Whether the root is a lateral root, if so different vision defaults were used.
Tip length	70	The length in pixels of the root tip used in angle detection.
Root width	70	The width of the root.
Close size	23	The size of the kernel used when closing the image. Should be about one third of the root width.
Open size	23	The size of the kernel used when opening to remove hairs. Should be similar to the close size.
Invert colours	1	Whether to take the complement of the initial image prior to processesing.
Absolute value	False	Whether to use the absolute change in intensity from the background, if set to false only light objects are detected.
Extraction threshold	15	The threshold used to detect a root.
World size	71 (or 151)	The size of the surrounding area used in background equalisation. This varied depending on the image quality with 151 being a common option.
Blur size	0	Size of initial blurring kernel used to decrease noise, this was not needed in the final version of the code but is included nonetheless.
Noise size	200	Size in pixels of small objects to be removed after segmentation.
Spur size	60	The length of small spurs to remove from the skeleton.
Angle method	'line'	Whether to use a line or an ellipse to fit to the root tip when detecting angle.